2017

Remote Sensing of World War II Era Unexploded Bombs Using Object-Based Image Analysis and Multi-Temporal Datasets: A Case Study of the Fort Myers Bombing and Gunnery Range

Bryan Byholm
Minnesota State University, Mankato

Remote Sensing of World War II Era Unexploded Bombs Using Object-Based Image Analysis and Multi-Temporal Datasets: A Case Study of the Fort Myers Bombing and Gunnery Range

By

Bryan Byholm

A Thesis Submitted in Partial Fulfillment of the

Requirements for the Degree of

Masters of Science

In

Geography

Minnesota State University, Mankato

Mankato, Minnesota

May 2017

5/15/2017

Remote Sensing of World War II Era Unexploded Bombs Using Object-Based Image Analysis and Multi-Temporal Datasets: A Case Study of the Fort Myers Bombing and Gunnery Range

Bryan Byholm

This thesis has been examined and approved by the following members of the student's committee.

_____

Cynthia Miller, Ph.D.

_____

Fei Yuan, Ph.D.

_____

Forrest Wilkerson, Ph.D.

Abstract

During World War II, United States Army and Navy pilots trained on several hundred bombing ranges encompassing more than 12 million acres of land, leaving behind crater-scarred landscapes across the country. Post-war estimates suggest that 10-15% of aerial bombs used failed to detonate as intended, so these areas today are contaminated by a large number of dangerous unexploded bombs (UXB) which remain under the surface. Until recently, detecting UXB has been a tedious and expensive process done in three stages: (1) identifying and mapping general areas of concentrated bomb craters using historical air photos and records; (2) intensely searching these areas at a larger scale for much smaller UXB entry holes; and (3) confirming the presence of individual UXB using magnetometry or ground-penetrating radar. This research aims to streamline the workflow for stage 1 and 2 using semi-automated object-based image analysis (OBIA) methods with multi-source high spatial-resolution imagery. Using the Fort Myers Bombing and Gunnery Range in Florida as a study area, this thesis determines what OBIA software and Imagery is best at locating UXB in this environment. I assess the use of LiDAR-derived DEMs, historical air photos and high-resolution color digital orthophotos in Feature Analyst and Imagine Objective, and discuss optimal inputs and configurations for UXB searches in karst wetlands. This methodology might be applied by the detection and clearance industry in former war zones, and aid in restoring former training ranges to safe land uses in the U.S.

Acknowledgements

I would like to take a moment and thank my committee who without their unwavering support and excitement, this process would have been much more anxiety filled then it was. Dr. Cynthia Miller was always available to help when needed and passed on much of her photo interpretation skills on to me, something that is very hard to come by these days. Dr. Fei Yuan was always very helpful to guide me writing and research in the correct direction with her vast knowledge of OBIA software and remote sensing. Last but defiantly not least, I thank Dr. Forrest Wilkerson for his determination to make sure I do great things with my thesis and his continued support throughout the process. Thank you all so much! I would also like to thank the Minnesota State, Mankato Geography Department for all of the added support throughout my time as an undergraduate and as a master's student. Everyone has always been very kind and knowledgeable when needed, and also very tenacious and to the point when needed. Next, I would like to thank my friends who dealt with me and helped me along the way whether that was helping proofread chapters, Rachel Ledding, or allowing me to relax when I got home from a long day, Scott Tessman, and every single person who I interacted with in this time helped me along the way even though you may not be named. Lastly, I want to thank my family, my brother Brett and nephew Ayden for not getting too upset when I couldn't be at many family gatherings. My girlfriend Mylissa Sauser who has stood by me in the worst times and then even worse times during this whole process. And especially my mom Cindy, who has nearly torn her hair out over the last two years in my almost complete absence. I love you all and thank you so much for your support!

Table of Contents

List of Figures

List of Tables

Chapter 1: Introduction

In today's world, people tend to forget the past and how it can affect the present. Growing up, history was one of my favorite subjects, along with the study of warfare and how it can change the landscape so much after the fighting has stopped. This interest was piqued through the video games I would play and one mission still stands out to me today. It was a simple bombing mission in preparation of Operation Husky, the Allied Invasion of Sicily. In the mission, the player is a bombardier in a B-24 Liberator and the targets are oil depots and ships. The bombs all fall on target and explode and the mission is over in only a few minutes. Throughout the war, and every war for that matter, bombs are dropped or fired at an enemy but a certain amount of them do not explode. This becomes a problem after the war when unexploded ordnance (UXO) can finally explode, killing whoever may be in the vicinity. The UXO issue has surfaced in Europe as well as in Southeast Asia, where the Obama administration recently allowed US tax dollars to be used for UXO removal in Cambodia (Lefevre and Petty 2016). Because modern ground methods for location are slow, dangerous, and expensive, this thesis attempts to locate UXO and unexploded bombs (UXB) remotely using object-based image analysis (OBIA) software and freely available "off the shelf" imagery.

This introduction will discuss UXO and UXB definitions, imagery used, the study area, and my research expectations. In Chapter 2, the historical background will discuss the planes flown and why this information is relevant to UXB locations. A literature review examining past UXB location methods and technologies comprises Chapter 3, and then a discussion of methods will follow in Chapter 4, covering my techniques used to locate these UXB and how their accuracies were tested. The results of these tests will be

shown and discussed in Chapters 5 and 6. The concluding chapter will summarize the findings and determine if the research expectations have been met.

1.1 UXB vs. UXO

The terms UXO and UXB are not interchangeable. UXO are any unexploded explosives which still remain under the ground after a battle and can include any explosive such as small arms ammunition, grenades, rockets, and aerial bombs. UXB are unexploded bombs which have been dropped from an aircraft and did not explode as designed. This delineation is important as more research has been completed on UXO mitigation. Some UXO have a tendency to be closer to the surface which makes them more readily visible, while UXB can burrow deeply into the ground and leave very little evidence of their existence. This thesis attempts to bridge the research gap between the remote sensing of UXO and UXB using both historical and present day imagery and Object Based Image Analysis (OBIA) software.

1.2 Purpose of the Research

Because of the need to train aerial bombing crews since the 1940s, the U.S. military created hundreds of training ranges throughout the United States. During World War II, the demand for qualified personnel was both immense and immediate, so the Army and Navy Departments quickly leased many parcels of land to use as training ranges. Most of these sites were used intensely for only two to three years and then returned back to the original land owners at the war's end with very limited clean up or "deduding" activities. A document released by the U.S. Army Corps of Engineers

(USACE) directly stated that the study site used in this thesis never had a certificate of clearance and that very little work had been done there since WWII (USACE 1996).

Most of these former ranges are listed on the USACE "formally used defense sites" database or FUDS list, and are awaiting evaluation as to whether or not UXO/UXB remain on the site. The largest and most dangerous ranges have been given priority for cleanup operations. Contractors working with USACE personnel have developed a variety of detection methods that use a combination of remote sensing and ground based analysis techniques that will be discussed in Chapter 3. These methods use time intensive analyses of custom acquired imagery and LiDAR data, and usually require years to accomplish at the cost of hundreds of thousands of dollars.

This research deliberately focuses on a smaller range that has yet to be selected for intense analysis by the USACE, but likely contains potently dangerous UXB. Because budgets have been limited for smaller ranges, this research will assess whether or not free or low cost data sets that already exist in archival collections can be used to locate UXB with new OBIA remote sensing software. If successful, this thesis will offer and effective, low cost means of UXB identification that the USACE can use to facilitate small range analysis.

The Fort Myers Bombing and Gunnery Range (FMBGR) was selected as a case study for this research because it fits these criteria. It is a small site that was used for approximately three years during WWII, but has been identified by the USACE as a range that likely contains large and potentially still dangerous unexploded general

purpose bombs that could pose risks to modern-day populations. A variety of imagery is available for analysis of the site, so it meets the criteria as a test case for providing the USACE the background data to facilitate cleanup in the near future.

1.3 Study Area

While this thesis will attempt to create a methodology which can be replicated worldwide, a previously documented USACE FUDS site serves as the study area. The location is known as the Fort Myers Bombing and Gunnery Range (FMBGR) due to its proximity to the city of the same name. Some WWII sources describe the site as the Bermont Bombing Range because of a nearby crossroads, but this name is not normally used in modern USACE records. This was a WWII bombing range used to train U.S. Army Air Force (USAAF) pilots from 1942 to 1945. The range is located about 20 miles north of Fort Myers, Florida, on the western side of Florida (Figure. 1.3.1). This land currently is in possession of the Florida Fish and Wildlife Conservation Commission under the name "Fred C. Babcock/Cecil M. Webb Wildlife Management Area" (Florida Fish and Wildlife 2016). This location was perfect for bombing during the war for two main reasons: the weather and its geographic location. Weather is very important for flying and safe, effective training conditions. Florida's climate allowed for a sufficient number of training days and allowed bomb crews to hone their communication and bombing skills in a calm, controlled manner. Its geographic location was also ideal in terms of the proximity to airfields that hosted training units stationed at Page Field in Fort Myers. At the time the range was created, the land had been clear cut and was only used for cattle grazing so little risk to civilians was anticipated.

Figure 1.3.2. Page Field and the FMBGR location

The landscapes of the former FMBGR consist of flat sandy scrubland mixed with clusters of palmetto tree stands. (USACE 1996 and 2009) Known as a karst region, layers of limestone bedrock are saturated with subsurface water, so this is why much of southern Florida consists of wetlands (Peterson, Sack and Gabler 2012). Searching for bomb craters and UXB in this environment can be difficult because karst features include

sinkholes and dolines, which are types of depressions that can be misidentified as bomb craters on imagery (Lane 1986).

The determining factor in delineating the two features on imagery is that bomb craters will have a visible rim on LiDAR-derived surfaces where the sediments were forced out from the blast, while a sinkhole will not. Even a UXB tends to have a very small rim and will have a more distinct profile into the middle of the hole, whereas a sinkhole will be more erratic in terms of its surface configuration. Another issue is the constantly variable land cover in a karst landscape, which can change very quickly because of the close proximity of the water table to the surface. In this environment, trees and other plants can grow very quickly and cover up exposed bomb craters that cannot be seen through the canopy or ground cover (Figure 1.3.3). Lastly, because of the relative softness of the sandy, wet shallow soil, the impacting bombs created much larger holes than bombed landscapes in Europe or other drier places in the United States. This can cause issues for crater identification because research has shown that bombs tend to have a regular crater diameter that can be used to identify the type and the size of the bomb (U.S. Army Office of the Chief of Ordnance 1944). In karst areas, the blast created a larger than normal visible surface impact mark, making confirmation with LiDAR an essential aspect of bomb crater identification. More detailed discussion of these issues can be found in Chapter 3.

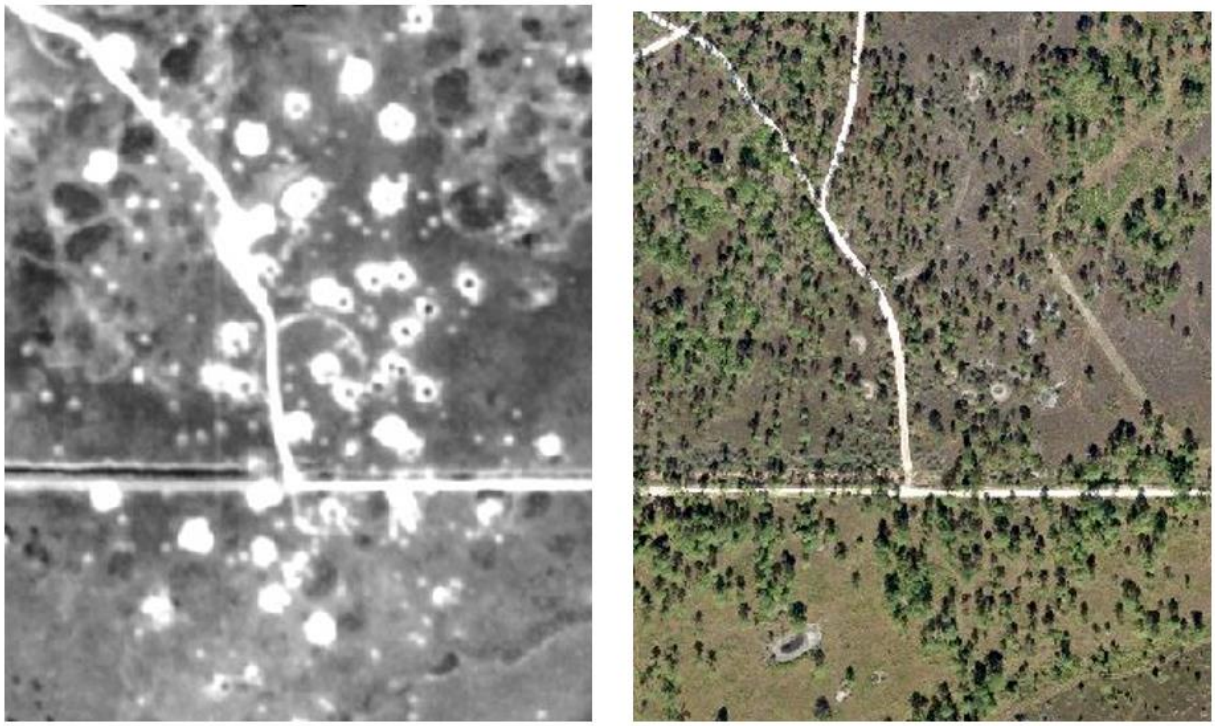

Figure 1.3.3. Comparison of the range between 1946 and 2014. These two images, the 1946 image on the left and the 2014 image on the right, shows the change in land cover over time. This entire impact area has been reclaimed by the landscape vegetation and shows only limited evidence of craters.

Taking all of this into consideration, this thesis will use the FMBGR as a case study site for locating the impact craters and UXB to create a locational methodology that can be adjusted to different environments and landforms.

1.4 Imagery

When locating UXB, it is necessary to first identify cratered features that mark the areas impacted by exploding aerial bombs. Given that approximately 10-15% of the

bombs dropped failed to explode, one can expect to find UXB at an approximately 1:10 or 1:15 ratio among crater fields. In effect, locating impact zones enables a researcher to find areas most likely to contain much less visible and sometimes invisible UXB entry holes. In compiling imagery for UXB research, historical air photos taken as soon as possible after impact are essential. These photos clearly show impact signatures ranging from only a few meters in diameter to twenty or more meters depending on the size of the bombs (Table 1.4.1).

Modern aerial imagery in the form of high resolution Digital Orthophoto Quadrangles (DOQs) reveals remaining impact craters as they exist after decades of exposure to weather, erosion and vegetation regeneration. Another critical layer for the study is freely available LiDAR data which has been processed into a Digital Elevation Model (DEM) to show modern day landscape surfaces underneath the growing canopy and to confirm the location of the craters.

IMAGE	SOURCE	RESOLUTION	BANDS
1946 HISTORICAL IMAGERY Figure 1.4.1	University of Florida Digital Collections of the Map and Imagery Library	600 dpi 1:20,000	Single - Black and White
2008 MODERN DOQ HIGH RESOLUTION IMAGERY Figure 1.4.2	USGS Earth Explorer	1 Foot	Three - CIR, Blue, Green
2014 MODERN DOQ HIGH RESOLUTION IMAGERY Figure 1.4.3	USGS Earth Explorer	1 Foot	Three - Red, Blue, Green
2006 LIDAR Figure 1.4.4	Southwest Florida Water Management District, Distributed by NOAA	1 Meter	Single - DEM

Table 1.4.1. Imagery layers used in the thesis.

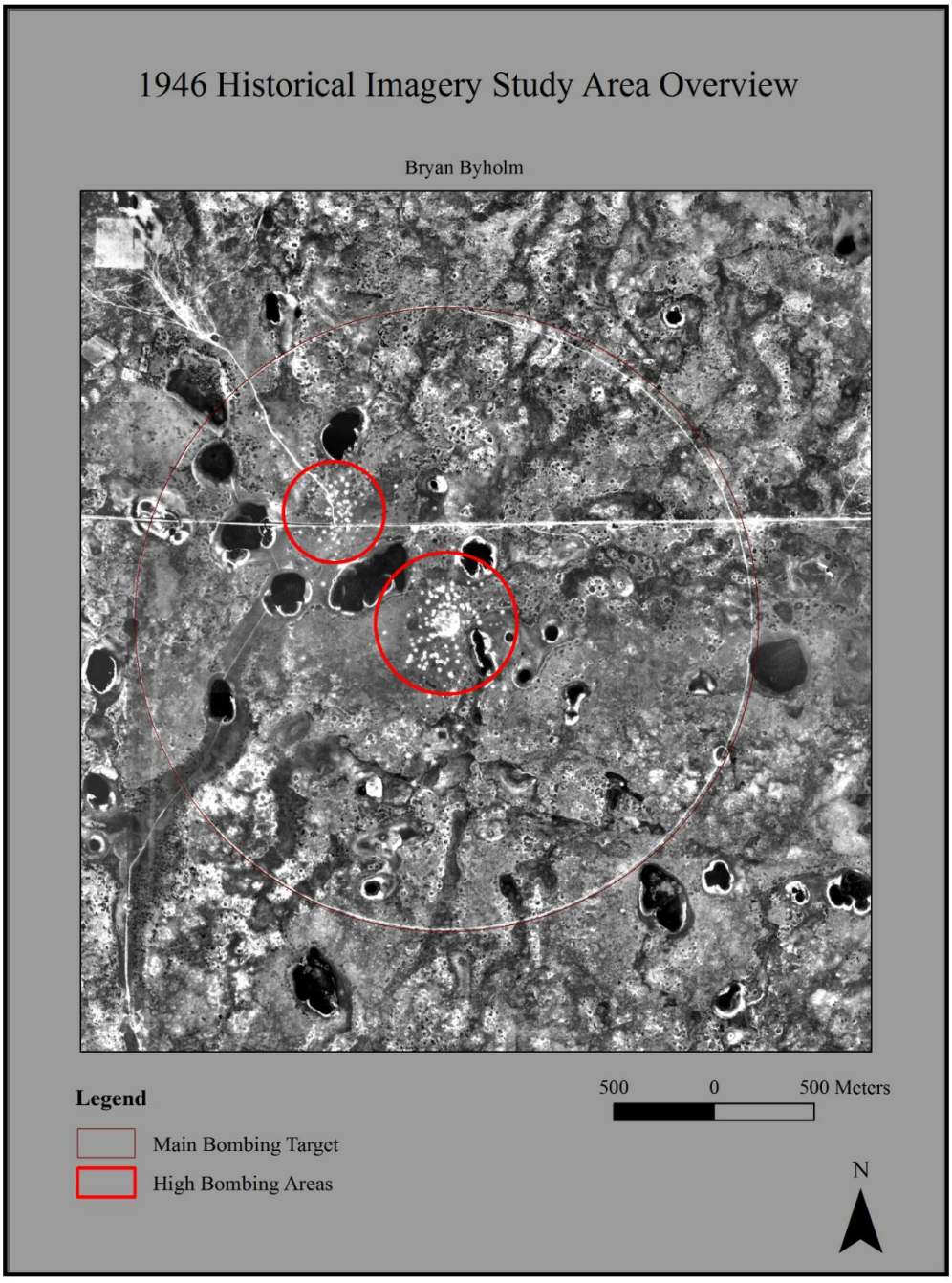

Figure 1.4.1. Map of study area in 1946. The two circles outline the highest concentration of bombing.

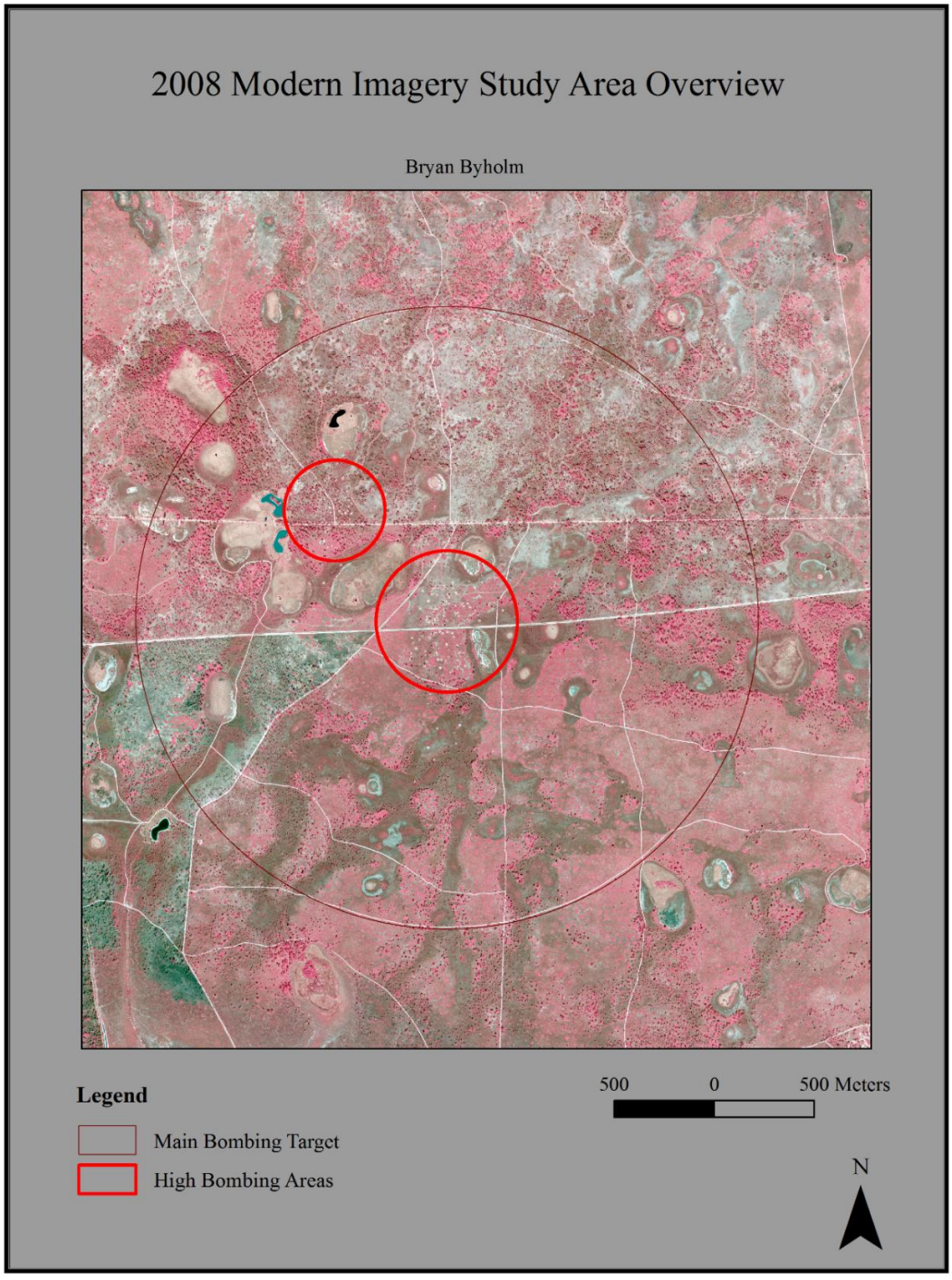

Figure 1.4.2. Map study area in 2008, shown in color infrared. The two circles outline the highest concentration of bombing

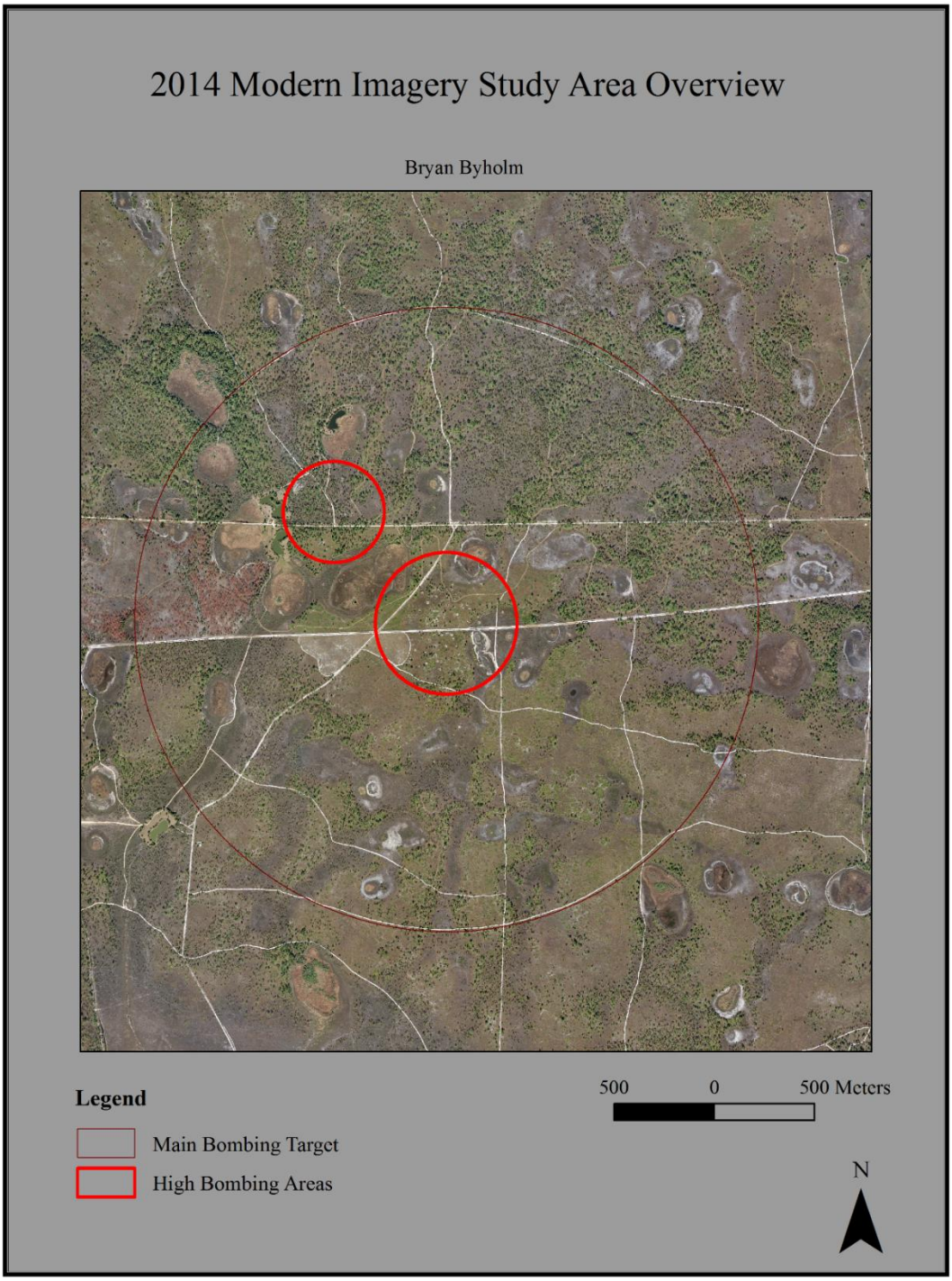

Figure 1.4.3. Map of the study area in 2014. The two circles outline the highest concentration of bombing.

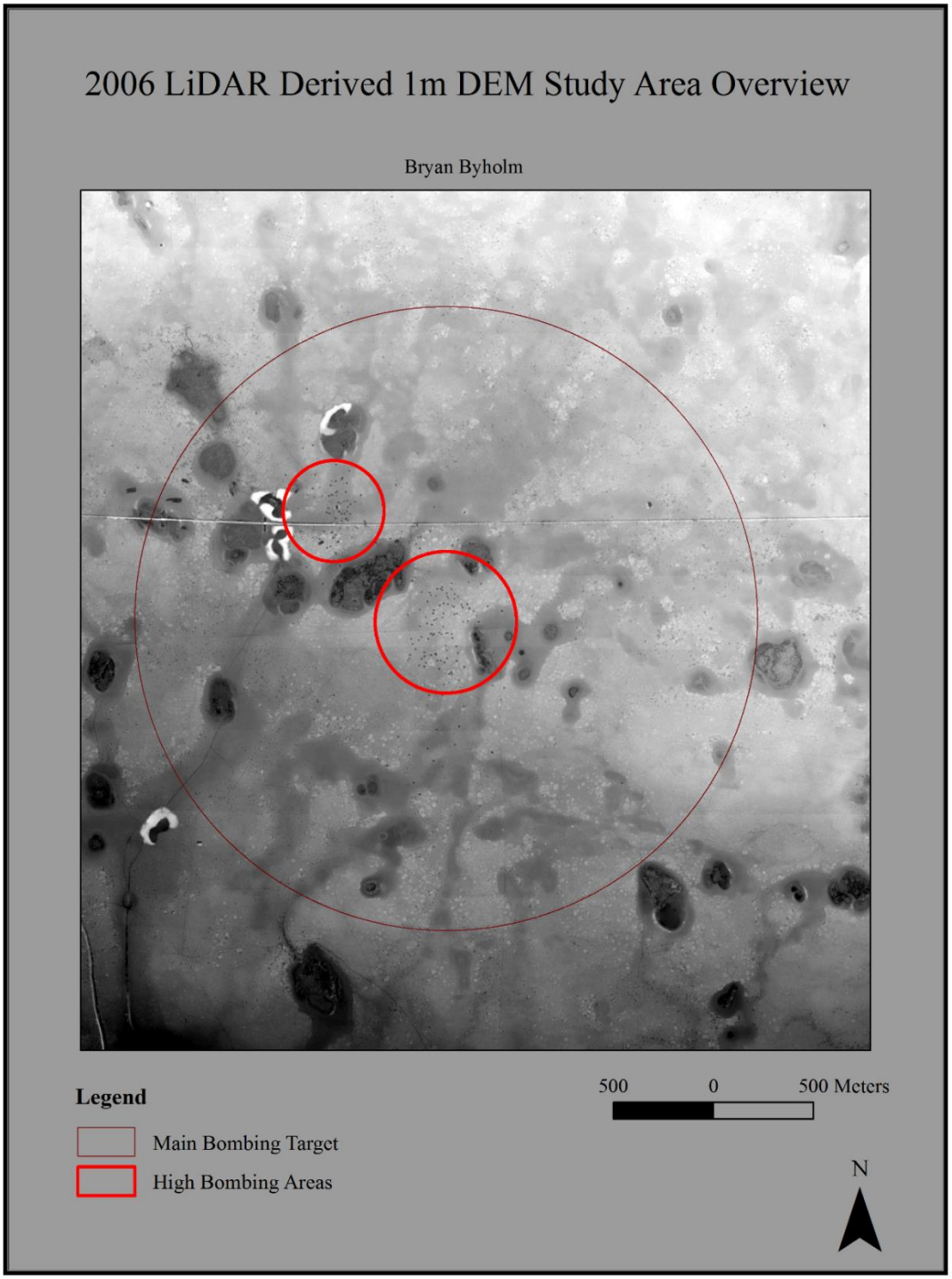

Figure 1.4.4. Map of the study area in 2006, shown in a LiDAR-derived DEM. The two circles outline the highest concentration of bombing, and the tiny black holes indicate craters.

1.5 Research Objectives

The objectives of this study are: (1) to determine which OBIA is better at delineating crater impact areas; (2) to determine which imagery is the best for UXB entry hole delineation; and (3) to learn if the methods work well enough to apply them for UXB delineation in other areas. These objectives will be tested to answer the primary research question: Using the Fort Myers Bombing and Gunnery Range (FMBGR) as a case study, can a new locational methodology be created using only low cost, readily available imagery and modern Object Based Image Analysis (OBIA) software? It is hypothesized that Overwatch Systems' Feature Analyst will have a more comprehensive ability to locate UXB entry holes as more data can be used at once in Feature Analyst compared to Imagine Objective. Another hypothesis is that the modern imagery will have a lower success rate in comparison to the imagery taken closer to the time of the bombing. This is because of the loss of the features, which is exacerbated in this study area due to the moist environment and the karst landscape. This creates an issue as LiDAR becomes less effective at UXB delineation as time goes on. This will likely have a negating effect on the multi-layer tests that can be performed successfully.

Chapter 2: Historical Information

Background information about which type of bombs were dropped and what method was used to drop them is important for delineating the UXB "pinhole" entry points and the patterns they leave on the ground. This information can also be used for remediation as these details can help assess risk in terms of the number of bombs dropped. While this information is useful, it can be very challenging to gather as many essential details were not recorded by training units during WWII. The need for aircrews was urgent and the pilots were trained quickly before being sent off to war, so the U.S. War and Navy Departments opened new airfields around the country and then closed them as soon as the war was over. By 1943, USAAF training units stationed at Page Field trained replacement fighter pilots in advanced flight tactics and how to use their planes to their full potential before they were sent to operational aviation units overseas. The airfield closed in 1945 at the war's end (Shettle 2009). This process included attack methods such as strafing and glide bombing techniques intended to support Allied troops on the ground during the final stages of the war. Page Field pilots used the Fort Myers Bombing and Gunnery Range for this phase of their training. (Figures. 2.1 and 2.2). Because of the short time that the range was in operation, very limited records about the types, sizes and quantities of ordnance used there can be found in the collections of the U.S. Air Force Historical Research Agency at Maxwell Air Force Base in Alabama. Fortunately, the Corps of Engineers site inspection report of the range includes a detailed analysis of munitions debris found in the target areas, and these are used in this thesis to interpret the craters and possible UXB entry holes that are visible on the imagery (USACE 2009).

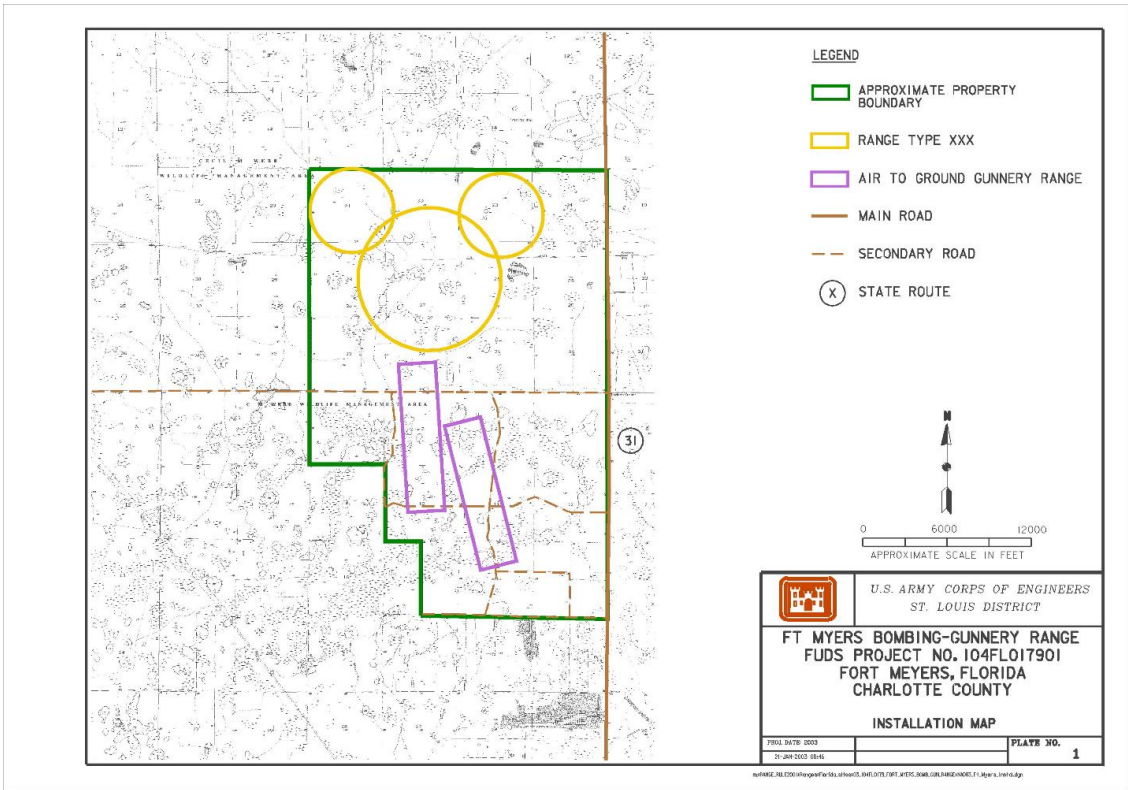

Figure 2.1. FUDS FMBGR Map. The main bombing target is the larger yellow circle between the smaller two to the north.

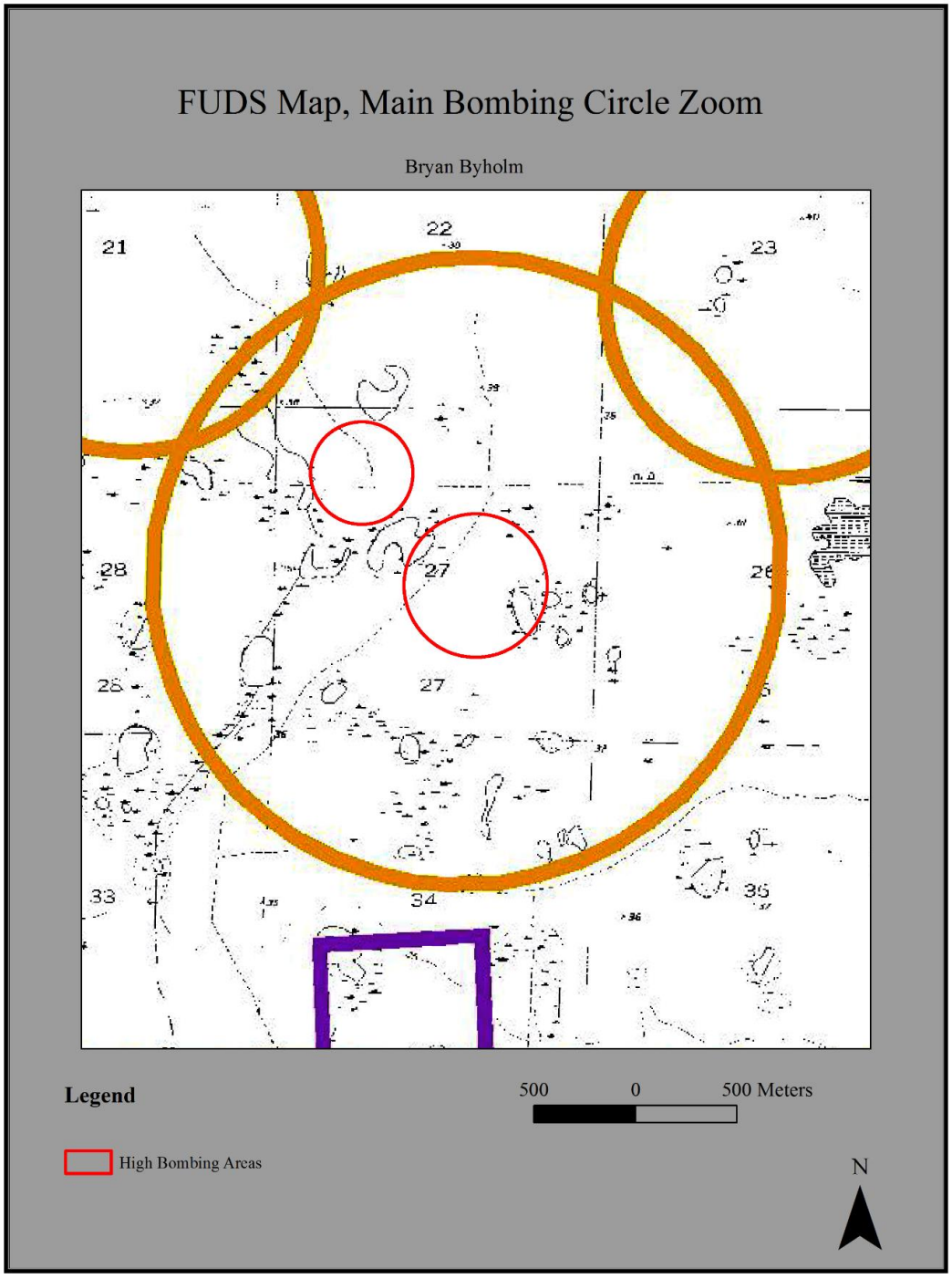

Figure 2.2. Zoomed FUDS FMBGR Map. This map is a zoomed version of Figure 2.1. In this image, the main bombing circle is shown in yellow and the main concentrations of bomb craters are highlighted in red.

2.1 Planes and Bombs

When work began on this thesis, it was assumed that the large craters at the FMBGR were made by 500 lb bombs being dropped from heavy bombers by crews training in aerial bombing techniques from their bases in the Tampa or Homestead areas. The problem with this assumption is that larger aircraft would have left many more craters in the target areas even in the two short years of operation, given that the typical B-17 and B-24 aircraft normally dropped ten bombs per run. Researchers who compiled the USACE archival research report found documentation confirming that only fighter pilot trainees based at Page Field used the FMBGR once it opened for use (USACE 2009). The pilots were taught to perform strafing runs using their .50 caliber machine guns and to drop bombs at a low angle and low altitude (Figure 2.1.1). This maneuver is called glide bombing and it was a standard ground support tactic for the USAAF during the final stages of the war (USAAF 1945).

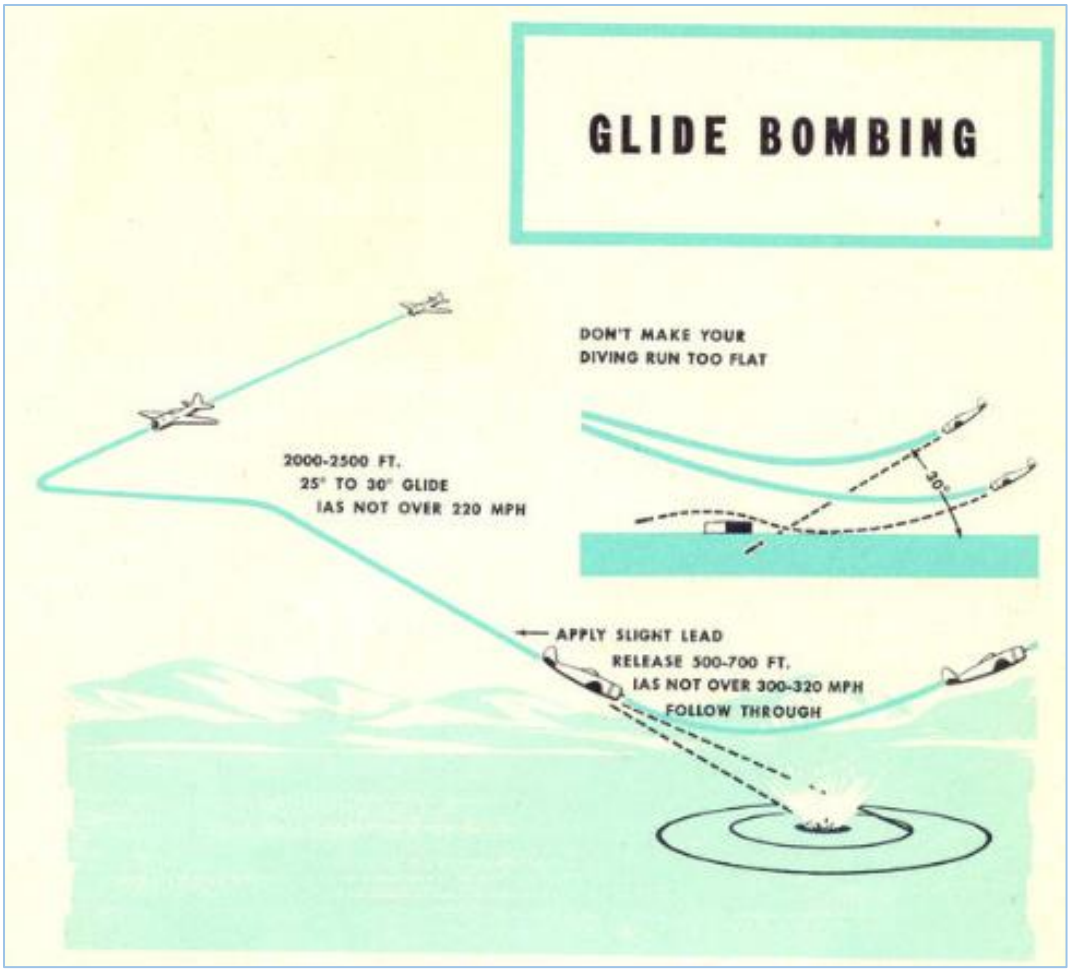

Figure 2.1.1. The Glide Bombing Maneuver. Unlike steeper dive bombing, this tactic used a low angle and low altitude approach that was safer for the heavier P-47 Thunderbolt fighter plane. (USAAF 1945)

Knowing which fighter plane models trained at the FMBGR can help us better understand the altitude, speed and possible direction of the attack used at the range and thus enable make more accurate interpretations of the crater and UXB entry holes shapes and sizes. In his comprehensive study of Florida's Army Air Fields, M.L.Shettle, Jr. states that training units at Page Field used two fighters and one fighter-bomber during

the time that the FMBGR was in service, confirming that ground support bombing tactics were done here (Shettle 2009). These aircraft are described in Table 2.1.1.

PLANE	CLASS	MAX SPEED	SERVICE CEILING	COMMON BOMB LOAD
CURTISS P-40L "WARHAWK"	Fighter	595 km/H	10,973 m	2 - 3 bombs (250 or 500 lb) or (2 x 250 or 500 lb and 1 x 1,000 lb)
REPUBLIC P-47N "THUNDERBOLT"	Fighter-Bomber	752 Km/H	13,106 m	2 -3 bombs (2 x 250 or 500 lb) or (2 x 1,000 lb and 1 x 500 lb)
NORTH AMERICAN P-51D "MUSTANG"	Fighter	703 km/H	12,771 m	2 bombs (100, 250 or 500 lb)

Table 2.1.1. Aircraft Specifications. This table describes the specifications of each aircraft model likely stationed at Page Field in 1944 and 1945. Ordnance is described by sizes of the general purpose high explosive bombs commonly used at the time for both training and combat (Shettle 2009, Dwyer 2014a, Dwyer 2014b, Dwyer 2014c, USAAF 1943, USAAF 1944 and USAAF 1945).

By early 1944, the USAAF began training fighter pilots to strike ground targets in anticipation of the Allies planed invasion of France. While the P-40 Warhawk was being replaced by the newer P-47 Thunderbolt and P-51 Mustang in the overseas combat zones, the USAAF still assigned the plane to fighter pilots who were learning tactical skills, and Shettle confirms that these older planes were in use at Page Field during the time the FMBGR was functional (USAAF 1943, Shettle 2009). The main focus of fighter-bomber training at the time, though, was the P-47 with its greater speed and robust structure. This aircraft could withstand more damage from enemy fire, allowing them to get closer to the

ground to deposit their bombs on target, and they, too, were used for pilot training at Page Field (USAAF 1945, Shettle 2009).

The P-51 Mustang was also capable of ground support bombing with its high speed and bomb load capacity, but the USAAF valued its air superiority role more in 1943 and 1944 due to its longer range as an escort for heavy bombers. It excelled in clearing the skies of enemy planes and its payload allowed the use of auxiliary fuel tanks to extend its range for longer escort missions, but this feature negated its ability to carry a full bomb load for ground support. As the Luftwaffe suffered increasing losses of its fighter planes in the European theater, P-51 pilots were able to devote more flight time to ground attack duties during the later months of 1944. Training on the P-51 at Page Field began in the spring of 1945, perhaps in anticipation of a land invasion of Japan, so we can assume that it played only a small role in the bombing runs conducted over the FMBGR before the war ended in August. Given these circumstances, it is likely that the majority of the bombs dropped on the FMBGR came from P-40 and P-47 aircraft engaged in glide bombing maneuvers.

Based upon the common bomb loads used by the P-40, P-47 and P-51 aircraft, we can determine the types of ordnance that was most likely used in training at the FMBGR. On the ground, pieces of the bombshells can be still seen scattered around the range, offering further confirmation of bomb types and sizes used. The USACE Site Investigation Report states that shrapnel was found on the site from exploded 250 and 500 lb. general purpose, high explosive bombs, and from 100 lb. training bombs in the main target area (USACE 2009). This information becomes very useful when interpreting

the 1946 image. Large craters likely caused by the explosion of 500 and 250 lb bombs are visible, but smaller pinholes can be seen as well (Figure. 2.1.2).

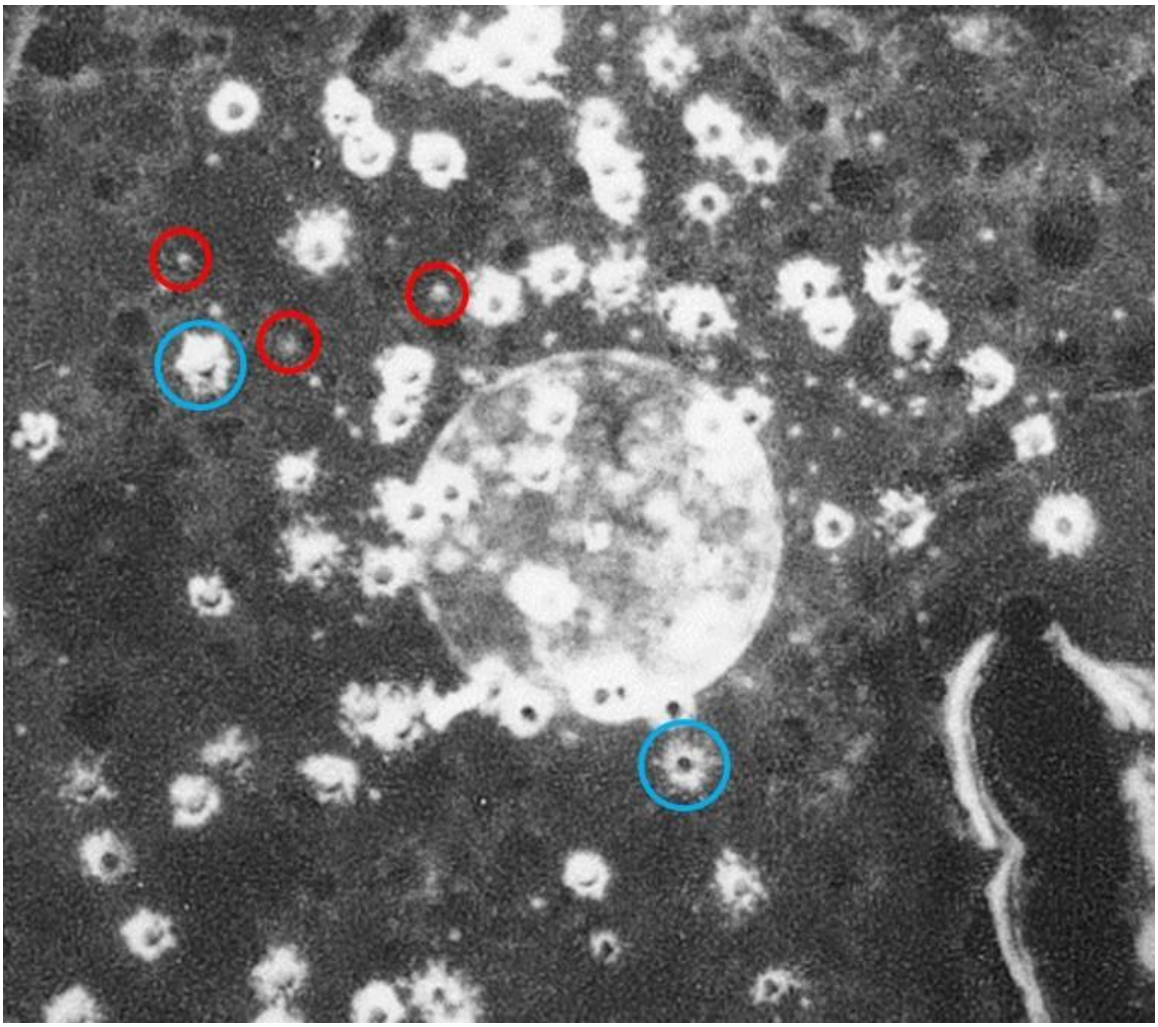

Figure 2.1.2. Main bombing target, 1946. Examples of small pinholes are circled in red and exploded bomb craters are in blue.

These pinholes could be either UXB entry holes or 100 lb training rounds but there is evidence present to suggest that they are indeed UXB signatures. In the demolition circle, the pinholes have a distinctive smaller non-explosive impact crater. It appears as if the bomb hit the ground and created an asymmetrical V-shape, shallower in

the direction of origin, and steeper when it stopped on the opposite side of the crater (Figure 2.1.3). These distinctive crater profiles at the pinhole sites appear to be the signatures of 250 and 500 lb. UXB in the main demolition target area.

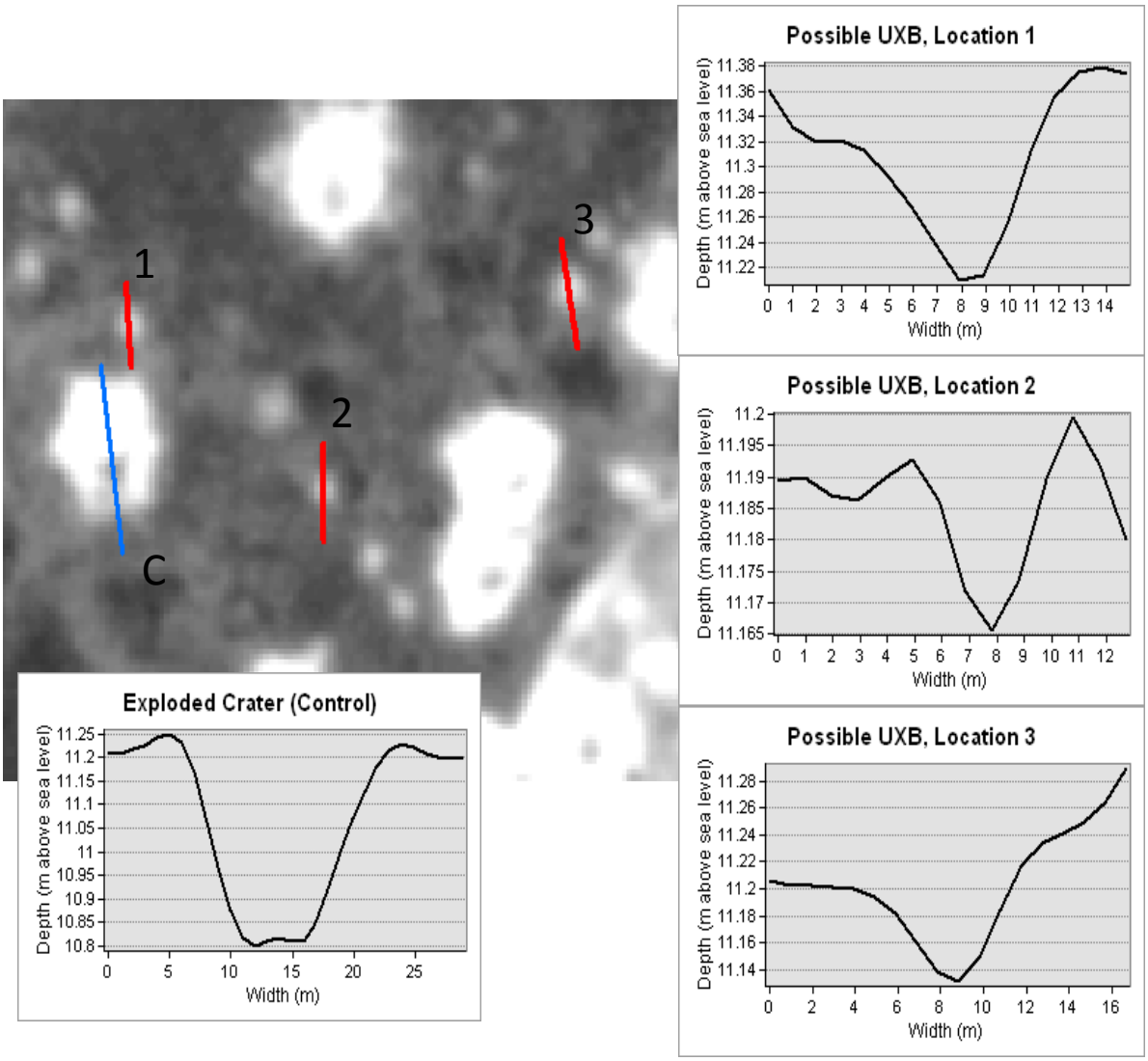

Figure. 2.1.3. Profiles detailing the craters. These profiles are based from the 2006 DEM overlaid with the 1946 historical imagery. The pinholes numbered 1-3 have a profile which matches the description of a UXB. These are shallow as they have refilled over time. The C crater, the control, is very distinctive of a U-shaped exploded crater.

Another issue related to the identification of the UXB signatures is the question of what type of impact mark was created by the 100 lb training bombs. These bombs only consisted of a small spotting charge, rather than high explosives, and emitted a puff of smoke upon impact. The USACE Site Inspection Report (2009) provides insight by describing a group of 100 lb training bombs that exploded on the nearby dive bombing range. Because the researchers found no evidence that 250 or 500 lb general purpose bombs were ever used on this range, we can assume that the identified cluster of 100 lb training bombs that are visible on the DEM are signatures of this type of ordnance. Thus, they will provide a reliable signature of their distinctive profiles as compared to those made by the 250 or 500 lb. UXB entry holes. As shown in Figure 2.1.4, these 100 lb training bombs created much smaller, shallower and more symmetrically U-shaped crater profiles, which are visibly different than the possible pinhole signatures of the 250 and 500 lb. UXB on the demolition range.

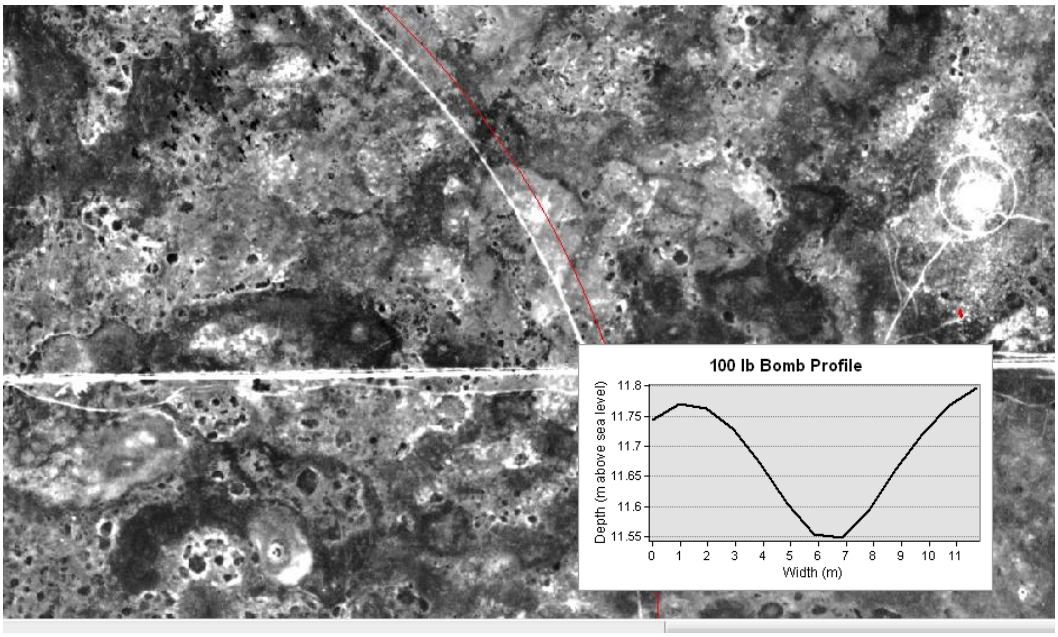

Figure. 2.1.4. A 100 lb. training bomb profile. Researchers confirmed that the crater was made by a 100 lb training bomb during a site inspection. (USACE 2009).

For the remediation process, these DEM profiles and signatures can serve as an indicator of how many UXB may exist in the study area. While this site does not have any historical documentation on sortie loads and sortie numbers used by Page Field trainees, these data do exist in more specific bomb loading documents compiled by USAAF units in the combat theaters, so this profile identification process could prove useful for UXB searches on actual bomb target areas in Europe and in the Pacific areas of operations.

Knowing how many bombs were dropped can also indicate how many could be UXB, as most nations have reported estimated dud rates. During WWII, the dud rate for U.S. high explosive aerial bombs ranged from 10% to 20%. For this thesis, the 10% rate

will be used as a conservative estimate (U.S. Army Corps of Engineers 2016, Sabour, Agarius, and Sadidi 2014).

While archival confirmation and ground truthing is also required for UXB analysis, the dud rate is invaluable factor for estimating how many possible UXB could remain on the training range. In effect, assuming that ten fighter planes completed a training run per day, each carrying two 500 lb. bombs, it is likely that two UXB were dropped on an average daily basis. This type of information would be very useful if the methods developed in this thesis are to be replicated for other ranges.

Chapter 3: Literature Review

UXO and UXB have been issues around the world and will continue to be a problem until warfare is completely eradicated. As this became a worldwide problem in the 20th century, the literature on the topic is extensive. While this thesis will focus on UXB in a Florida case study, it is important to remember that the threat of UXB exist in war zones around the world and on hundreds of other training ranges throughout the United States. These areas are dangerous as UXO are still present (Michael 2004). Most U.S. bombing ranges are classified as Formally Used Defense Sites (FUDS) and most are recorded on both the national FUDS database and the Munitions Response Site (MRS) Inventory (Department of Defense 2005). The Department of Defense has investigated ways to remediate the land for safety and environmental purposes for decades, but this is an expensive and time consuming process (Department of Defense 2005). Making this a cheaper and quicker process has been a goal for the past decade, but as new methods of detection are created, the cost of detection continues to rise (Hooper and Hambric 1998).

The major methods of detection currently in use can be broken down into two methodologies that work in tandem: remote sensing and ground methods. While the focus of this thesis is on remote sensing methods, ground methods will also be discussed to provide context into the strengths and weaknesses of each.

3.1 Background

This next section will describe three different kinds of imagery that will be used in this research as well as how it has been used for UXB and UXO detection elsewhere. Understanding the history of the imagery and its benefits and shortcomings will allow for

a better understanding of why it was used on this project. The last portion of this section will discuss historical landscape reconstruction which is invaluable for UXB location and extraction.

3.1.1 Aerial Photographs

Aerial photography began in 1858 when Gaspar Tournachon placed camera equipment into a hot air balloon and took an image of Paris (St Joseph and Coombe 1977). This method of photography remained popular through the turn of the century, with militaries adapting the technology to perform reconnaissance on opposing armies (Kuhn 1910). After the technological advances in aviation which occurred in the early 1900s, airplanes quickly became the new means of taking aerial photographs. The process is fairly straightforward; a plane goes up with a camera pointed toward the surface, and images are taken at certain intervals to obtain maximum coverage.

The United States government used this technology throughout the Depression era to analyze agricultural production on the land, with the Agricultural Adjustment Administration (AAA) being responsible for flying imagery for most of the country (Monmonier 2002a). The height of the aircraft, as well as the length of the camera lens determine the scale of the images taken. Most imagery flown by the AAA is 1:20,000 in scale (Macdonald 1992). At the time, these images were needed to allow massive amounts of land cover to be surveyed quickly and accurately. Most of these images have survived and have been scanned into online databases for easy download, and they are essential to historical landscape analysis.

Aerial photography became a military asset again throughout the World Wars and the Cold War with better cameras and higher flying aircraft. Overtime, images became very clearer and smaller ground features could be seen and interpreted (Monmonier 2002b). One of the more famous uses of aerial photographs was during the Cuban Missile Crisis in 1962. Soviet missiles were found to be deployed in Cuba, which caused a geopolitical crisis between the two superpowers of the U.S. and the U.S.S.R. (George, Hall and Simons.1971). As time moved forward, aerial photography has evolved from aircraft borne cameras to digital images taken from satellites. Modern aerial photos with increasingly higher resolution will remain relevant research tools into the future (Macdonald 1992, Lillesand, Kiefer and Chipman 2015).

3.1.2 Satellite Imagery

Because the Cold War created the necessity to perform up-to-date reconnaissance over the Soviet Union and its client states, the United States launched the CORONA program in 1959, sending six different satellites into space between 1960 and 1972 (Powers 1997). These images were taken by a camera inside of the satellite and sent back to earth by ejecting a film cartridge, which was then caught by an aircraft as it entered the atmosphere. The resolution on these images was not very good at first, having pixels of 8 m. By the last missions in the late 1960s, resolution had improved to 2 m, almost as good as high altitude imagery flown by aircraft but with much greater coverage (Powers 1997). By 1972, the Landsat satellite program began and these new satellites were being sent into space to capture images for the Department of the Interior and NASA (Baumann 2009). These new satellites carried multispectral sensors that allowed the images to have

multiple bands which can be used for different spectral analyses. Because of this, the market for the public use of these images range widely from base mapping to diagnosing crop health via infrared images.

After laws controlling who could send cameras into space were lifted, commercial companies launched satellites to compete with the federal government's Landsat imagery (Baumann 2009). This led to the enormous amount of information that is readily available today for the users to download either from government or private entities. Weather plays a large role in how useful the images can be. If it is cloudy over a study area because the light energy is scattered and reflected by the clouds back to the sensor before it can reach the ground. Cost can be an issue as well, because the newest high resolution imagery is expensive but can ultimately be cheaper than contracted aircraft-derived photos. For large area coverage, satellite imagery often remains the best option (Lillesand, Kiefer, and Chipman. 2015). The last issue with satellite imagery is its nadir value. Nadir is the intersection between the center of the camera on the craft and the center of the image. If the image is not taken close to perpendicular to the ground, tall objects on the image can have odd angles and radial tilt. Because the satellite is so much farther from the earth than an aircraft, nadir becomes a significant problem if the image is to be rectified correctly (Paine and Kiser 2003). While satellite imagery has its application problems, it is very useful because it can cover large areas and is available over the entire world.

3.1.3 LiDAR

LiDAR (Light Detection and Ranging) is a method that began in the 1970s to model and map the surface of the Earth (Lillesand, Kiefer, and Chipman. 2015). This technology has been expensive and not widely available from government sources until the last decade, when more LiDAR-derived digital elevational data became more readily available (Bennett 2008). Modern LiDAR is usually flown from a low-flying aircraft with a GPS unit and a laser scanner aboard which will scan the surface and determine the distance from the aircraft to the surface by calculating the time the laser pulses take to be reflected back to the aircraft. The airborne GPS unit is monitored by an earth-based GPS which tracks the movement of the aircraft and determines where each point is in space (Paine and Kiser 2003). These datasets are typically range in size from whole counties or as small as individual study areas only a few hectares in size. As LiDAR data is increasingly becoming available in more locations, new innovative applications of the data are being created every year (Risbøl 2013). Because LiDAR data can easily be converted to digital elevation models (DEMs), these derived surfaces, in effect, can be used to provide 3-D context to other forms of imagery. Bare earth DEMs that depict only the terrain surface will increasingly be essential for UXB detection. The use of LiDAR-derived surface DEMs will be discussed in detail below.

3.1.4 Historical Landscape Reconstruction

Multiple imagery types can now be layered together in a geographic information system database to recreate the landscape. Historical landscape reconstruction is a

method that uses available imagery in an attempt to recreate the landscape of a certain location at a specific point in time. Geographer Craig Colten demonstrated the value of the process in assessing hazardous wastes in Illinois (Colten 1990). With the help of GIS and LiDAR, very interesting landscapes can be created to show objects from the past that may have been missed with standard visible imagery alone. In 2013, a study on locating Mayan ruins in Belize was completed using imagery and LiDAR (Chase, Chase and Weishampel 2013). This study used bare earth LiDAR data to map the surface of the ground which was then used to rebuild the buildings in the correct locations in ArcMap.

Another study published in 2013 created a DEM of Boston in 1775 using historical maps and modern LiDAR (Maio et al. 2013). This study used a handwritten map from the revolutionary period as well as an 1847 coastal survey to create a DEM of Boston before much of the land was filled in. This DEM can be used in context with battle maps from the war to show where troops were located and how the British Navy provided cover for the army on the land, something that was very hard to display as ships would have been located on modern streets (Maio et al. 2013). This study shows that overlaying historical imagery with DEMs can provide essential 3-D perspectives allowing for a more detailed interpretation.

In 2015, a group of German researchers used LiDAR to model prehistoric terrain surfaces (Höfler, Wessollek and Karrasch 2015). While this does not pertain specifically to UXO detection, the study demonstrates how pre and post-bombing landscapes can be compared.

3.2 Methods of Location

In this section, the two basic methods of detection will be discussed in detail using individual case studies from sites around the world.

3.2.1 Surface Truthing

If surface imagery cannot detect UXB signatures, other methods must be employed. Two of the most common methods are the use of magnetometry to find the metallic casings of UXO or the use of ground penetrating radar to locate anomalies under the surface of the ground.

3.2.1.1 Magnetometry

Most magnetometry methods use a multi-magnet system that is dragged along the surface of the ground to detect subsurface anomalies. This process is efficient for covering a large area efficiently as the detecting equipment can be swept quickly to produce digital displays of magnetic responses (Butler 2001). This method also has the benefit of being able to find most types of UXO consisting of bullets, missiles, warheads and aerial bombs at deep depths (15 m or more). Chen and Peters attempted to use this method in 1997 by using a magnetometer to determine the frequency of detecting different natural objects below the surface, and then attempting to find man-made anomalies. While this method is faster than searching for the UXO by hand, it is still time consuming as the scanner is giving the researcher a constant output and the targets are unknown (Chen and Peters 1997). In 1998, Nelson et al. completed a study to determine

how effective these magnetometry detection methods performed in areas of high soil perturbation like a FUD site. This methodology used a Multi-Sensor Towed Array Detection System (MTADS) to locate the UXO along with other metallic objects. Throughout the procedure, the MTADS was tested over control surfaces which contained different materials to determine what the signatures would be. They found that the signatures could be determined accurately in the field and the process resulted in lower false positives of other metal objects under the surface compared to previous methods (Nelson et al. 1998). Fridon Shubitidze and other researchers expanded upon this method in 2012 by using an upgraded time domain electromagnet sensor. The MTADS concept was expanded to determine the detection timing which improved the directional aspect of the target signature (Shubitidze et al. 2012). This method allowed the sensors to determine the location as well as size of the target UXO.

While both methods do locate UXO, they also detect almost all ferrous or magnetic material in the soil. While the researchers attempted to minimize noise (unwanted signatures) while still locating small ordnance, many false detections remained problematic. Three other studies attempted to model signatures differently to help suppress noise. Sanchez and his team used the same basic method as Nelson, but instead of using a single dipole sensor, they used a quad and octopole sensor which would allow the team to model objects in 3D (Sanchez 2008). This method successfully modeled the object and its trajectory and angle under the surface, and also increased the accuracy of the dragged magnetometry method of detection. This is very important because this 3D model can be used to identify the object which would help in extraction.

In 2007, a different methodology was employed by boring a hole and placing a magnetometer into the ground which would allow for side profiling of items at depths of over 20 m (Zhang, Al-Nuaimy and Huang 2007). This assists in finding bombs dropped from a higher altitude, as some UXO can penetrate more than 20 m deep into the ground if they did not explode at or near the surface as intended. The Zhang method could be used in tandem with the methodologies used in this thesis to ground truth the surface signatures.

The last method discussed here is actually four different tests in one. A 2001 article compared a likelihood ratio technique, maximum likelihood algorithm, a neutral network, and a fuzzy clustering technique (Collins et al. 2001). These methods used in tandem were able to minimize much of the noise that is attributed to this method. Only issue with using all of these methods at once is the amount of calculation required and the fact that a small discrepancy in the numbers can compound errors in whole test.

3.2.1.2 Ground Penetrating Radar

Like the use of magnetometry, ground penetrating radar (GPR), is a method which involves moving a sensor on the surface. Instead of attempting to determine magnetic returns, the sensor emits radar waves which are reflected back to the surface sensor where the output can be recorded (Butler 2001). GPR has a much smaller window then the magnetometry methods because the sensing unit is smaller, but the radar tends to have a high accuracy, significantly reducing background noise. Radar cannot detect smaller objects as well as larger objects, so GPR is better suited for finding larger

ordnance at shallower depths. While this seems counterintuitive to a high attitude bomb being dropped and being buried deep, this method could be useful in an area where the surface soil density was resistant to bomb penetration. In 1998, the U.S. Army attempted to use this method to locate UXO by taking the radar sensor and attaching it to a moving boom and aiming the radar beam from a height of 50 m. (DeLuca et al. 1998). This method had two positives: it was accurate up to 5 meters under the surface with a lower amount of noise and, because the unit is remote controlled, it is safer as it does not put the operator at risk of an accidental explosion.

3.2.2 Remote Sensing Applications

Remote sensing methods should be the way of the future as ground methods are not only dangerous but also expensive. These techniques can narrow down a search area lowering the risk and raising efficiency running tests on a computer. Four main methods will be discussed: the use of imagery, use of LiDAR, mathematical methods and Object Based Image Analysis (OBIA).

3.2.2.1 Using Imagery

Remote sensing methods use digital imagery just as analog aerial photography has been used to located bombed areas since WWII (St. Joseph and Coombe 1977). While hard-copy methods have become outdated, the analysis of digitalized imagery has become the core of almost every current technique used, including the one used in this thesis. Howard (2001) applied airborne thermal infrared imaging for the detection of unexploded ordnance. This study used multiple infrared bands of modern imagery to

locate land mines near the surface of the earth. By flying the images shortly after a rain event, the ground around the mines would remain wet and cool for a few hours, and the soil in close proximity to the surface over the mines would warm more quickly than the surrounding area, showing a hot spot on infrared imaging (Howard 2001). In a much simpler process, Foley (2008) demonstrated how WWII range markings can still be visible on digital orthophotos in desert environments, thus allowing UXO search methods to be employed there more efficiently.

3.2.2.2 LiDAR Applications

As LiDAR is a newer detection method, its usage in UXO detection has only become feasible within the last fifteen years as the ability to collect higher resolution data enables researchers to identify bomb craters as well as the smaller pinholes made by UXB penetrating into the ground. LiDAR has been used to locate UXO in FUD sites in New Mexico, and a specific technique has even been patented by Johnson and Minor in 2012 for their Data Fusion Framework for Wide-Area Assessment of Buried UXO methodology (Padilla 2007, Johnson and Minor 2012). The Department of Defense's Strategic Environmental Research and Development Program (SERDP) and the Environmental Security and Technology Certification Program (ESTCP) performed a ground magnetometer scan to locate the bombs and narrow down the study area using LiDAR-derived hill shade surfaces (Bennett 2008, Padilla 2007). This is very important to my own research as this is the basic structure of my thesis methodology. As my own research will focus on publicly available LiDAR and less expensive custom-flown digital

imagery, my methodology will be cheaper and possibly more accurate when high resolution imagery is available.

The Department of Defense has also focused on LiDAR applications with success. In 2008, Jack Foley from Sky Research, Inc. demonstrated that LiDAR could be used to locate bomb craters greater than 1 m in size quickly and accurately (Foley 2008). The ESTCP also released its own report examining three different locations in New Mexico, California, and Colorado (Bennett 2008). The ESTCP conceived a methodology to locate these craters before using a magnetometry-based system to determine exact target locations on the ground. This method worked very well in most locations and the LiDAR images contained evidence of exploded or unexploded ordnance (Bennett 2008). Both of these findings showed that the government was prepared to use this new technology to attempt to locate these signatures and pave the path for future UXO and UXB locational studies.

3.2.2.3 Mathematical Methods

Another remote detection method involves the usage of single or multiple complex mathematical equations. These mathematic equations can be used to automate the detection method based on inputs solely from the imagery used. This directly correlates to my own research as the OBIA software uses algorithms and machine based learning for detection. While I won't be writing my own code and will depend on commercial software, this will shed light on how this technology has developed as well as how it can be applied.

Because of the complexity of the imagery required, much of this research is recent, paralleling improvements in computing. The first method was completed in 2004 by a team of Brazilians and a Briton who determined that a Digital Elevation Model (DEM) could be used to delineate craters from the surrounding landscape (Portugal, de Souza Filho and Bland 2004). Using the data gathered by the Shuttle Radar Topographic Mission, the DEM was created and then many algorithms were developed to determine the roundness of signatures on the ground. These algorithms, based off the Hough Transformation, were able to detect a 460 m wide asteroid crater in Chile, which was remarkable as the two images used had resolutions of 90 m and 15 m (Portugal, de Souza Filho and Bland 2004). This established the precedent that these algorithms could be used to find large terrestrial craters, but not on the scale needed to locate bomb craters, an application that would have to wait until higher resolution imagery became available.

Before this happened, researchers in Italy used historic air photos to map the risk of UXO in Trentino, a province in northern Italy (Merler, Furlanello and Jurman 2005). This method used the adaboost algorithm to quickly analyze the aerial photos and identify clusters of exploded ordnance craters which could then be mapped using the current borders of the province. This is an important step in the process as this shows that a semi-automated method can simplify the process of locating these UXB on historical imagery. In the United States, similar aerial photos of training ranges can be obtained from government archives, allowing for a lower overhead cost to ground truth areas that are not already mapped.

In 2012, a DEM for Mars had become available, meaning that a test of this type could be attempted on an extraterrestrial object (Stepinski, Ding and Vilalta 2012). The DEM had a high resolution of 12.5 m and used the same adaboost method used by Merler, Furlanello and Jurman (2005), but this technique used a more complex set of training data which raised the accuracy of the test significantly and was able to detect craters on Mars smaller than the crater in Chile (Stepinski, Ding and Vilalta 2012).

3.2.2.4 Object Based Image Analysis (OBIA)

OBIA is a relatively new method in remote sensing technology that allows users to no longer rely on classification methods which continuously take inputs from the user to find pixels which match the user inputs. OBIA takes an area of interest layer (AOI), much like the past classification methods, but OBIA treats these AOI layers as objects, and these objects are then tested for reflectance, context and texture (Yuan 2008). This raises the accuracy of the method and automates the location of these objects (Opitz and Blundell 2008). In the short time OBIA software has been on the market, its potential in UXB extraction has been noted. As the former Yugoslavia fragmented during a civil war in the 1990s, countless mine fields were planted Bosnia, Croatia, and Kosovo. These areas have become the study area for researchers who are looking for signatures that would serve as an indicator of mined areas. One such method uses a line detection process to find linear features of disturbed ground in aerial photographs (Vanhuysse et al. 2014; Lacroix and Vanhuysse 2014). The researchers applied Trimble's eCognition OBIA software to extract the lines from the surrounding earth. Lacroix's team then modified the process to detect circles in 2015. This new method searched for bomb

craters and delineated them from the background by analyzing the angle gradient of the crater itself as well as the shape of the circle (Lacroix and Vanhuysse 2015). This thesis will employ a newer OBIA software to make the process more efficient as the Lacroix method takes a lot of time to process, as well as back checking to make sure that the information is correct and the algorithm is not finding shadows or water (Lacroix and Vanhuysse 2015). While the literature does use additional custom algorithms in tandem with the OBIA, this thesis will be assess two newer types of OBIA, Imagine Objective and Overwatch Feature Analyst.

Imagine Objective is a software by Hexagon Geospatial that employs a segmentation method for detection. This means that the input AOI layer is used to help classify the image into a series of polygons which are statistically linked to the object being located (Marpu et al. 2010). This entire process uses machine learned algorithms which take the AOI layer and adjusts the statistics for a best fit to delineate the object. While very complex, this is still less complex than other OBIA on the market as Objective is designed to be more user friendly, which translates into lower accuracy as compared to other OBIA (Chepkochei 2011). Objective was used to delineate trees in Kenya quite successfully, but the author also commented on the unforgiving AOI layers which, if not carefully selected, will completely throw out results as it interprets the pixels to be in the background of the image (Chepkochei 2011). This also creates an issue as the software cannot handle black and white imagery, which is the basis of this thesis research.

Developed by Textron's Overwatch System, Feature Analyst is a more complex and expensive software extension that runs in ESRI's ArcMap. It differs from Objective because it can handle more imagery and multiple layers at one time to create output results (Yuan 2008). Objective can also accept more than one layer of imagery at a single time, but the software suffers a fatal crash that appears to be unavoidable using the layers of FMBGR data. This suggests that Objective is not as refined as Feature Analyst at processing multiple layers of differing types of imagery such as black and white historical photos, DEMs and modern orthophoto imagery. Multiple layer input becomes very useful to give more depth to the extraction process (Blundell et al. 2008). Multiple layers were used in an analysis to locate sinkholes in Kentucky in 2015 (White et al. 2015). This study used multiple iterations of Feature Analyst and multiple layers of LiDAR data to locate these sinkholes with varying results. This work demonstrates the versatility of Feature Analyst as well as the numerous trial and error iterations of input settings that are required to complete an analysis. Feature Analyst also uses edge detection in lieu of segmentation which means that the surrounding pixels are used as context to extract the pixels which could be the object (Yuan 2008). This is done by using a Foveal Representation which focuses the algorithms on the main pixel but will also use the surrounding pixels and information in different fashions (Figure. 3.2.2.4). While this representation can be adjusted and changed, the idea of using a main pixel and context pixels around the main pixel is used throughout.

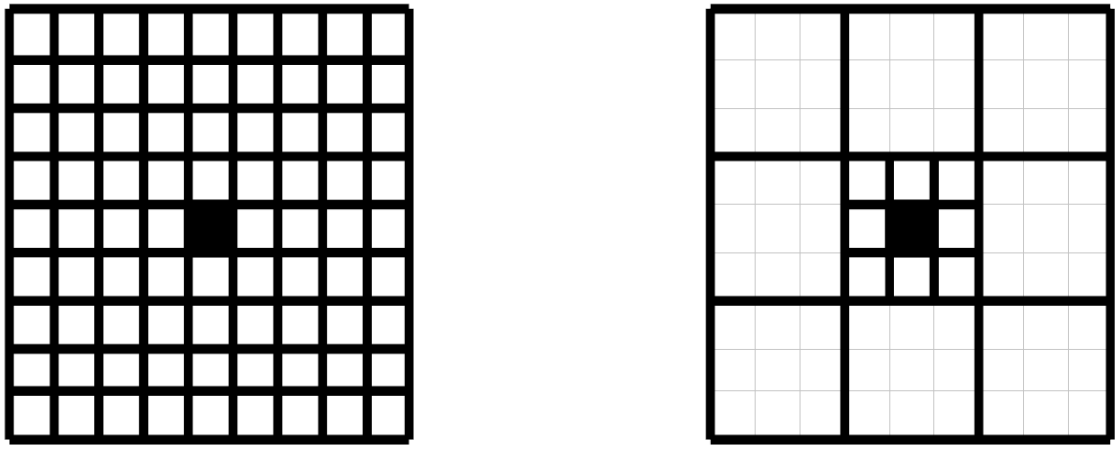

Figure. 3.2.2.4. Foveal Representations. This shows the standard representation on the left and a classic Foveal Representation on the right. The standard representation only views the main dark pixel whereas the Foveal views the dark pixel as well as the other pixels with lowering weights as the surrounding pixels only provide context for the main pixel (Opitz and Blundell 2008).

While this discussion of methods and imagery is not all inclusive, these are the most successful and recent methods of detection and they will be used for a basis for my own methods and research. Although the remote sensing methods are useful and accurate, some of the imagery and software is expensive and hard to find, and the analysis is complex and time consuming to understand. The following methodology is intended to overcome these problems as well as apply a new method that can be used in different locales as long as sufficiently high resolution past and present imagery is available.

Chapter 4: Methodologies

This chapter will describe the methodologies used to locate UXB at the Fort Myers Bombing and Gunnery Range (FMBGR). The first section explains the creation of the control and how it will be used to assess the other methodologies. The last sections will discuss the use of different imagery in Imagine Objective and Overwatch Feature Analyst. These assessments will be discussed in the next chapters. These methodologies use the imagery layers described in Chapter 1 and they will be illustrated throughout the discussion of each test.

4.1 Control and Assessment test

4.1.1 Control

In scientific analysis, a logical control is created as a standard of comparison. The control for this study was created using the original 1946 black and white aerial photography covering the central demolition range at the FMBGR. Four overlapping photos were georeferenced to the USGS world imagery layers in ArcGIS and mosaicked into a single image. Flown less than a year after the range closed, the images clearly show a large circle containing and surrounded by numerous craters that was the primary bombing target for the pilots. Around the large exploded craters are smaller white pinholes which could be possible UXB. Because the pinholes are so small, the study area was narrowed to the larger bombing circle. A point layer was created and the location of the UXB targets were found and displayed in the ArcMap viewer.

4.1.2 Assessment

All of the outputs from the individual assessments will be tested in the same manner (Figure 4.1.2.1). The output from the individual OBIA will be a polygon shapefile that can be taken into ArcMap for the assessment.

The polygons will be then turned into points by locating the X and Y of the center of the polygons. This will done by adding two new fields into the data table of the polygon and filling both with the X and Y coordinates using the calculate geometry feature. The data table will then be exported and displayed as an X and Y shapefile which produces the centroid of the polygon. These centroids will then be tested for density using a cell size of 10 m and a neighborhood search of 100 m. These parameters were selected because the standard exploded crater is approximately 9 m to 10 m in diameter and the standard dud rate was 1 out of 10 (U.S. Army Corps of Engineers 2016). Given that the bomb craters would cover a large area, the neighborhood search radius needed to be high as well. The 100 m radius found enough points to create a continuous surface without diluting the outcome. (Figures 4.1.2.2 and 4.1.2.3)

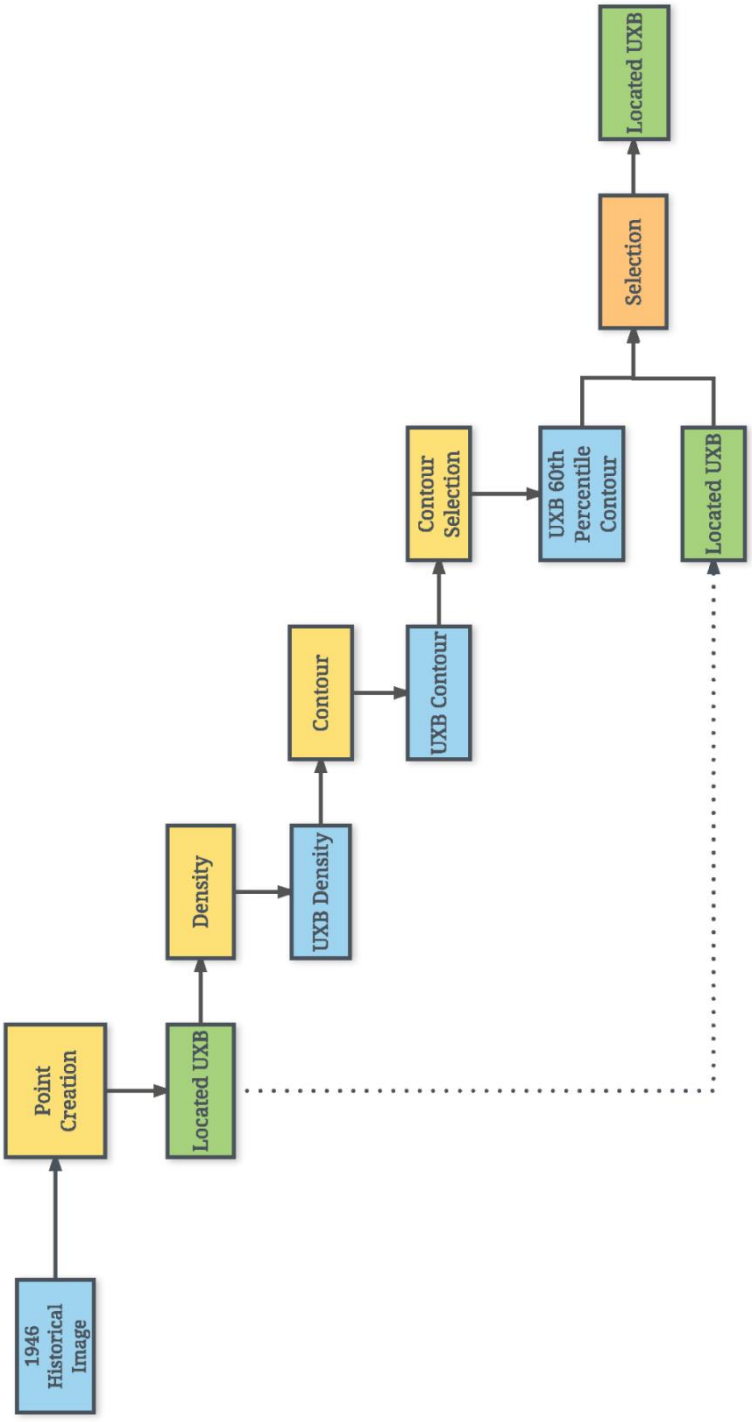

Figure 4.1.2.1 Control workflow.

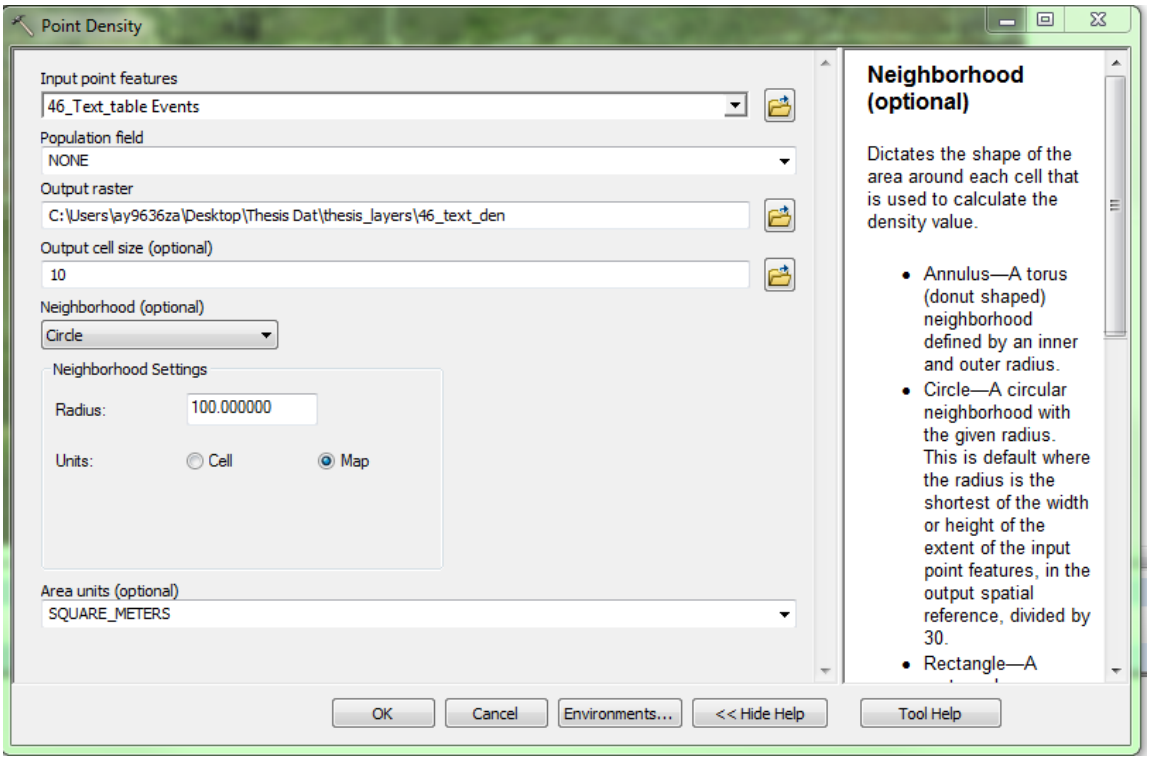

Figure 4.1.2.2. Point Density inputs.

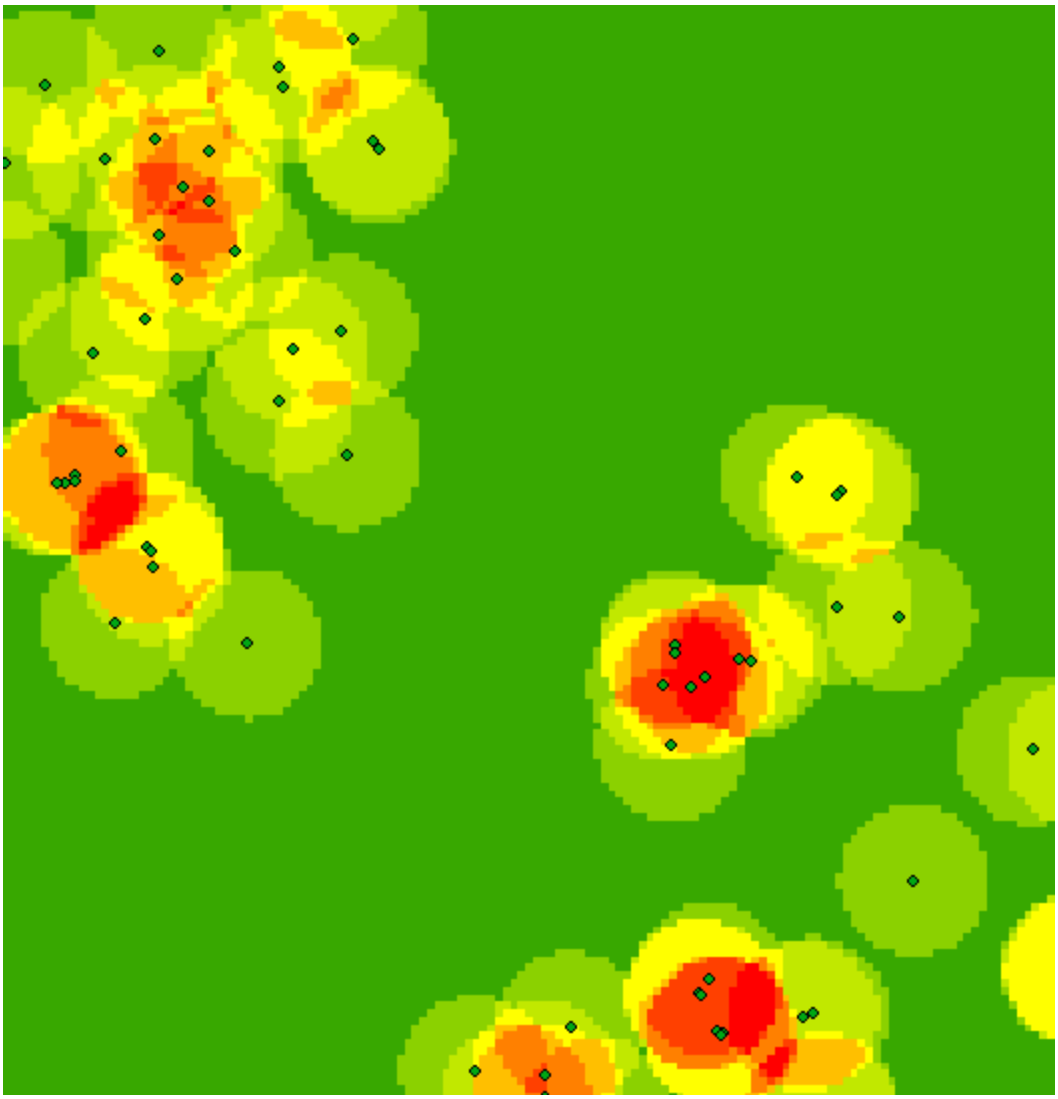

Figure. 4.1.2.3. Point Density output. The input settings for the statistical test and the output raster used to assess accuracy.

Once the output is created, the symbology is changed to a quantile, then set to ten classes giving a percentile. The percentile will be further broken down into contour lines by taking the maximum value of the density and divide that value by ten, producing a set of percentile contour lines. The 60th percentile contour line will be used for the

assessment. This 60th percentile contour line was selected because it covers over half of the located points and will be a solid representation of the tested data (Figure. 4.1.1.4).

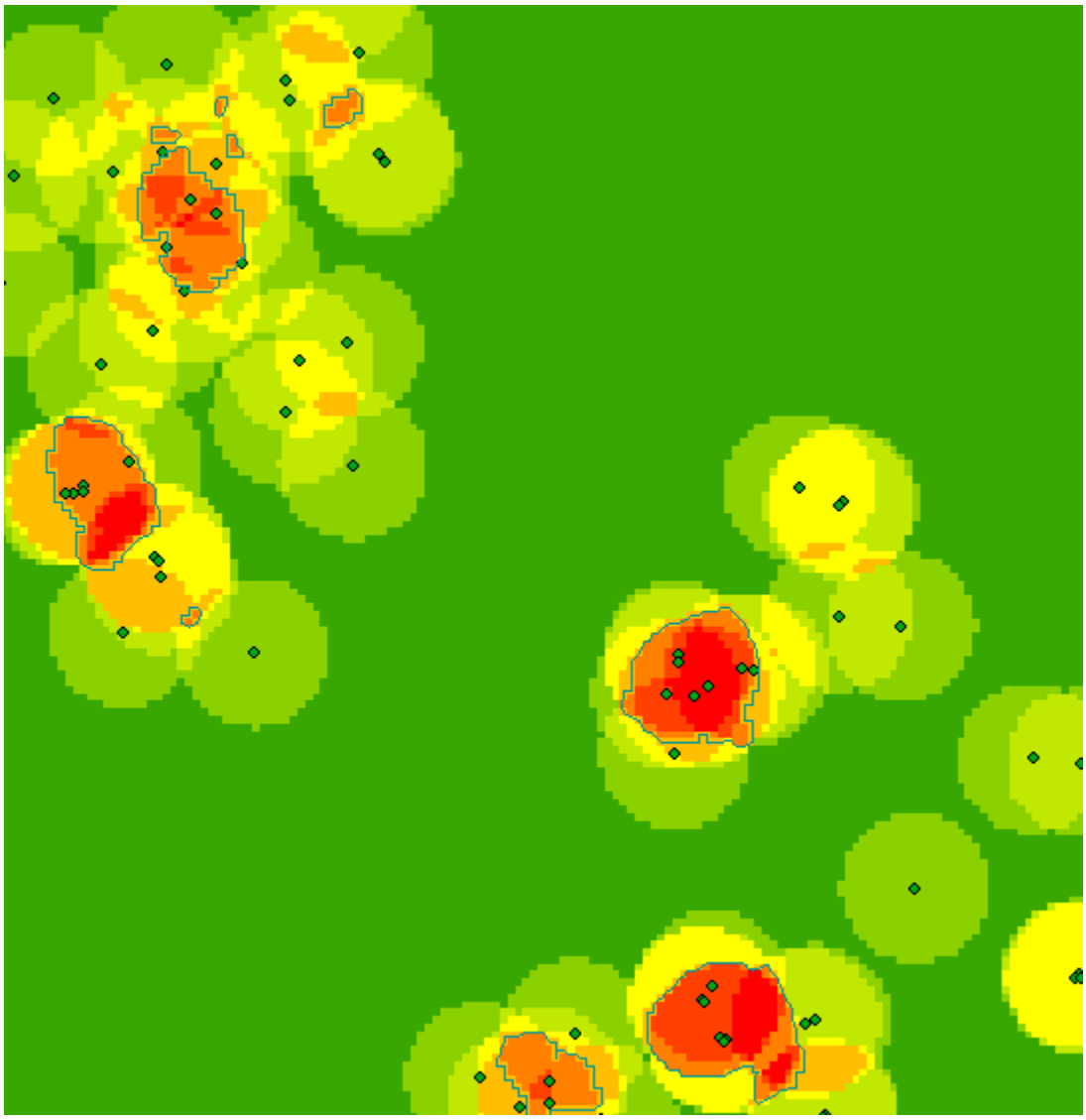

Figure. 4.1.2.4. Density output with 60th percentile line.

This 60th percentile line will then be used to assess the original visually located possible UXB points located by hand on the 1946 imagery. This assessment will be referred to as the "meter stick test" throughout the rest of this thesis.

4.2 Imagine Objective

This method uses the Imagine Objective object-based image analysis software. With the four sets of imagery, only one assessment was successful. The Imagine Objective software had problems locating the small UXB holes on the 1946 air photo and the newer imagery from 2008 and 2014. The 1946 imagery is black and white, and the software could not identify the small white holes. The software instead selected out pockets of white in areas like road ditches and larger areas of reflection. Even after refining the search method and reducing the contrast of the image, the UXB holes could not be located correctly. The 2008 and 2014 imagery contained three bands of color, which were adjusted in an attempt to create a larger contrast between the smaller UXB holes and the background. However, the problem with this imagery is the ground had changed so much since 1946 that the holes had been recovered by the landscape. Even when the actual craters were selected, the software was not sensitive enough to find a large enough quantity to test, resulting in the location of only three to seven craters. Finally, the LiDAR-derived DEM did have high enough contrast so that the craters stood out and could be properly selected. Because the 1 m LiDAR-derived DEM does not have a fine enough resolution to locate only the small UXB holes, the test located the likelihood of a UXB and not a UXB itself.

4.2.1 Imagine Objective and LiDAR

The LiDAR-derived DEM was opened in Imagine Objective and tested extensively. Only one series of variables found enough craters to complete a test. The

feature extraction testing is very straightforward as each step of the extraction is in the order in the table of contents to the left of the viewer in the Objective Workstation (Figure. 4.2.1.1).

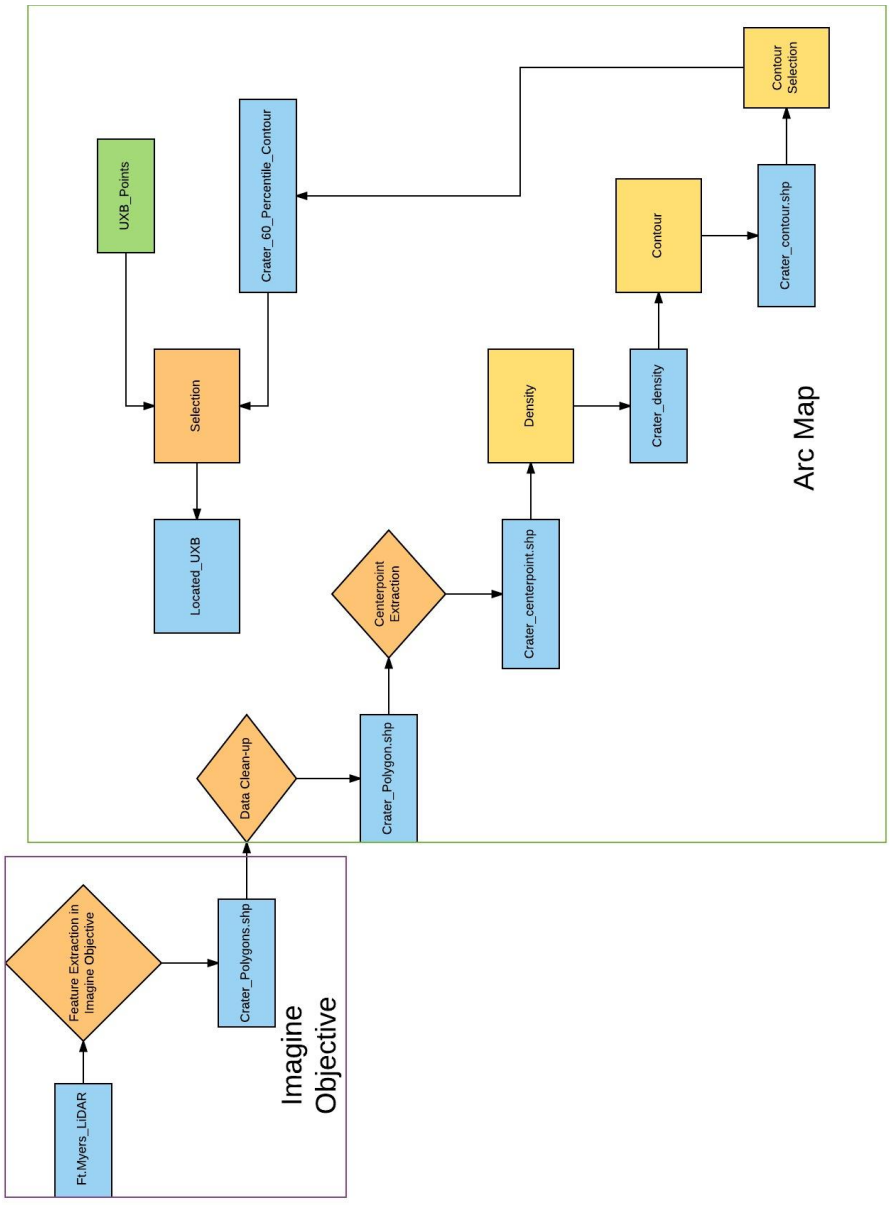

Figure. 4.2.1.1 Imagine Objective Workflow.

The first step is the Raster Pixel Processor which tells the program how to view the image throughout the test. The Pixel Classifier used was a Multi-Bayesian Network which creates a network where the probability of each pixel is assessed. The Multi-Bayesian allows the output pixel value to be adjusted by the surrounding values and creates a continuous surface (ERDAS Imagine Help: Multi-Bayesian Network 2016). The other option, a single Bayesian Network, could not locate the craters as well because the algorithms are slightly different and separate the located areas in the viewer. Next, the 2006 DEM is designated as the input raster variable. The last step is a two-step process, first, describing how the AOI layers will be used and then creating the AOI layers. Describing how the layers will be used employs a pixel cue designation. The pixel cue designation selected was the Single Feature Probability (SFP) because it worked the best to locate the craters. It does this because it takes a given AOI layer and assigns the pixel with a value between 1 and 0, 1 being the best (ERDAS Imagine Help: SFP 2016). From this point, the AOI layers themselves can be created. This is not as straight forward as it would seem because there are four designations for each AOI layer: pixel, object, both or background. For this test, the "both" option was used on a few large craters clearly visible in the middle of the bombing area. The background AOI layer was created by selecting random areas that were at the same elevation which had no craters. This would give a contrast for the software to delineate the craters faster.

The next step involves the Raster to Object creators which takes the output from the last step and segments it into what the software believes to be the object. The segmentation method used was threshold and dump. This seemed to work the best as it

creates statistic thresholds, in which the probabilities of the target pixel being the object fall into and are clumped into each group. The method works well because of the small size of the craters and the window for the probability will be small. Threshold and dump will group the output and quickly determine if they are the object the user has selected. The statistic threshold selected was 90% because this would find the largest amount of craters while still giving the user a large amount of output.

The third step allows the user to create filters and control the output directly. There are a large amount of filters that can be used, but the one selected was the size filter as it will save time during data clean up. The size filter that was used was 55-250 pixels. This will vary from place to place because the average size of the craters was about 100 pixels, which would allow for some smaller and larger craters to be located.

The last step in the process is converting the raster produced in the previous step into a vector. This step only has two variables, polygon trace and line trace. Because the output would be groupings of pixels, the polygon trace was used. After this step, the shapefile can be brought into ArcMap to be cleaned for the statistical testing discussed in section 4.1. This is the only test which moves an output from one software to the next. All of the following tests will take place in ArcMap.

4.3 Overwatch Feature Analyst

Feature analyst is an extension for ArcMap from Overwatch. This OBIA uses edge detection instead of segmentation to locate the object the user designates (Opitz and Blundell 2008). This also allows the software to accept multiple layers as an input to

deepen the analysis. This section will be divided into single-image analysis and multiple image analysis, starting with the former.

4.3.1 Feature Analyst, Single-Image Input

All of the images follow the same steps because the input is the only thing that would change (Figure. 4.3.1.1). These steps could be varied, but the same analysis was completed on every image due to the effectiveness of this sequence. Feature Analyst also works in a step format starting with the AOI layer creation. All of the images were assigned an AOI layer which located craters as well as the pinholes that could be seen in the viewer. A new AOI layer was created for each image even though a single AOI layer could be used throughout.

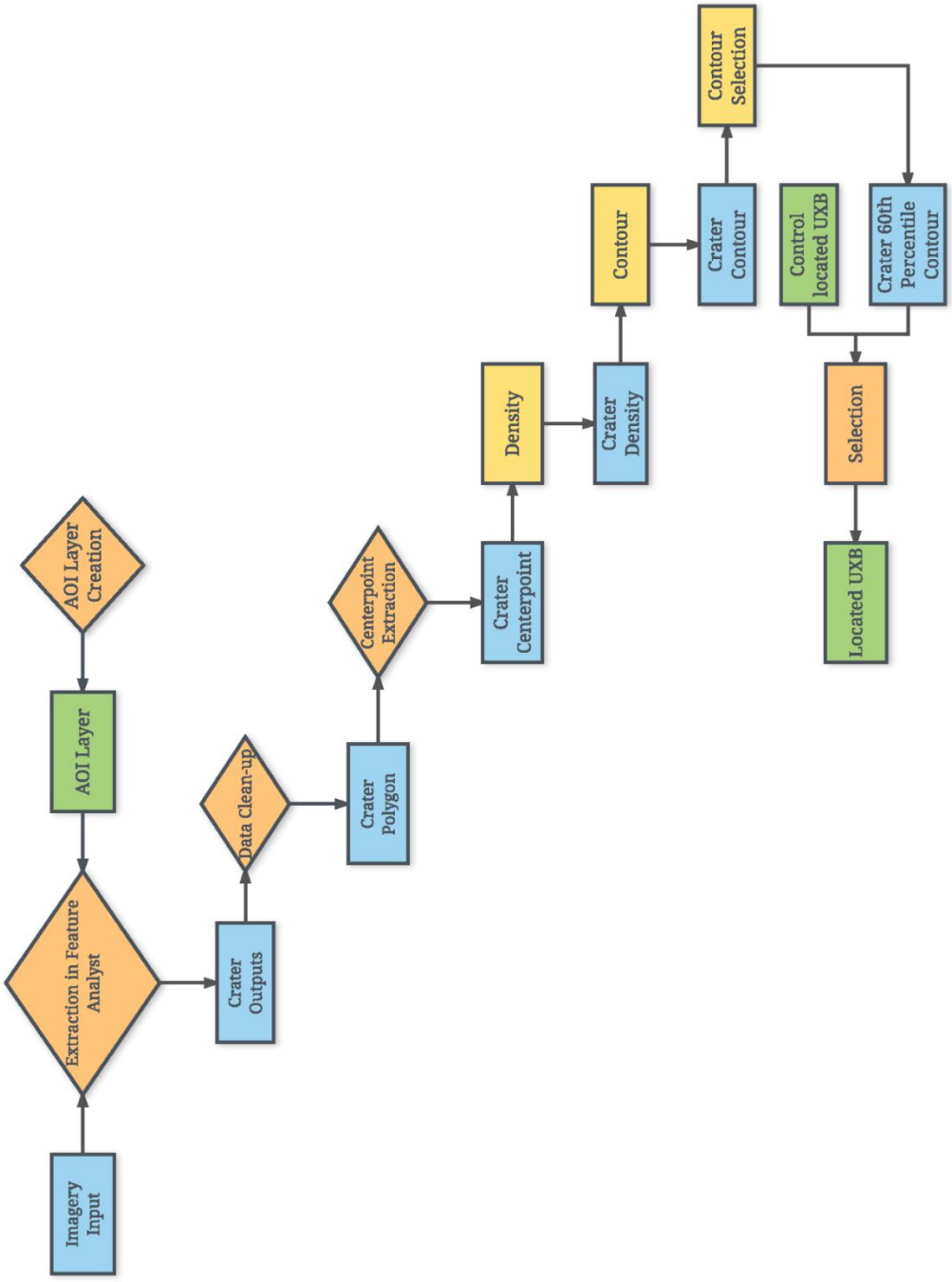

Figure. 4.3.1.1 Feature Analyst single image workflow.

The next step is the supervised extraction which uses the AOI layer created in the last step as the input. The AOI layer is selected in the table of contents and the supervised

extraction button on the Feature Analyst tool bar is selected. This will open the Feature Analyst window which allows the user to control the extraction process (Figure. 4.3.1.2).

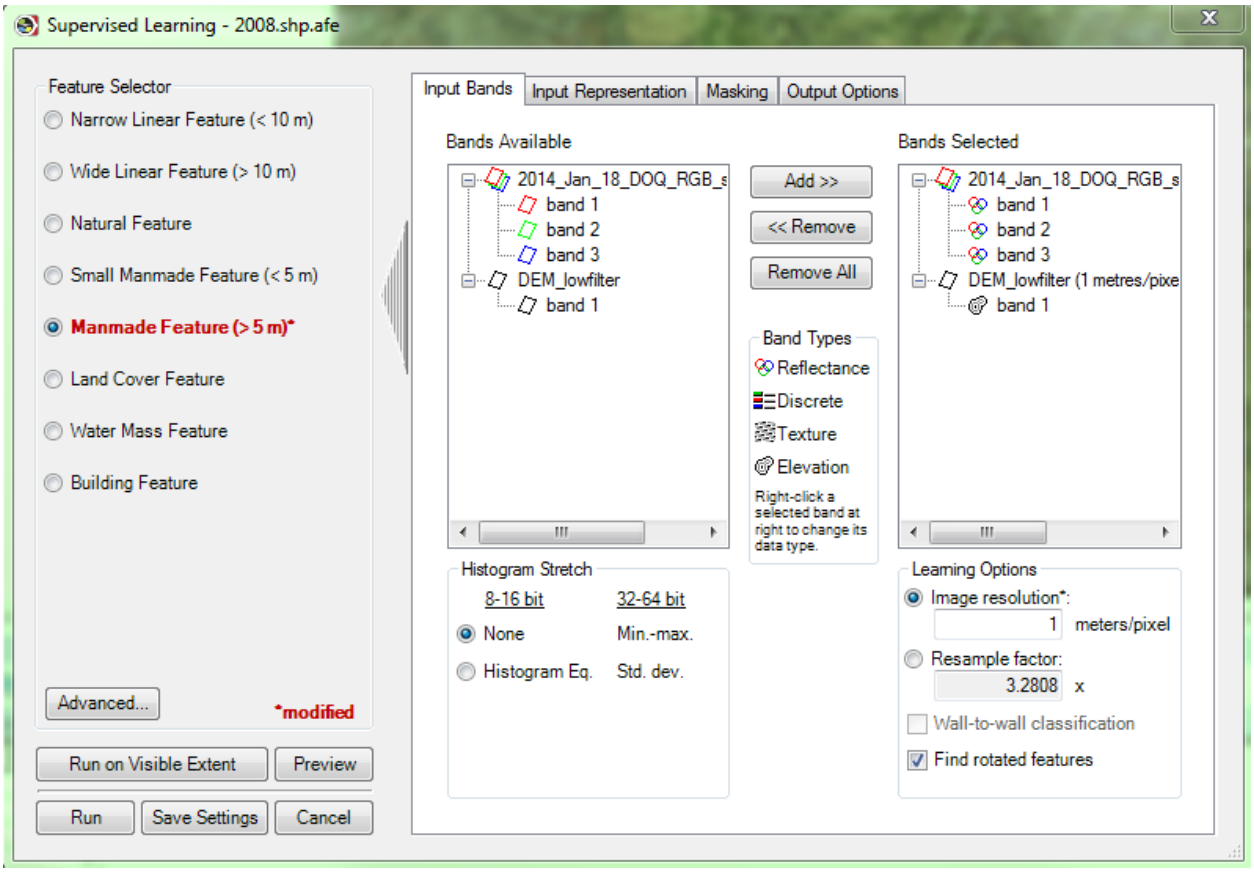

Figure. 4.3.1.2. Feature Analyst input window.

On the left side of the window, the default extraction settings are described. These methods used the natural feature setting because of the size and shape of the features being extracted. On the right of the window, four tabs represent the input bands, input representation, masking, and output options. For the single-image assessments, the user selects the image being tested in the bands available window and then add them to the bands selected window. The band type can then be assessed by right clicking on the icon under the image layer. The user also needs to confirm that the input will be viewed as

reflectance. In the next tab, the representation can be adjusted. Feature Analyst uses a Foveal Representation which can be adjusted in this step. The standard bulls-eye 3 representation that is the default for the natural feature selector will be used throughout all tests for the single-images (Figure. 4.3.1.3).

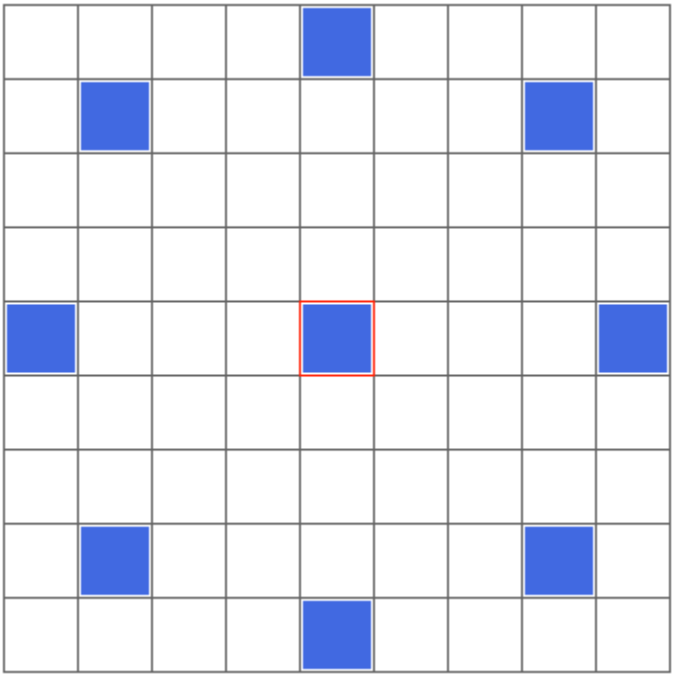

Figure. 4.3.1.3. Bulls-eye 3 representation.

The only variable that will be changed from image to image will be the pattern width of the bulls-eye. These widths will be described in the following table (Table 4.1).

Imagery	Pattern Width (m)
1946 Historical	7
2014 Modern	35
2006 LiDAR	12
2008 Modern	35

Table 4.1. Widths of the bulls-eye patterns used for crater extraction.

The next tab, masking, designates a layer which can be used to mask out areas that the test should not use as inputs. Masking showed no significant changes in the output, so it was not included in the test. The last tab is the Output Options which has many different options that can be selected. The output format was selected as a vector to keep the final outputs in the same format. Under this selection, the post processing options can be selected which performs a quick clean up on the data before the user can access it. For these tests, none of these options was selected to get raw data from the images. At this point, the analysis can be run and the output will be deposited into the viewer for data cleanup inside of Feature Analyst. This is done by selecting the Begin Removing Clutter Tab which creates a new layer in which the user can identify output as correct or incorrect. The layer is then is reprocessed and returned. This creates an automated cleanup process which speeds up the post processing manual clean up. The manual cleanup uses a size filter that was applied by adding a field to the table of the output shapefile, and then fills the field with the area of each polygon. Each test also uses different size tolerances for the size clean up and is shown in Table 4.2.

Image	Size Tolerance (m^2)
1946 Historical	1-45
2014 Modern	60-400
2006 LiDAR	20-200
2008 Modern	60-400

Table 4.2. Size tolerances of the size filters used to extract out craters.

From this point the data will be subjected to the same statistical test as the Objective outputs.

4.3.2 Feature Analyst, Multiple Image Input

Feature analyst has a unique trait of being able to process multiple images in a single run (Figure 4.3.2.1).

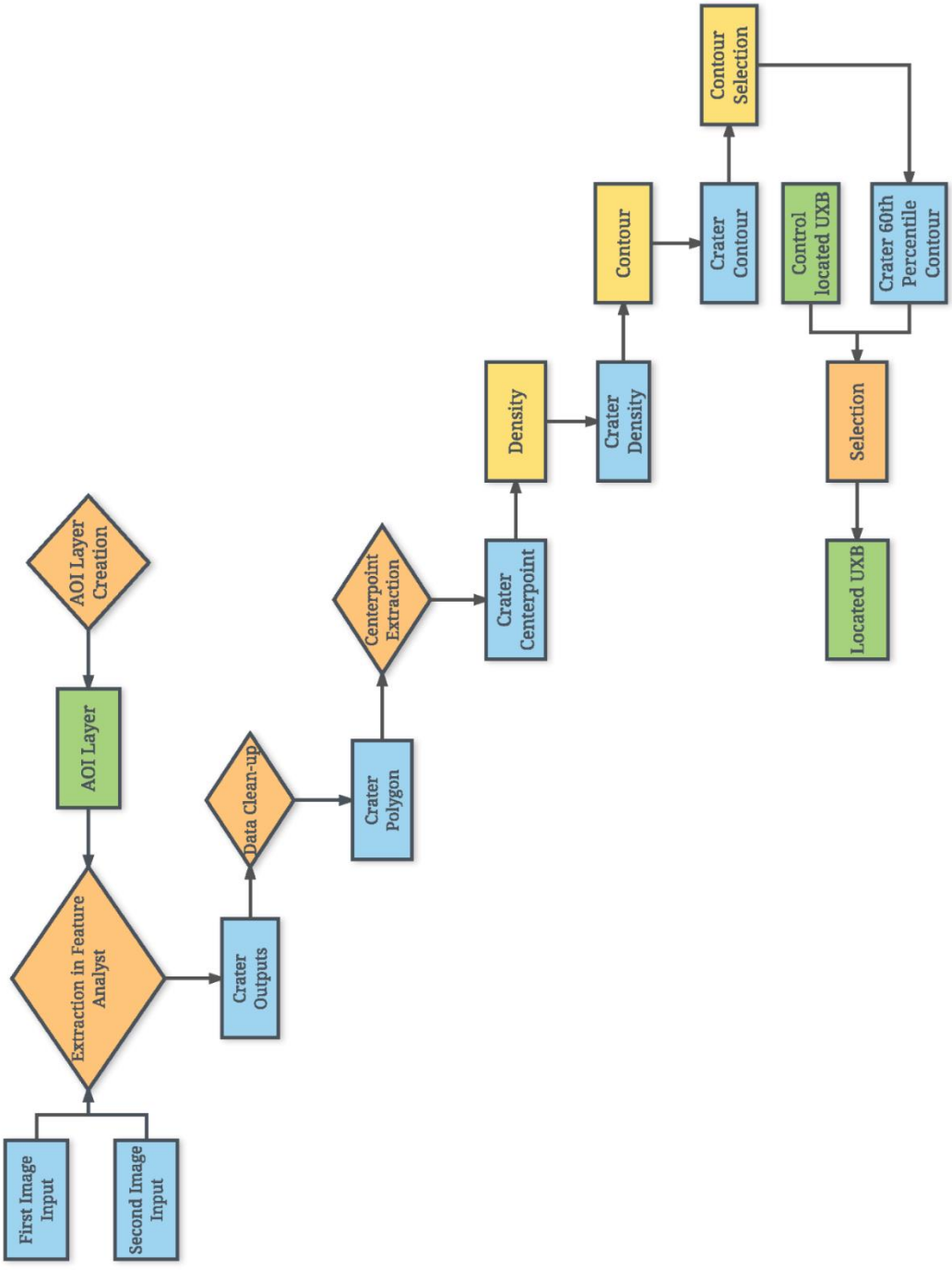

Figure 4.3.2.1. Multi-image Feature Analyst workflow.

This process is very similar to the single-image input with the only difference being that in the image input window, two or more images can be used to provide different digital pixel characteristics of the same target objects. The images can then be adjusted from reflectance to texture or elevation by clicking the icon below the image in the bands selected window. This change determines how the software views each set of images and affects the output. Each image will be viewed using the input image as reflectance and texture of itself, meaning that the same image will be used in two different manners at the same time. The images will also be tested using an image as reflectance and the 2006 LiDAR DEM as the elevation and texture layers. In total, eleven iterations of the test were completed with varying results, and they will be discussed in Chapter 6. As for the bulls-eye settings, these varied with every test, and were adjusted with each new set of imagery. These changes are listed in Table 4.3 and Figure 4.3.2.2.

Image Set	Foveal Representation	Pattern Width (m)
1946 Historical Reflectance / 1946 Historical Texture	Bulls-eye 3	7
2008 Modern Reflectance / 2008 Modern Texture	Bulls-eye 4	9
2014 Modern Reflectance / 2014 Modern Texture	Bulls-eye 4	9
2006 LiDAR Reflectance / 2006 LiDAR Texture	Bulls-eye 3	9
1946 Historical Reflectance / 2006 LiDAR Texture	Bulls-eye 3	7
2008 Modern Reflectance / 2006 LiDAR Texture	Bulls-eye 4	9
2014 Modern Reflectance / 2006 LiDAR Texture	Bulls-eye 4	9
1946 Historical Reflectance / 2006 LiDAR Elevation	Bulls-eye 3	9
2008 Modern Reflectance / 2006 LiDAR Elevation	Bulls-eye 4	9
2014 Modern Reflectance / 2006 LiDAR Elevation	Bulls-eye 4	9
2006 LiDAR Reflectance / 2006 LiDAR Elevation	Bulls-eye 3	7

Table 4.3. Representation and Pattern Widths for each test.

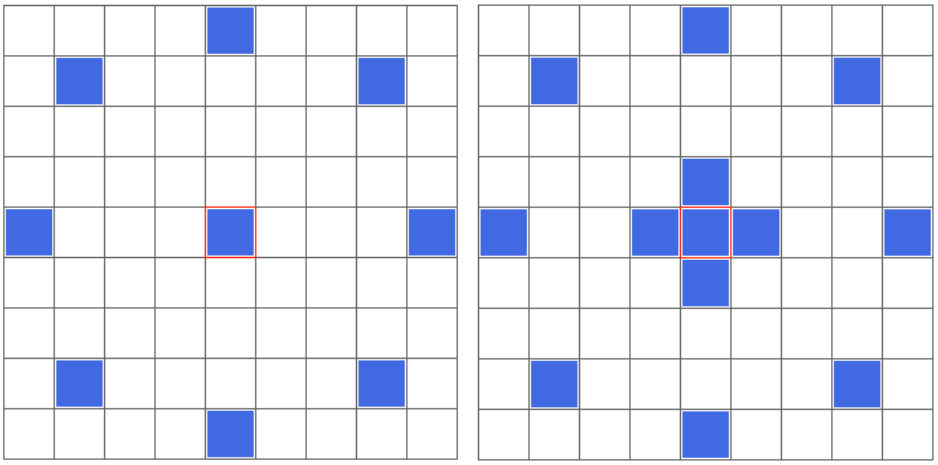

Figure 4.3.2.2. Bulls-eye 3 and Bulls-eye 4 representations. These two represenations allow for more or less of the surrounding pixels to be seen by the viewer.

During the post processing, the same size filters were used in respect to the reflectance. For example, in the case of the 2008 Modern Reflectance and 2006 LiDAR Elevation test, the size filter would be the same as that was used for the 2008 Modern imagery seen in Table 4.2. At the end of the post processing, the resulting shapefiles are run through the same statistical assessment as described in chapter section 4.1.

Chapter 5: Results

In this chapter, all statistical results of the tests described in Chapter 4 are presented. The imagery input and specific number and percent of control points located by each test are listed. In effect, these tables and figures present the sequential results of the tests using both software packages. These findings will be summarized and discussed in Chapter 6.

The tables and figures are organized by the software that was used to complete the analysis. They follow the same content and heading layout: Imagery, which describes what imagery or combination of images were used; Located Points, which designates how many points were found after the analysis; Located Control Points, which shows how many of the initial control points were located by the 60^{th} percentile line; and Percent of Control Found, which shows the percentage of the 230 initial control points that were found.

5.1 Control Results

Imagery	Located Points	Located Control Points	Percent of Control Found
1946 Historical	230	92	40

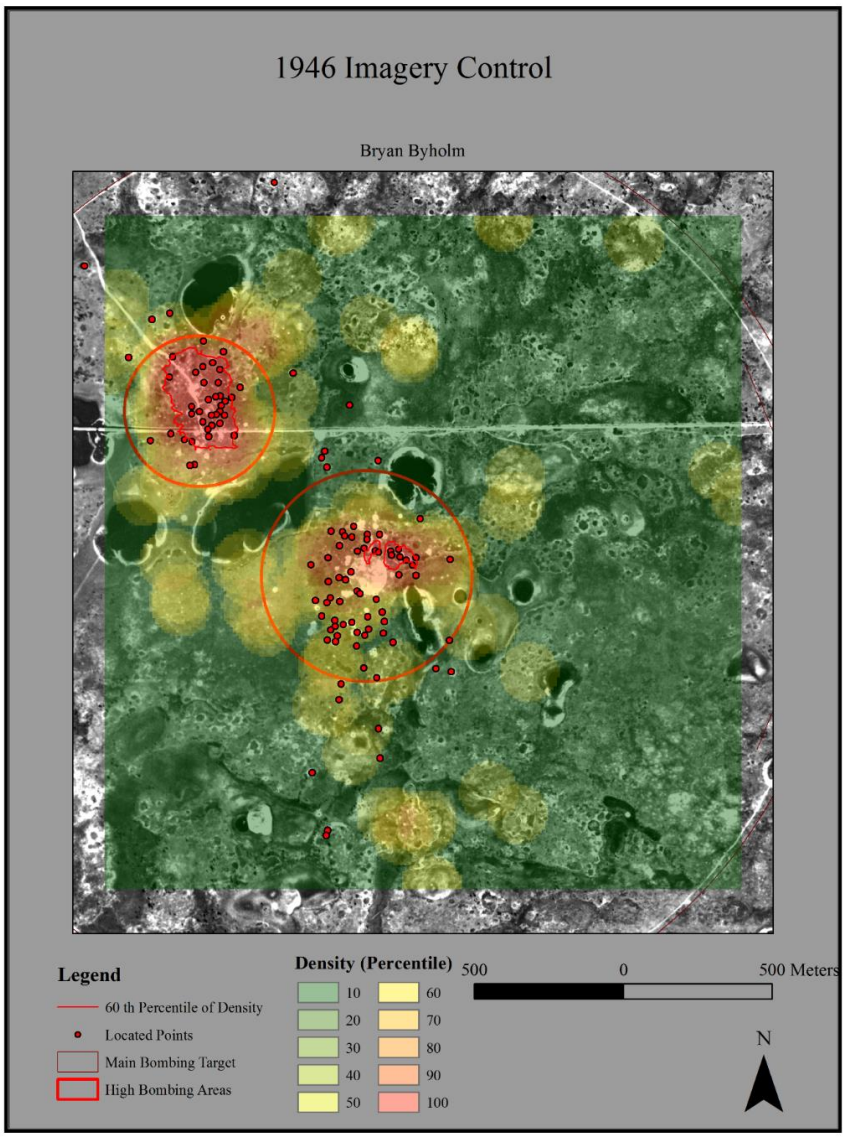

Figure 5.1.1 Control Output

5.2 Objective Results

Imagery	Located Points	Located Control Points	Percent of Control Found
2006 LiDAR Figure 5.2.1	121	67	29.1

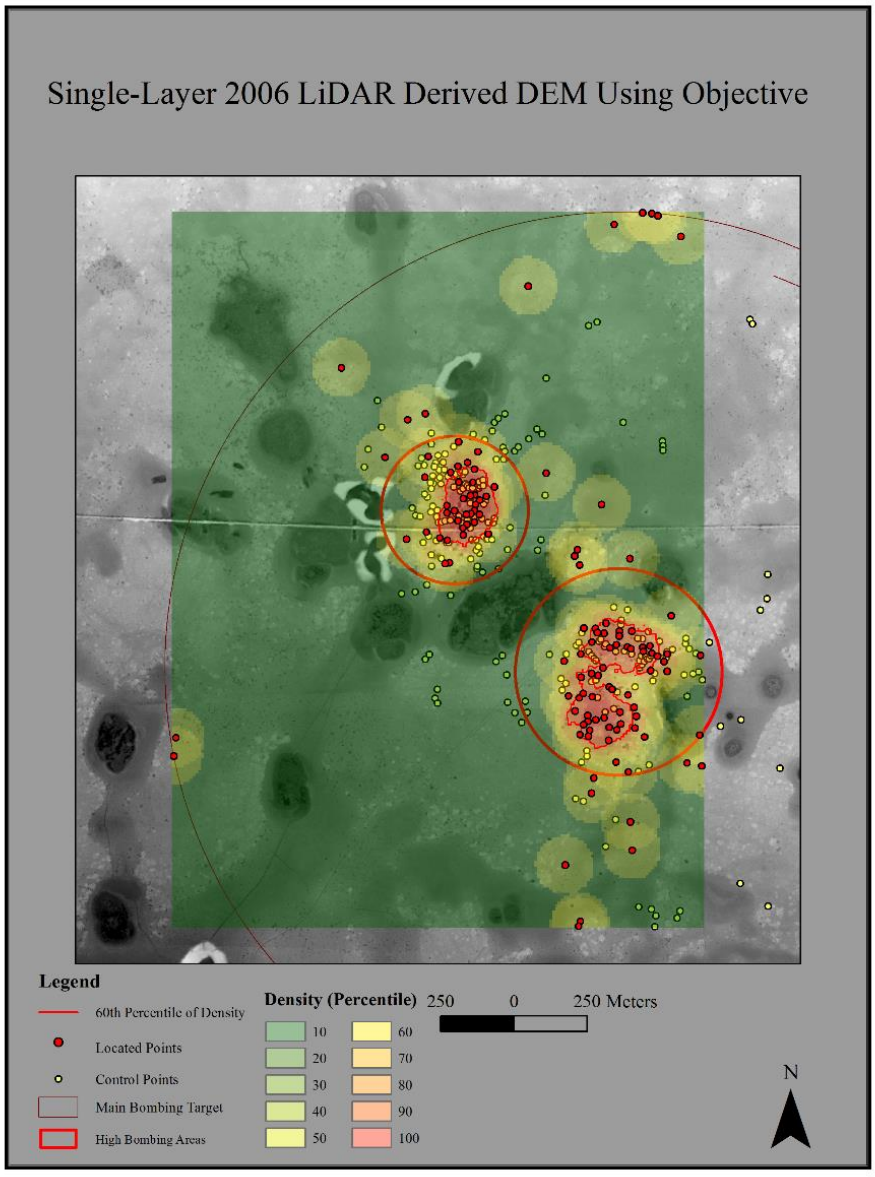

Figure 5.2.1 Imagine Objective output.

5.3 Feature Analyst Single-Image Results

Imagery	Located Points	Located Control Points	Percent of Control Found
1946 Historical Figure 5.3.1	205	85	37
2014 Modern Figure 5.3.2	61	34	14.8
2008 Modern Figure 5.3.3	79	55	23.9
2006 LiDAR Figure 5.3.4	164	65	28.3

Table 5.3 Feature Analyst Single Image Results

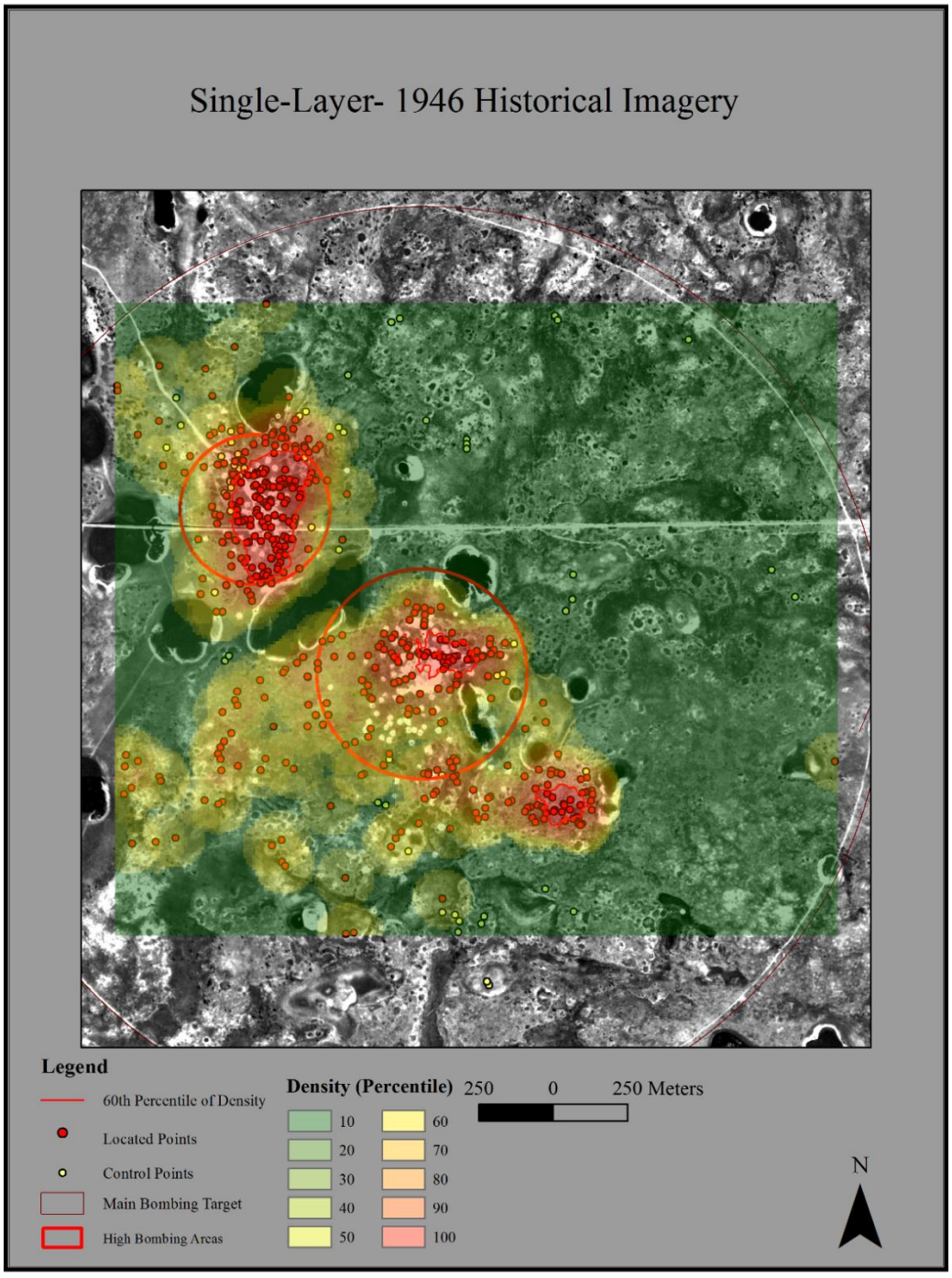

Figure 5.3.1 Single image Feature Analyst historical imagery output.

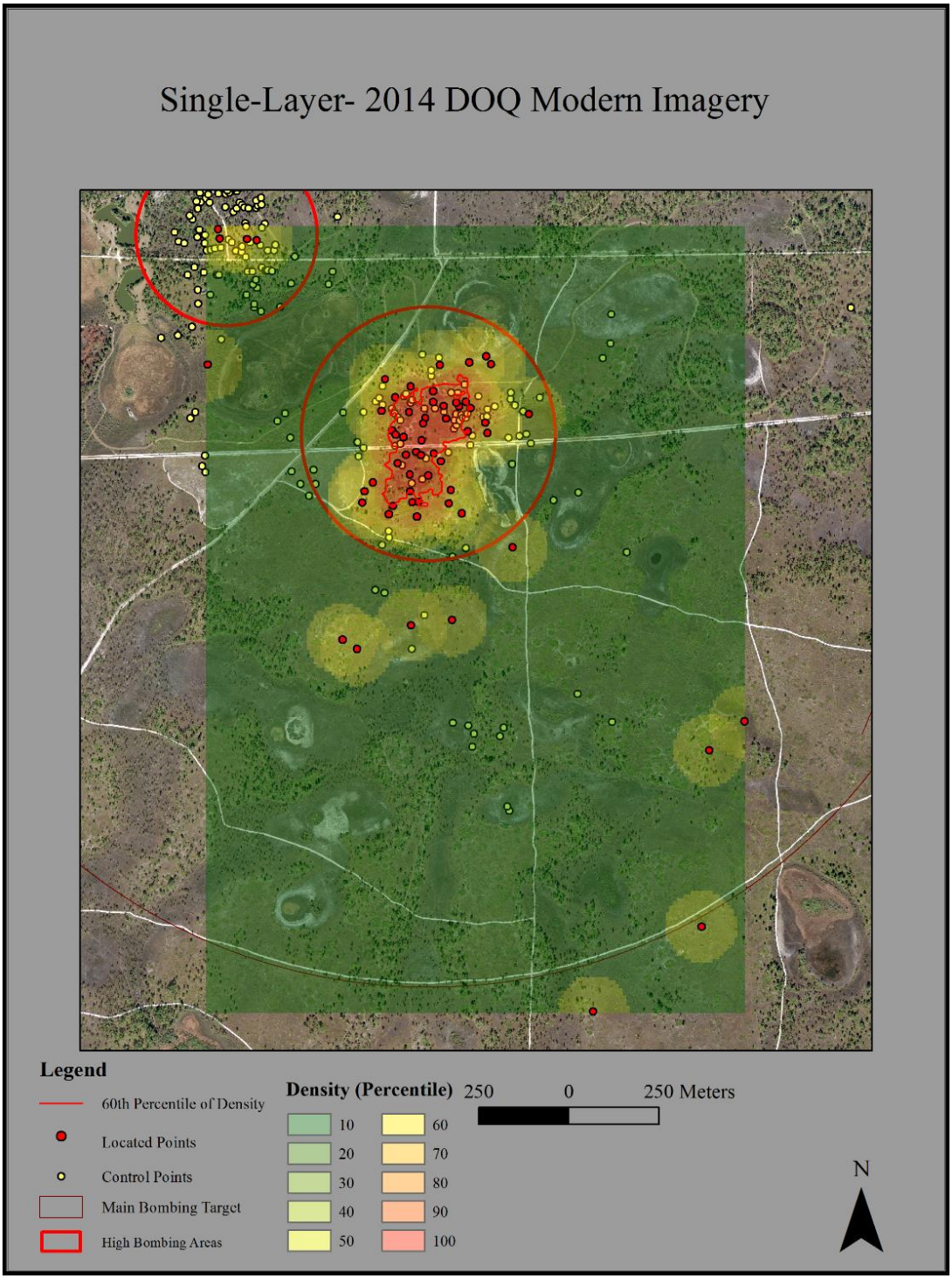

Figure 5.3.2 Single image Feature Analyst 2014 DOQ output.

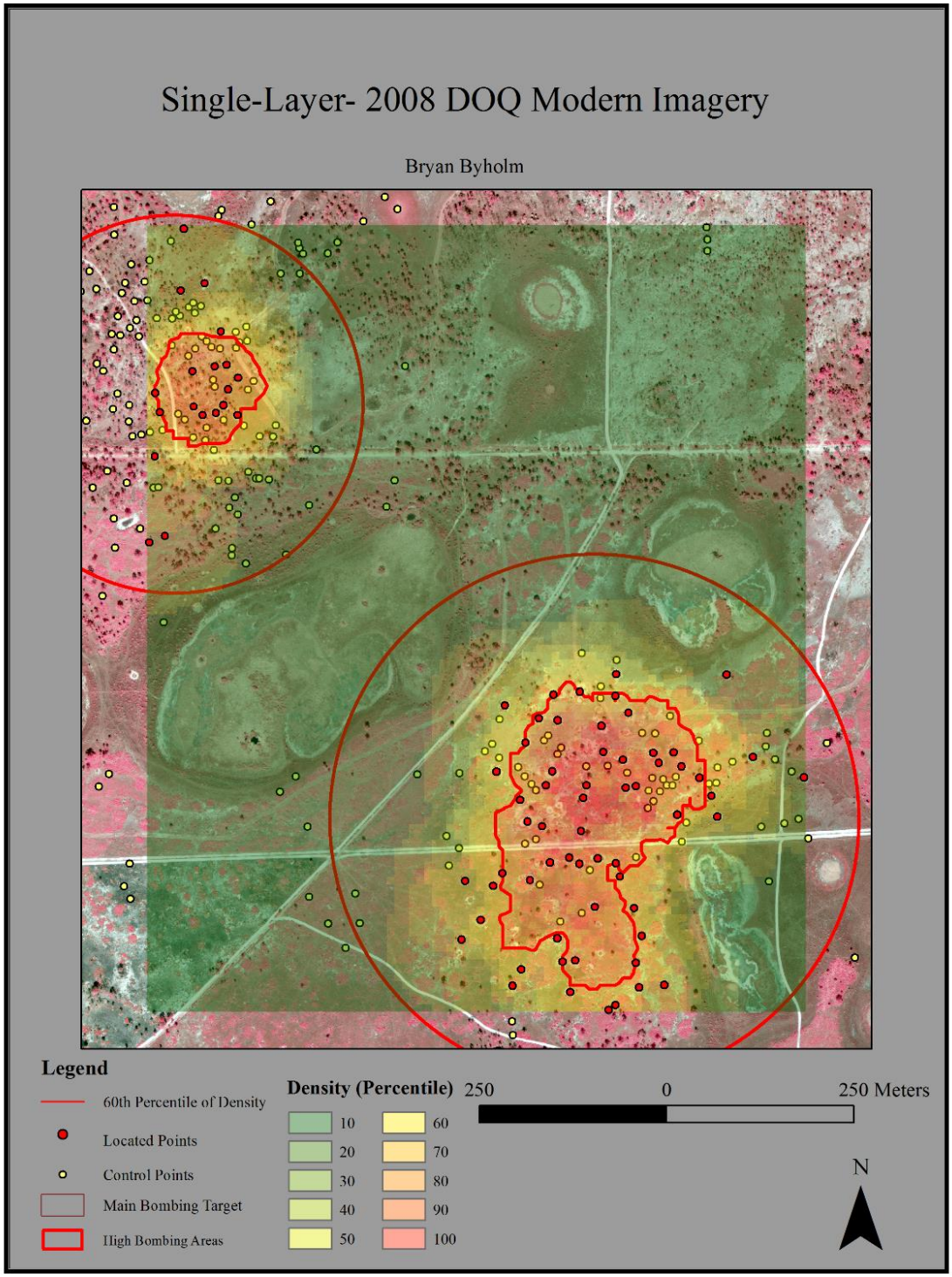

Figure 5.3.3 Single image Feature Analyst 2008 DOQ output.

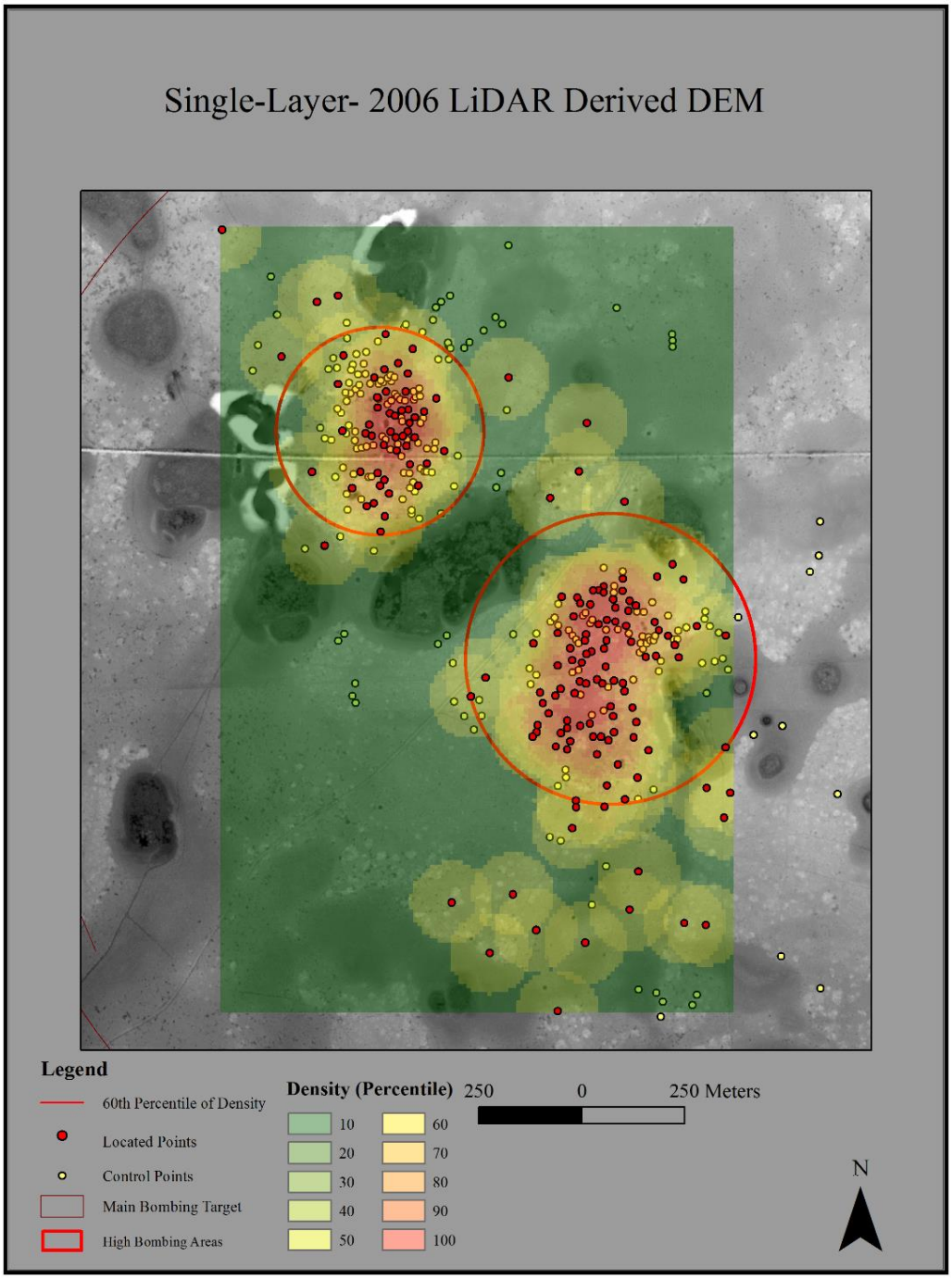

Figure 5.3.4 Single image Feature Analyst 2006 LiDAR output.

5.4 Feature Analyst Multiple Image Results

Imagery	Located Points	Located Control Points	Percent of Control Found
1946 Historical Reflectance/ 1946 Historical Texture Figure 5.4.1	43	37	16.1
2008 Modern Reflectance/ 2008 Modern Texture Figure 5.4.2	37	6	2.6
2014 Modern Reflectance/ 2014 Modern Texture Figure 5.4.3	59	34	14.8
2006 LiDAR Reflectance/ 2006 LiDAR Texture Figure 5.4.4	124	24	10.4
1946 Historical Reflectance/ 2006 LiDAR Texture Figure 5.4.5	69	35	15
2008 Modern Reflectance/ 2006 LiDAR Texture Figure 5.4.6	101	46	20
2014 Modern Reflectance/ 2006 LiDAR Texture Figure 5.4.7	59	34	14.8
1946 Historical Reflectance/ 2006 LiDAR Elevation	1	NA	NA
2008 Modern Reflectance/ 2006 LiDAR Elevation Figure 5.4.8	166	67	29.1
2014 Modern Reflectance/ 2006 LiDAR Elevation Figure 5.4.9	152	57	24.8
2006 LiDAR Reflectance/ 2006 LiDAR Elevation Figure 5.4.10	96	29	12.6

Table 5.4 Feature Analyst Multiple Image Results

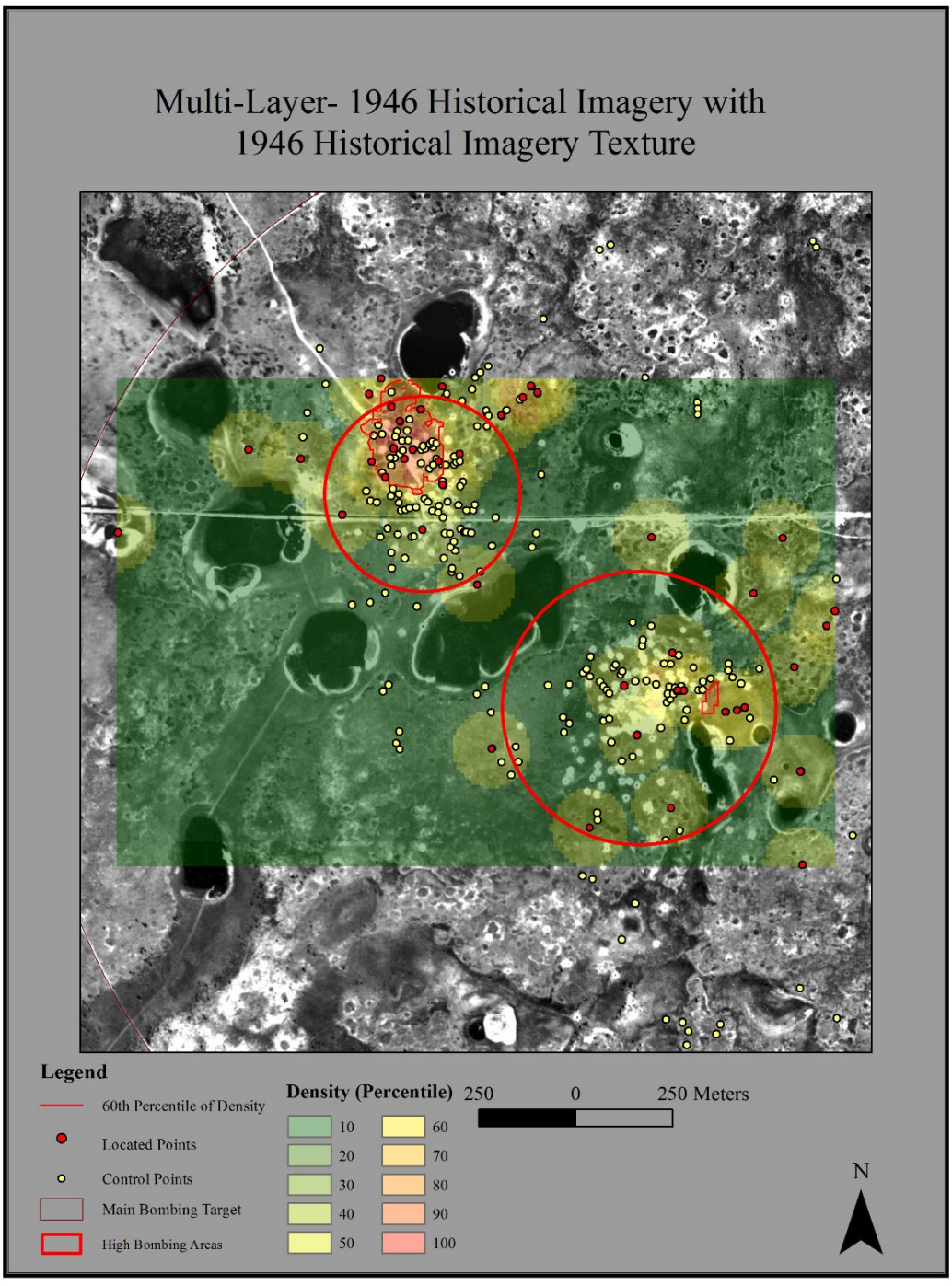

Figure 5.4.1 Multi-Imagery Feature Analyst, 1946 Historical Imagery as reflectance and texture in Feature Analyst.

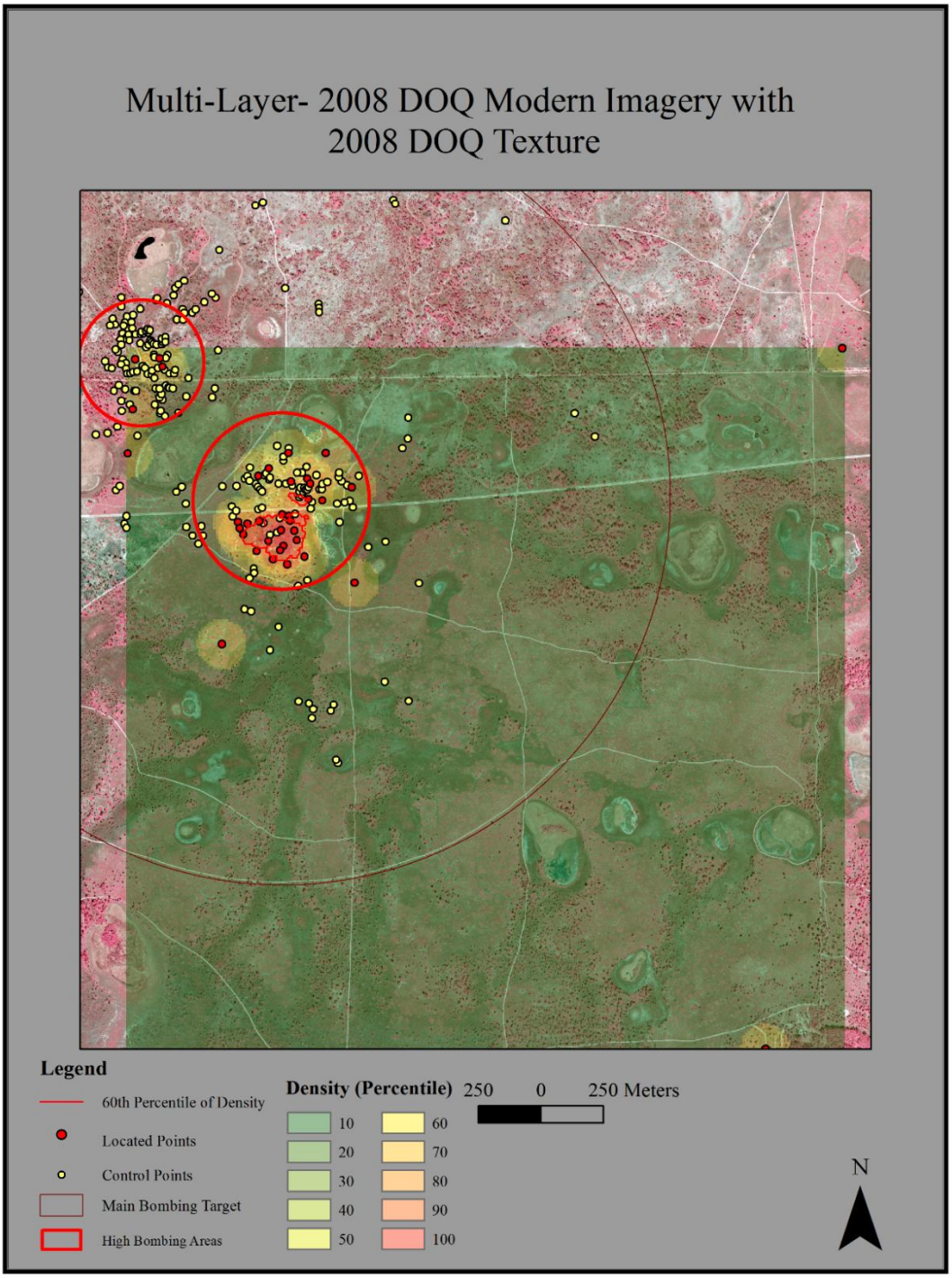

Figure 5.4.2 Multi-Imagery Feature Analyst, 2008 Modern Imagery as reflectance and texture in Feature Analyst.

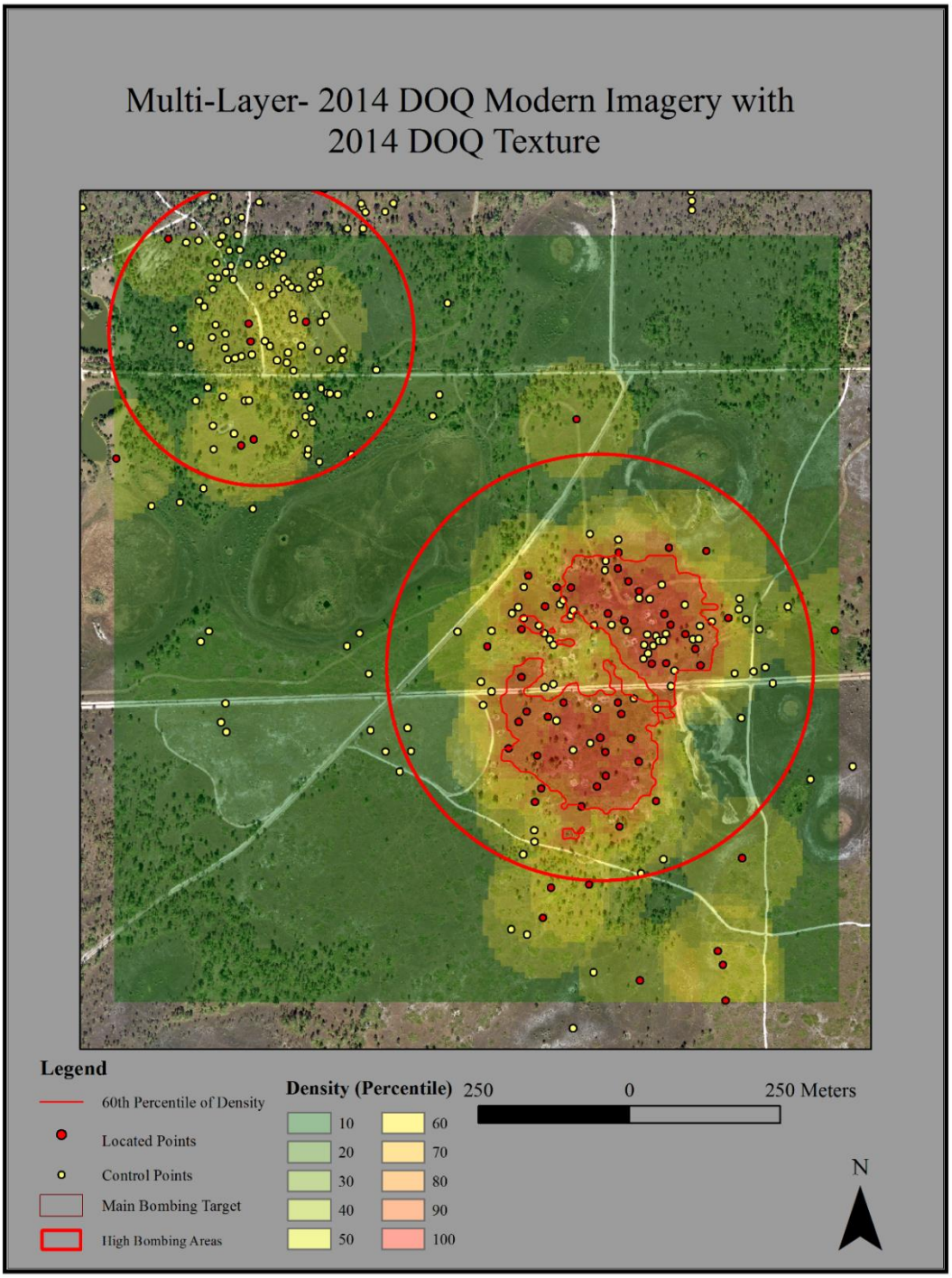

Figure 5.4.3 Multi-Imagery Feature Analyst, 2014 Modern Imagery as reflectance and texture in Feature Analyst.

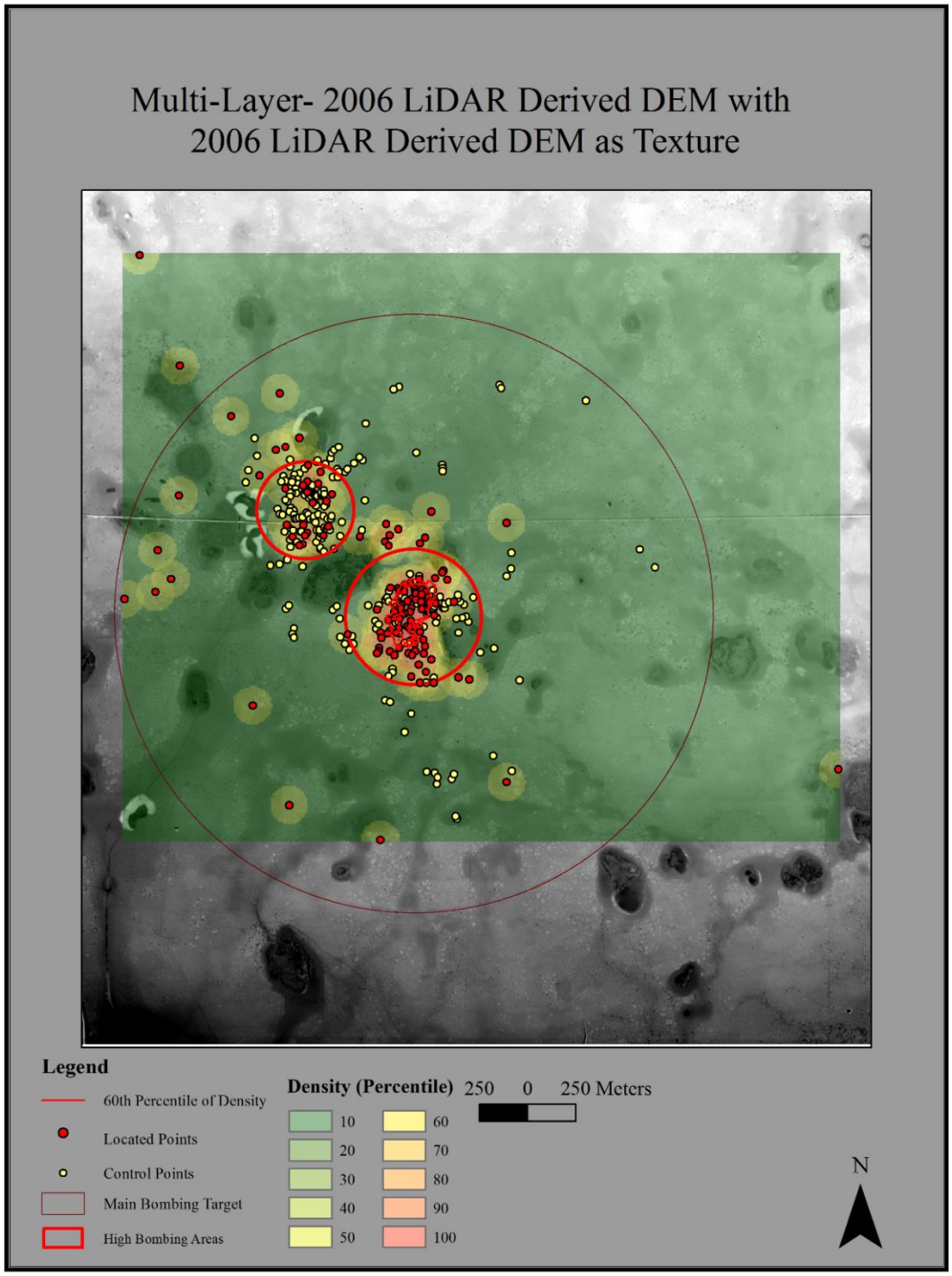

Figure 5.4.4 Multi-Imagery Feature Analyst, 2006 LiDAR-derived DEM as reflectance and texture in Feature Analyst.

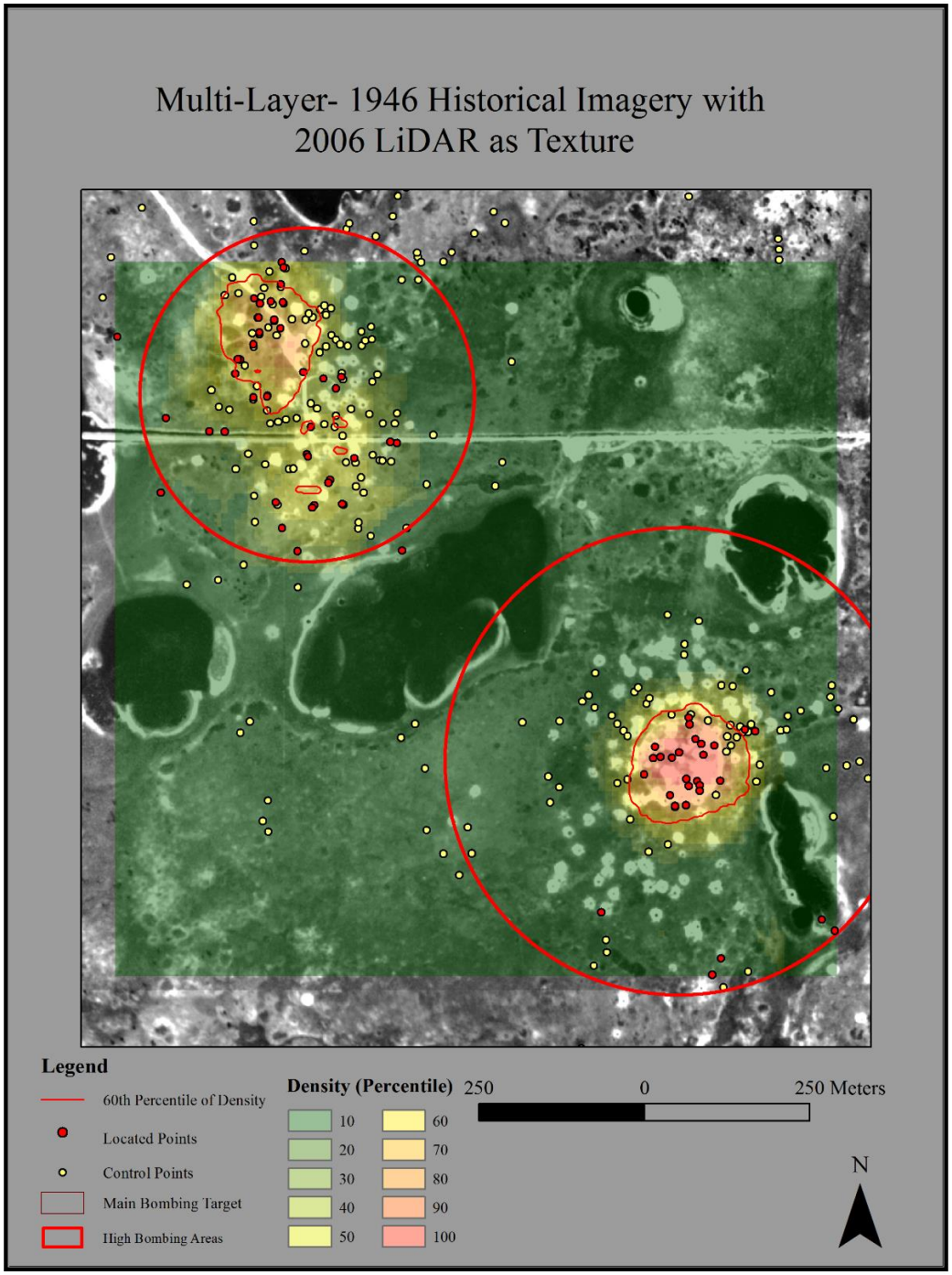

Figure 5.4.5 Multi-Imagery Feature Analyst, 1946 Historical Imagery as reflectance and the 2006 LiDAR-derived DEM as a texture layer in Feature Analyst.

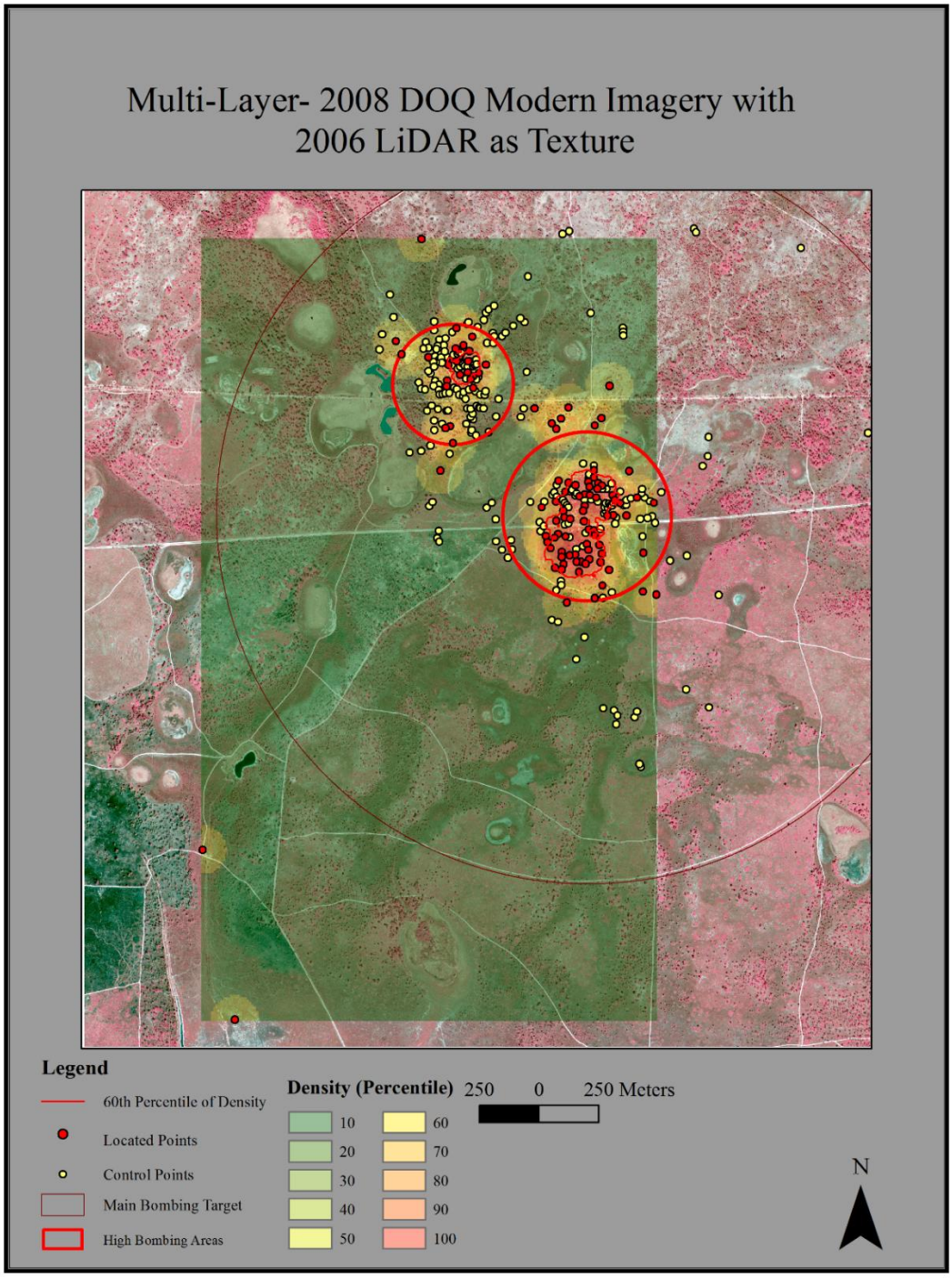

Figure 5.4.6 Multi-Imagery Feature Analyst, 2008 Modern Imagery as reflectance and the 2006 LiDAR-derived DEM as a texture layer in Feature Analyst.

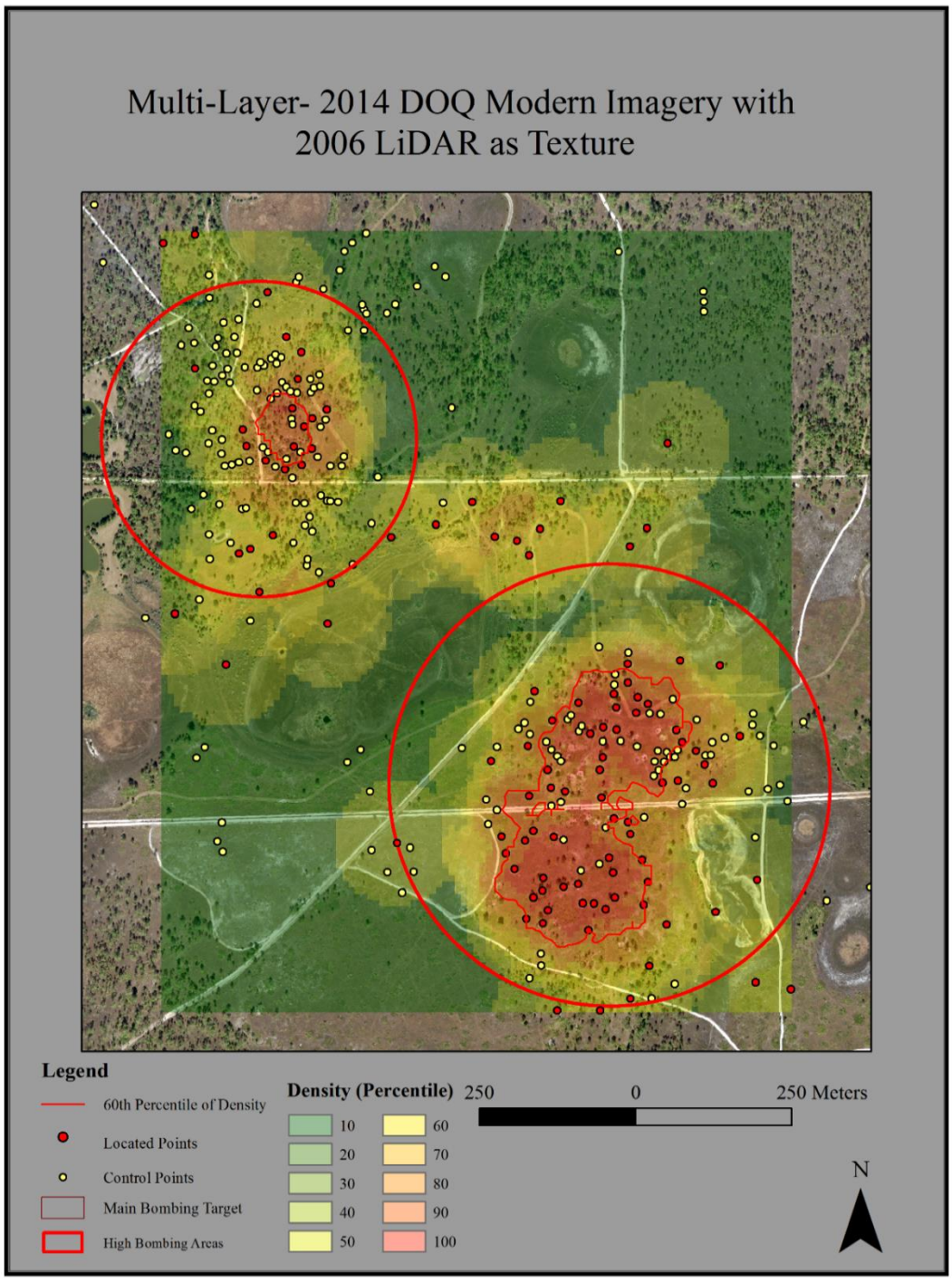

Figure 5.4.7 Multi-Imagery Feature Analyst, 2014 Modern Imagery as reflectance and the 2006 LiDAR-derived DEM as a texture layer in Feature Analyst.

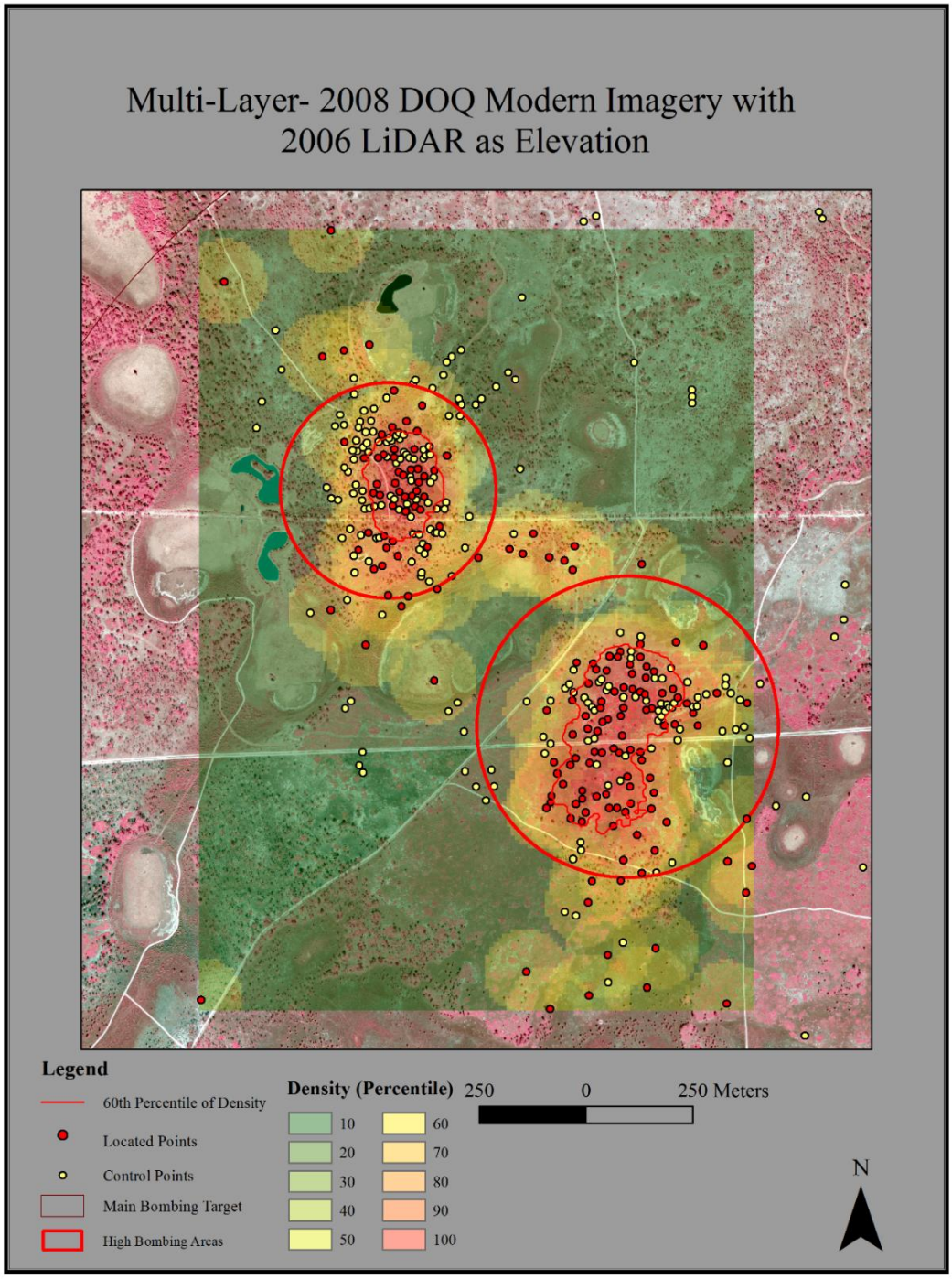

Figure 5.4.8 Multi-Imagery Feature Analyst, 2008 Modern Imagery as reflectance and the 2006 LiDAR-derived DEM as an elevation layer in Feature Analyst.

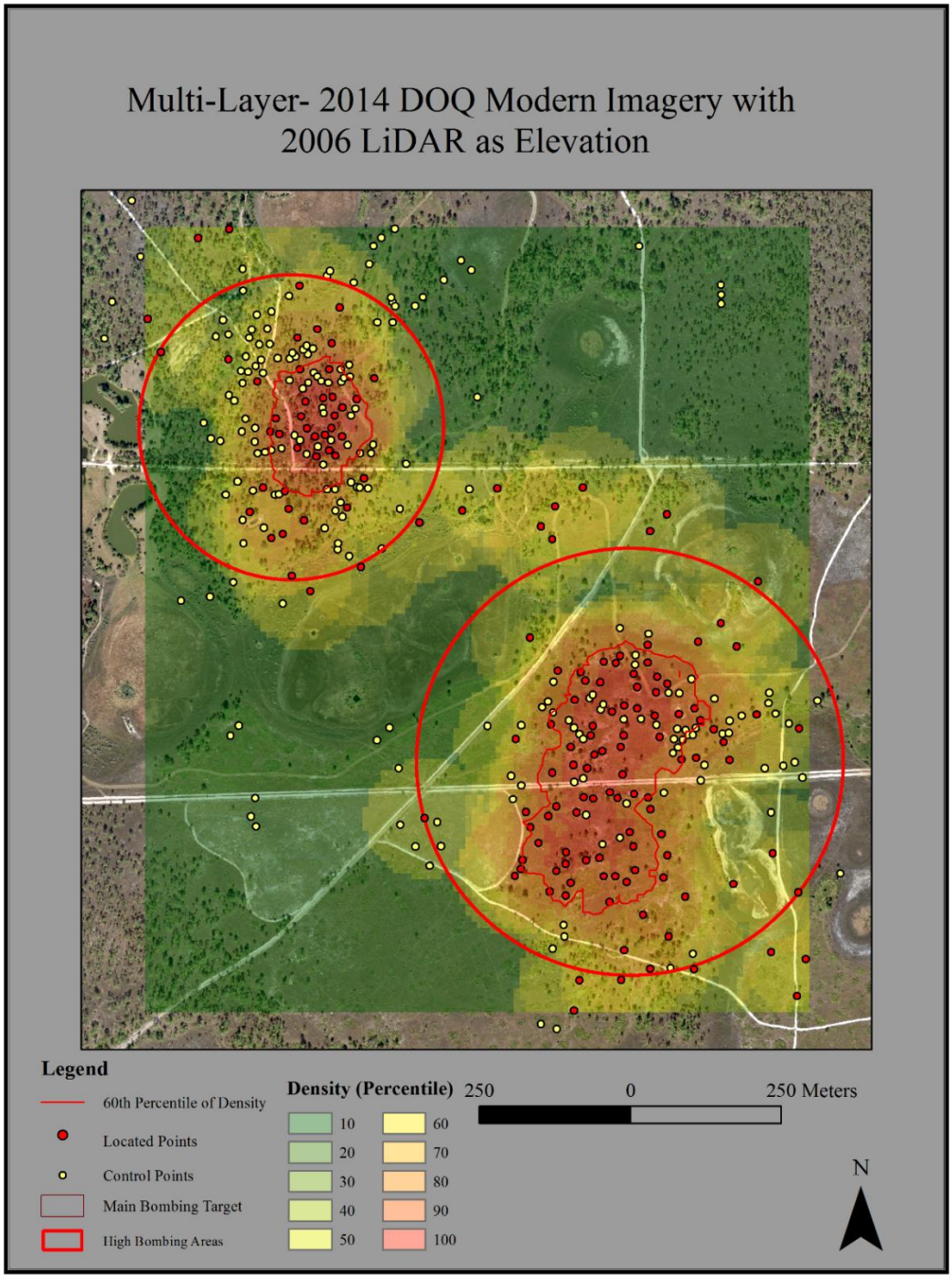

Figure 5.4.9 Multi-Imagery Feature Analyst, 2014 Modern Imagery as reflectance and the 2006 LiDAR-derived DEM as an elevation layer in Feature Analyst.

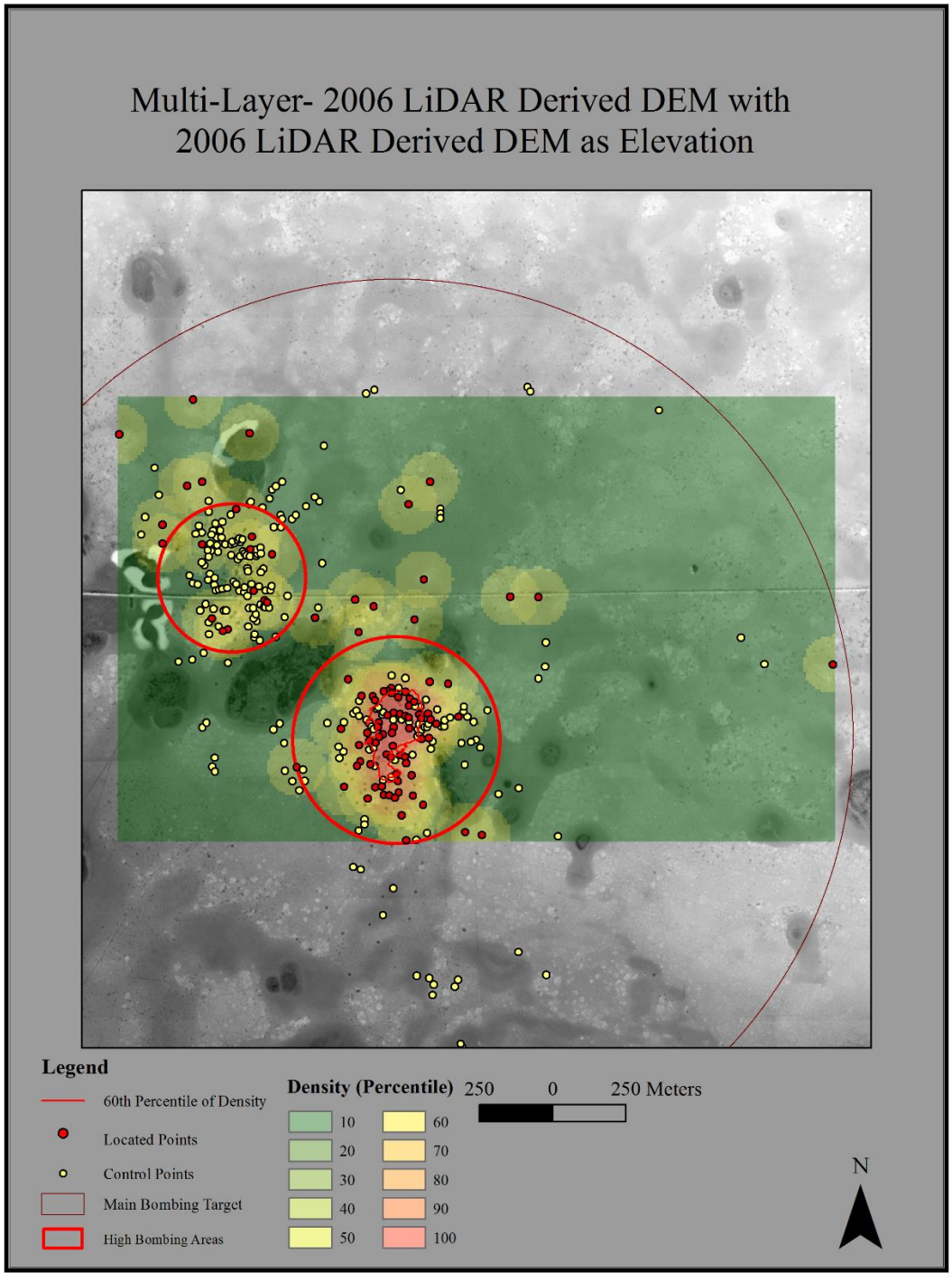

Figure 5.4.10 Multi-Imagery Feature Analyst, 2006 LiDAR-derived DEM as reflectance and the 2006 LiDAR-derived DEM as an elevation layer in Feature Analyst.

Chapter 6: Discussion of Results

Because this thesis was designed to test the effectiveness of both the software and the imagery, the discussion will address the results individually, starting with the software and then the imagery, and finally the effective combinations.

6.1 ERDAS Imagine Objective vs. Feature Analyst

Imagine Objective is a new object-based image classifier and it is straightforward to use. All of the menus have many different options to perfect the extraction and they also have help tabs to assist the user to understand what each option does. This feature became very useful as the help tabs explained what each test would do and how it worked. Objective is also very straight forward. Step by step, the software guides the user through the extraction setup. Once the setup is complete, the "Run" button will become active and the test can be run completely. If it does not activate, there is a button to check to see why the model is not ready to run. This feature becomes very handy as time is not wasted on allowing the test to run improperly. Conversely, Objective was not sensitive enough to extract a sufficient number of points on the modern imagery to test and could not use the black and white historical imagery. This hinders the software in actual testing because both modern and historical panchromatic imagery would most likely be inputs in a UXB search. Objective also has a multi-layer input feature, but it is not as refined as the same feature in Feature Analyst. In Objective, the during the image import stage, multiple files can be imported and the test continues in the same manner as a single-image test. Unfortunately, this feature continuously caused crashing issues and would not create an output. For these purposes, Objective would not be the ideal software to use.

Comparatively, Feature Analyst was not as intuitive and required much more background reading to understand. This learning time could have been shortened by a built in help section like in Objective. Feature Analyst does have an accessible help tab but it is not as intuitive as in Objective and uses more terms that are not easily understood by a novice user. Feature Analyst was easy to use and very powerful with a smaller amount of input throughout the menus. All types of imagery produced an output that could be tested against the control points, giving Feature Analyst the highest amount of user input flexibility. The software did an excellent job extracting craters on the combined LiDAR and modern imagery raising the accuracy by almost 20%. The only problem layer was the imagery that did not show many craters. On the historical imagery, the possible UXB pinholes were clearly located and extracted, thus creating the best result at 37%. This flexibility is also reflected in the multilayer input feature which allows for a much more comprehensive test of the imagery. This feature allows the modern imagery to become much more viable as an input by adding accuracy to the tests. These findings indicate that Feature Analyst is the better software for crater extraction on the FMBGR even though the learning curve for the user is much steeper.

6.2 Single layer Imagery

6.2.1 LiDAR

The LiDAR DEM was the only imagery to work in both Objective and Feature Analyst, but it does have some performance issues. The image itself is quite large for data storage and can require ArcGIS extensions to work with completely. In ArcMap, the user needs the LAS toolbar and the 3D analyst to process the raw point cloud data files. The

LiDAR point cloud originated from the Southwest Florida Water Management District and it was downloaded in tiles from the United States Interagency Elevation Inventory hosted by the National Oceanic and Atmospheric Administration (Southwest Florida Water Management District 2006). Created in 2006, these point cloud datasets are the only publicly available LiDAR coverage for the FMBGR in existence. As such, there was no other source available for the creation of high resolution DEMs, so the limitations of the data could not be avoided. Most significantly, the average point density of the bare earth returns used for the DEM layer was 0.51 points per meter^2 which is relatively course by current standards, and is more appropriate for the production of DEM products at a resolution of 2 or 3 m per pixel (Finn, Velasquez and Yamamoto 2015). Initial bare earth surfaces at 2 m resolution were run in the tests, but they did not perform well enough for the OBIA analysis. Instead, a DEM of 1 m resolution proved effective when generated using the natural neighbor void filling option during the LAS dataset to Raster conversion process. This option is consistent with the findings of Finn, Velasquez and Yamamoto (2015) relative to quality LiDAR DEM creation.

LiDAR can "see" around most vegetation to the ground below allowing the production of a bare earth image. This enables the user to create a profile of the crater on the ground which can provide surface information about it without needing to ground truth it. In this imagery, individual craters can be identified and the DEM profile can be generated in ArcGIS to estimate the size of the bomb. Both software packages found about 65 points inside of the 60th percentile lines showing that they were fairly consistent. The only issue is that the LiDAR is not sensitive enough to extract UXB pinholes due to

its resolution, but it can locate the exploded craters very well, which can then be statistically linked to likely UXB location. The density heat maps generated by both packages also look very much alike as they both locate the two main pockets of UXB activity very well. This research demonstrates that even relatively low density LiDAR can be used to generate DEMs of sufficient quality to locate crater signatures. Procuring the next generation of publically available higher density point cloud datasets might enable the creation of higher resolution DEMs to detect UXB pinholes more effectively using OBIA.

6.2.2 Modern Airborne Imagery

Modern Imagery is now available all around the world and often has a fine enough resolution to locate UXB pinholes. The only major issue with this imagery is that the land cover change that can occur in the years after the bombs are dropped. This is reflected in the software tests as the pinholes could not be located, but some of the craters could be. The test on the 2014 imagery did locate 34 likely UXB holes, only 14.8 percent of the control. These 34 control points were only extracted due to the overgrowth of the northern pocket of activity. This means that only objects the sensor can detect on the surface can be located with OBIA, which creates a problem as many bombed areas from the past have been regrown or developed into a new land use. The 2008 imagery was also flown during a wet period with a lower amount of foliage, allowing the image to preform much better in the tests, finding 55 of likely UXB, a comparatively better 23.9 percent of the control.

The study area has also experienced significant change in the land cover because of the karst landscape and the regrown vegetation. If the imagery is not taken near the time of bomb explosion, there is a smaller probability of location success using OBIA methods. In areas of recent conflict such as Southeast Asia and the Middle East, modern imagery would be very useful as the landscape would likely have less change over a shorter period of time. Desert landscapes would also likely show the entry holes much better as plant cover is sparse as compared to denser foliage in a tropical or subtropical region.

Another advantage of modern imagery is that multiple bands of the imagery can be ordered to show different information. Because of timing and location, the modern three band imagery was less effective in the single-image tests.

6.2.3 Historical Imagery

Finding suitable historic imagery of bombed areas is the most problematic aspect of UXB research as it is either available or not, depending on the specific context of the time and place. In the case of the FMBGR, it was fortunate that high quality aerial photos of Charlotte County were flown in January 1946 and include the range area. Many other FUDS-listed ranges lack historical imagery flown in close temporal proximity to the bombing process, making identification of both the exploded craters and UXB pinhole entry points difficult or impossible. In Objective, the black and white image was not able to delineate the bombing holes but Feature Analyst was able to locate the possible UXB holes very well by finding 85 pinholes and craters. Most importantly, this number is

higher than the control in which 75 pinholes were manually located. The historical imagery was also the easiest to work with as the images only had one band of data and only needed to be georeferenced and mosaicked to be processed as a layer. As noted above, two limitations of historical imagery is availability and the fact that Objective was unable to analyze a single band panchromatic image. Had color been available, the historical imagery could have been analyzed in the Objective suite. Even with these issues, the historical image proved to be the best OBIA performer, producing the most target points and most points inside of the 60th percentile.

6.3 Multi-Layer Imagery

All of the prior tests have only used a single-image in each test. Feature Analyst has an added feature which allows the user to use multiple layers of input to create a more comprehensive output. All the imagery was tested in the same manner as before, the only difference being that the inputs were used as a reflectance layer as well as a texture layer, adding depth to the tests. Every image would also use the LiDAR as a texture layer as well as an elevation layer, adding even more depth to the tests.

6.3.1 LiDAR/LiDAR

The LiDAR data could only be tested in two ways: by using the DEM as a reflectance layer and a texture layer, or as a reflectance layer with a DEM elevation layer. Both tests yielded mediocre results, only locating 24 points and 29 points of the control respectively. This lackluster performance can only be explained by the likelihood that the

edges of the craters were lost because the edge detection cannot detect the craters on the DEM image as well with the texture and elevation layers beneath it.

6.3.2 Modern Imagery/LiDAR

6.3.2.1 2008 Imagery

In the single-image tests, the 2008 imagery identified 55 located points from the control and was the most accurate of the modern imagery. This was because of the lower amount of tree cover which gave a cleaner image of the craters on the ground. The first test assessed the 2008 reflectance to the same image used as a texture layer. This surprisingly did not create an accurate output, only finding six points, a low 2.6 percent of the control. This was a surprising result as this test essentially uses the input twice and allows the software to double check the image during the test. After changing the underlying image to the LiDAR imagery, the accuracy rose significantly as the files complemented one another in the analysis. Using the LiDAR as a texture layer, the accuracy increased to 46 points, 20 percent of the control. The most success test came from the use of the LiDAR data as the elevation layer. This output found 67 points of the control, a respectable 29.1 percent of the control located.

6.3.2.2 2014 Imagery

The 2014 imagery tests reflected the same successes as the 2008 in that the addition of the LiDAR as a texture and elevation layer raised the accuracy. The LiDAR used as a texture located 46 control points and as an elevation layer located 57 points, an

increase of 23 points from the single-image test where the 2014 imagery proved less effective. Using the 2014 image as a texture layer of itself located the exact same amount of points as the single-image had in a prior test, 34 in all. This is to be expected if the single-image location is done correctly. What this suggests is that using the LiDAR as an elevation or a texture layer will raise the accuracy of modern imagery to a point where it can actually be used, and is almost comparable to the historical imagery in single-image tests.

6.3.3 Historical/LiDAR

The historical imagery had the best showing in the single-imagery tests finding 85 control points or 37 percent of them in total. In the multiple image assessment, the historical imagery struggled to locate this many points throughout its tests. Using the historical image as the reflectance as well as the texture layer only located 37 points which is less than half of the located points in the single-image analysis. This could be attributed to the resolution of the image. While 600 dots per inch resolution provides a relatively sharp image, the texture layer could be causing the software to disregard matches with the reflectance layer because of this lower pixel density. The most significant issue arose with the addition of the LiDAR data as the texture and elevation layers. Only 35 points were located with the texture layer and none were located with the elevation layer. This can likely be attributed to the software attempting to locate both the craters and pinholes while few of the pinholes were identifiable in the LiDAR. This also could be attributed to the creation of the AOI layer, which had located both craters and pinholes. This assumption was tested with an AOI layer consisting of only craters and the

output looked much like the initial results, finding almost no points. From this assessment, it seems that the historical data should be tested on its own and not in conjunction with any other layers.

6.4 Combinations and Conclusions

In the end, the software is only as good as the imagery tested. Objective lacks the sensitivity to extract objects effectively from black and white imagery so the historical test was null. The LiDAR information did produce a testable result but the vegetated surface in the modern imagery was too grown over to extract a high amount of craters to test. Feature analyst was able to take the small amount of information gathered and locate a few more craters to allow the information to be tested, but it was still not ideal. The LiDAR and historical imagery was able to be separately tested extensively and produced very good results. This leads to the conclusion that using Feature Analyst and inputting imagery gathered closest to the times of the explosions results in the best identification of possible UXB entry holes.

LiDAR also works very well as an input layer in Feature Analyst, but custom flown LiDAR is very expensive and study areas might not have freely available coverage. This makes the LiDAR data a useful luxury. If craters in a study area are recent enough to have multiple sets of modern imagery available, several criteria should be considered when selecting imagery. Sun angle, time of the year and wetness of the ground can significantly affect the extraction process, so multiple tests should be run to determine the most useful imagery characteristics. Of these, the time of the year is the most important

owing to the fact the leaf-off 2008 image preformed much better than the leaf-on 2014 image. Also, if LiDAR data sets are available, the modern imagery becomes viable through the usage of the multi-layer tests that increase the accuracy of the results. If the land has changed significantly over time since the bombing, historical imagery becomes the most valuable input layer.

Chapter 7: Conclusion

This thesis proposed a more cost effective and easier method of UXB location than the intense ground methods and complex programming computer based methods that have previously been used to locate possible UXB. Throughout the testing process, multiple methods of location have been created with varying levels of success based on what imagery is available. Through these assessments, the research objectives posed in the introduction have been met:

- Which OBIA is better at delineating possible UXB pinholes?
    - Imagine Objective was able to extract a comparable amount of UXB from the LiDAR data. With that being said, the software could not effectively process any other imagery. This leaves Feature Analyst as the best option for OBIA analysis in this respect as it was able to extract possible UXB pinholes and craters from different imagery layers. This resulted in very clear concentrations of likely UXB throughout the study area on a very consistent level.
- Which imagery is the best for UXB delineation or combination there in?
    - This also depends on when the bombs were dropped as stated in the discussion chapter. For this study area, the historical image did locate the highest concentrations of possible UXB entry holes. In other locations based on what is available and the timing of the bombings, newer imagery may be the better option. The closer to the timing of the bombing, the better. The LiDAR-derived DEM also complements the modern imagery

very well, raising its accuracy to useable levels. This multilayer workflow becomes very useful when working with the modern imagery.

- How this could be applied to other study areas for UXB delineation?
    - The major hope with any new method is its successful application in actual scientific analysis. While this study area is relatively well-documented for a small, obscure WWII training range, and has sufficient imagery for testing, the underlying theme of how to apply this in an actual war zone was perpetuated throughout the thesis. First, historical information would need to be gathered including what kind of bombs were used in the study area, how many, and what additional information is available. Next would be the location of both historical imagery and quality LiDAR, and this would be the most difficult and variable stage of the application. Next, the same tests can be run using the parameters set in the methodologies chapter. The methodologies for both Feature Analyst and Imagine Objective shown in Chapter 4 are recommended as starting point for developing a workflow appropriate to specific characteristics of the study area. Then finally, the output data can be cleaned and presented as demonstrated in Chapter 5.

By answering these questions, these methods will hopefully be applied to study areas around the world and ultimately help to save lives. For future research, actual application of these methodologies to a historic conflict area should prove valuable and effective.

Works Cited

Baumann, P. “History of Remote Sensing, Satellite Imagery, Part II.” Last modified 2009.https://www.oneonta.edu/faculty/baumanpr/geosat2/RS%20History%20II/RS-History-Part-2.html

Bennett, D. 2008. *High Density LiDAR and Orthophotography in UXB Wide Area Assessment.* Arlington, VA: Department of Defense. https://www.serdp-estcp.org/Program-Areas/Munitions-Response/Land/Sensors/MR-200534

Butler, D. K. 2001. “Potential fields methods for location of unexploded ordnance.” *The Leading Edge* 20 (8):890-895.

Charlotte County, FL. 2014. High Resolution Orthoimagery of Charlotte County, FL. Flight date 18 January 2014. Retrieved from https://earthexplorer.usgs.gov/

Chase, A. F., D. Z. Chase, and J. F. Weishampel. 2013. “The use of LiDAR at the Maya site of Caracol, Belize.” In *Mapping Archaeological Landscapes from Space*, edited by Comer, Douglas C., and Michael J. Harrower. 187-197. New York, NY: Springer.

Chen, C. C., and L. Peters. 1997. “Buried unexploded ordnance identification via complex natural resonances.” *IEEE Transactions on Antennas and Propagation* 45 (11):1645-1654.

Chepkochei, L. C. 2011.”Object-oriented image classification of individual trees using Erdas Imagine objective: case study of Wanjohi area, Lake Naivasha Basin, Kenya.” Paper presented at Kenya Geothermal Conference, Nairobi, Kenya, 21 November 2011. https://www.imarisha.le.ac.uk/academic-report/conservation-remote-sensing/253

Collins, L. M., Y. Zhang, J. Li, H. Wang, L. Carin, S. J. Hart, S. Rose-Pehrsson, H. H. Nelson, and J. R. McDonald. 2001. “A comparison of the performance of statistical and fuzzy algorithms for unexploded ordnance detection.” *IEEE Transactions on Fuzzy Systems* 9 (1):17-30.

Colten, C. E. 1990. “Historical Hazards: The Geographhy of Relict Industrial Wastes.” *The Professional Geographer* 42 (2):143-156.

Dean, F. H. (1997) *America's Hundred Thousand.* Atglen, PA: Schiffer Publishing Ltd.

DeLuca, C. C., V. R. Marinelli, M. A. Ressler, and T. T. Ton. 1998. "Unexploded ordnance detection experiments using ultra-wideband synthetic aperture radar." Proceedings of SPIE, Detection and Remediation Technologies for Mines and Mine-like Targets III, Volume 3392: 668-677. doi: 10.1117/12.324239

Dwyer, L. 2014a. *Curtiss P-40 Warhawk*. http://www.aviation-history.com/curtiss/p40.html.

------. 2014b. *P-51 Mustang*. http://www.aviation-history.com/north-american/p51.html.

-------. 2014c. *Republic P-47 Thunderbolt*. http://www.aviation-history.com/republic/p47.html.

ERDAS Imagine Help: Multi Bayesian Network. 2016. Hexagon Geospatial.

ERDAS Imagine Help: SFP. 2016. Hexagon Geospatial.

Finn, M., F. Velasquez and K. H. Yamamoto. 2015. "Determining Optimal Post Spacing for Lidar DEM Creation Using Open Source and Commercial Software." Paper presented at the GIS in the Rockies Conference, Denver, CO 23-24 September 2015. https://cegis.usgs.gov/projection/pdf/lidarPointSpacingAbstractGITR_V05_clean-%20elu.pdf

Florida Fish and Wildlife. 2016. *Babcock/Webb – History* http://myfwc.com/viewing/recreation/wmas/lead/fred-babcockwebb/history/.

Foley, J. 2008. *Demonstration of LiDAR and Orthophotography for Wide Area Assessment at Pueblo Precision Bombing Range #2, Colorado*: Sky Research, Inc. http://www.dtic.mil/dtic/tr/fulltext/u2/a495570.pdf

George, A., D. Hall and W. Simons. 1971. *The Limits of Coercive Diplomacy: Laos, Cuba, Vietnam*. Boston: Little, Brown.

Höfler, V., C. Wessollek, and P. Karrasch. 2015. "Modelling prehistoric terrain models using LiDAR-data: a geomorphological approach." Proceedings of SPIE, Volume 9644: Earth Resources and Environmental Remote Sensing/GIS Applications VI. http://spie.org/Publications/Proceedings/Paper/10.1117/12.2194290

Hooper, A. E. and H. N. Hambric. 1998. "Unexploded ordnance (UXB): the problem." In *Detection and Identification of Visually Obscured Targets*:1-8. Edited by C.E. Baum. Philadelphia: Taylor and Francis.

Howard, G. B. 2001. "Application of airborne thermal infrared imaging for the detection of unexploded ordnance." Proceedings of SPIE, Volume 4360, Thermosense XXIII, 149. 23 March. doi:10.1117/12.420986

Hexagon Geospatial. 2016. Imagine Objective the Future of Feature Extraction, Update, & Change Mapping. Hexagon Geospatial: Norcross, GA.

Johnson, K. and C. Minor. Data Fusion Framework for Wide-Area Assessment of Buried Unexploded Ordnance. U.S. Patent 8,150,794 B2 filed June 23, 2009 and issued April 3, 2012.

Kuhn, A. K. 1910. "The Beginnings of an Aerial Law." *The American Journal of International Law* 4 (1):109-132.

Lacroix, V., and S. Vanhuysse. 2014. "Indicators of Mine Presence: Focus on trenches." *South-Eastern European Journal of Earth Observation and Geomatics* 3 (2):635-639.

———. 2015. "Crater Detection using CGC-A New Circle Detection Method." Proceedings of the International Conference on Pattern Recognition Applications and Methods. 20-23 January 2015, 320-327. Lisbon, Portugal.

Lane, E. 1986. *Karst in Florida*. Tallahassee: Florida Geological Survey.

Lefevre, A., and M. Petty. 2016. "U.S. gives Laos extra $90 million to help clear unexploded ordnance." *Reuters*, 6 September 2016. http://www.reuters.com/article/us-laos-obama-uxo-idUSKCN11C0GV

Lillesand, T., W. Kiefer, and J. Chipman. 2015. *Remote sensing and image interpretation*. 7th ed. Hoboken, NJ: John Wiley & Sons.

Macdonald, A. 1992. "Air photography at Ordnance Survey from 1919 to 1991." *The Photogrammetric Record* 14 (80):249-260.

Maio, C. V., D. E. Tenenbaum, C. J. Brown, V. T. Mastone, and A. M. Gontz. 2013. "Application of geographic information technologies to historical landscape reconstruction and military terrain analysis of an American Revolution Battlefield: Preservation potential of historic lands in urbanized settings, Boston, Massachusetts, USA." *Journal of Cultural Heritage* 14 (4):317-331.

Marpu, P., M. Neubert, H. Herold, and I. Niemeyer. 2010. "Enhanced evaluation of image segmentation results." *Journal of spatial science* 55 (1):55-68.

Maurer, M. 1982. *Combat Squadrons of the Air Force: World War II*, Maxwell AFB, AL: Office of Air Force History. http://www.dtic.mil/get-tr-doc/pdf?AD=ADA128026

Merler, S., C. Furlanello, and G. Jurman. 2005. "Machine learning on historic air photographs for mapping risk of unexploded bombs." Paper presented at International Conference on Image Analysis and Processing. 6-8 September 2005. Cagliari, Italy.

Monmonier, M. 2002a. "Aerial photography at the agricultural adjustment administration: acreage controls, conservation benefits, and overhead surveillance in the 1930s." *Photogrammetric engineering and remote sensing* 68 (12):1257-1262.

———. 2002b. *Spying with maps: Surveillance Technologies and the Future of Privacy* Chicago: University of Chicago Press.

Nelson, H., T. W. Altshuler, E. M. Rosen, J. McDonald, B. Barrow, and N. Khadr. 1998. "Magnetic modeling of UXB and UXB-like targets and comparison with signatures measured by MTADS." Proceedings of UXO Forum 1998. http://citeseerx.ist.psu.edu/viewdoc/summary?doi=10.1.1.41.1534

Opitz, D., and S. Blundell. 2008. "Object recognition and image segmentation: the Feature Analyst® approach." In *Object-Based Image Analysis: Spatial Concepts for Knowledge-Driven Remote Sensing Applications*, edited by T. Blaschke, S. Lang and G. Hay, 153-167. Berlin: Springer-Verlag.

Padilla, M. 2007. Sandia searches for Unexploded ordanance. *Sandia Lab News*, 21 February. https://share ng.sandia.gov/news/resources/releases/2007/uxo.html

Paine, D. P., and J. D. Kiser. 2003. *Aerial photography and image interpretation*: John Wiley & Sons.

Peterson, J., D. Sack, and R. Gabler. 2012. *Physical Geography* 10th ed: Belmont, CA: Cengage Learning.

Portugal, R. S., C. R. de Sousa Filho, and P. A. Bland. 2004. Automatic Crater Detection Using DEM and Circular Coherency Analysis - A Case Study on South American Craters, ed. t. A. M. S. Meeting.

Powers Jr, F. 1997. “Foreword: From the U-2 to Corona.” In *CORONA between the Sun and the Earth: The first NRO reconnaissance eye in space*. Edited by R. McDonald. https://www.cia.gov/library/publications/intelligence-history/corona-between-the-sun-and-the-earth

Republic P-47 Thunderbolt. Retrieved from http://www.asisbiz.com/il2/P-47D/Republic-P-47-Thunderbolt.html

Risbøl, O. 2013. “Cultivating the ‘Wilderness’ - How LiDAR Can Improve Archaeological Landscape Understanding.” In Cowley, D. and R. Opitz. *Interpreting archaeological topography: Airborne laser scanning, 3D data and ground observation*. 51-62: Oxbow Books, Oxford.

Sabour, S. T., J. Agarius, and J. Sadidi. 2014. Calculation of Per Parcel Probability for Dud Bombs in Germany. *The International Archives of Photogrammetry, Remote Sensing and Spatial Information Sciences* 40 (2):261.

Sanchez, V., Y. Li, M. N. Nabighian, and D. L. Wright. 2008. Numerical Modeling of Higher Order Magnetic Moments in UXB Discrimination. *IEEE Transactions on Geoscience and Remote Sensing* 46 (9):2568-2583.

Shettle, M. L. 2009. *Florida’s Army Air Fields of World War II*. Roswell, GA: Schaertel Publishing Company.

Shubitidze, F., J. P. Fernandez, I. Shamatava, B. E. Barrowes, and K. O’Neill. 2012. Joint diagonalization applied to the detection and discrimination of unexploded ordnance. *Geophysics* 77 (4):WB149-WB160.

Southwest Florida Water Management District. 2005-2006 Peace River South LiDAR. Charlotte County, Florida: Southwest Florida Water Management District. Retrieved from https://coast.noaa.gov/inventory/

———. 2008. High Resolution Orthoimagery of Charlotte County, FL. Flight date 1 February 2008. Retrieved from https://earthexplorer.usgs.gov/

St Joseph, J. K. S., and D. Coombe. 1977. *The uses of air photography*. London: J. Baker.

Stepinski, T., W. Ding, and R. Vilalta. 2012. Detecting impact craters in planetary images using machine learning. In *Intelligent Data Analysis for Real-Life Applications: Theory and Practice.* Edited by D. Pevec, E. Sapozhnikova, S. Sakurai, J. Gamez and R. Vilalya, 146-159. Hershey, PA: IGI Global.

United States Army Air Forces. 1943. *Pilot Training Manual for the P-40*. http://www.avialogs.com/viewer/avialogs-documentviewer.php?id=3136

——. 1944. *Pilot's Flight Operating Instructions, Army Model P-51-D-5, British Model Mustang IV Airplanes,* Technical Order AN 01-60JE-1. Retrieved from http://www.wwiiaircraftperformance.org/mustang/P-51D-manual-5april44.pdf

——. 1945. *AAF 51-127-3 Pilot Training Manual for the P-47 Thunderbolt*. http://www.avialogs.com/en/aircraft/usa/republic/p-47thunderbolt/aaf-51-127-3-pilot-training-manual-for-the-p-47-thunderbolt.html

United States Army Corps of Engineers. 1996. *Archives Search Report, Fort Myers Bomb and Gun Range*. St. Louis, MO: United States Army Corps of Engineers.

——.2009. *Final Site Inspection Report, Fort Myers Bombing and Gunnery Range, Charlotte County, Florida*. Jacksonville, FL: United States Army Corps of Engineers.

——.2016. "Former Lowry Bombing and Gunnery Range – Project Information." http://www.flbgr.org/project/project.html

United States Army Office of the Chief of Ordnance. 1944. *Terminal Ballistic Data - Volume 3 - Bombs, Artillery, Mortar Fire and Rockets*. http://cgsc.cdmhost.com/cdm/ref/collection/p4013coll8/id/2375

United States Department of Defense. 2005. Report of the Defense Science Board Task Force on Unexploded Ordnance. http://www.denix.osd.mil/mmrp/archives/reports/unassigned/defense-science-board-dsb-report-task-force-on-unexploded-ordnance/

University of Florida Map and Imagery Library Digital Collections. Aerial photographs of Charlotte County. 1:20,000. Flight 1. DDM 1-28, 1-30, 1-51 and 1-53. January 26, 1946.

Vanhuysse, S., D. Hoelbling, B. Friedl, E. Hanson, A. Krtalic, M. Hagenlocher, I. Racetin, and E. Wolff. 2014. "Object-based image analysis for detecting indicators of mine presence to support suspected hazardous area re-delineation." *South-Eastern European Journal of Earth Observation and Geomatics* 3 (2):525-529.

White, M., J. Zhu, B. L. Blandford, and T. H. Grossardt. 2015. *Identifying Significant Environmental Features Using Feature Recognition*. University of Kentucky, Lexington: Kentucky Transportation Center.

Yuan, F. 2008. “Land-cover change and environmental impact analysis in the Greater Mankato area of Minnesota using remote sensing and GIS modelling.” *International Journal of Remote Sensing* 29 (4):1169-1184.

Zhang, Q., W. Al-Nuaimy, and Y. Huang. 2007. Interpretation of borehole magnetometer data for the detection and characterisation of unexploded bombs” J*ournal of applied geophysics* 61 (3):206-216.